CHARACTERISTICS OF THE DYNAMIC RESPONSE OF THE SULTAN AHMET MOSQUE (ISTANBUL) TO EARTHQUAKES

by

Kökcan Dönmez

B.Sc., Civil Engineering, Namık Kemal University, 2016

Submitted to the Kandilli Observatory and Earthquake
Research Institute in partial fulfillment of
the requirements for the degree of
Master of Science

Graduate Program in Earthquake Engineering

Boğaziçi University

2021

ACKNOWLEDGEMENTS

I would like to express my gratitude to Prof. Eser Çaktı, my supervisor, for broadening my horizons and for everything that she has taught me. Prof. Çaktı instilled my interest in heritage structures and paved my way. I am privileged for being her student, and she has been and will be a role model for me not only as an academic but also personally.

I am very grateful to Prof. Erdal Şafak for sharing his in-depth and valuable knowledge in structural monitoring and supporting the computational steps in this thesis.

I kindly thank Prof. Deniz Mazlum for reviewing the narrative section about the mosque and making it more reliable architecture-wise.

Ultimately, just as they dedicated themselves to me, I would like to dedicate this work to my parents, Gönül and Sebahattin, as a modest token of appreciation. They have always been my pioneering advisors in life, and I am the luckiest one as long as I feel their love and support.

ABSTRACT

CHARACTERISTICS OF THE DYNAMIC RESPONSE OF THE SULTAN AHMET MOSQUE (ISTANBUL) TO EARTHQUAKES

The 400-year-old Sultan Ahmet Mosque is located southwest of the ancient hippodrome in Istanbul's historical peninsula. This historic structure, which has survived from the Ottoman period, experienced many damaging earthquakes in the North Anatolian Fault, especially in the fault segments within the Marmara Sea, since its construction was completed in 1617. The mosque is prominent as a cultural heritage element in the city. Therefore, its primary structural system has been monitoring since 2012. The Structural Health Monitoring system deployed in the mosque consists of ten triaxial (two horizontal, one vertical) accelerometers functioning at a sampling rate of 200 Hz. Sensors were installed as four at the main dome, four at the upper galleries of the pillars, one at the ground level, and the last one on the basement floor. Over two hundred recorded earthquakes between October 2012 and November 2020, whose magnitudes ranging from minor to strong, were processed and assessed through scripts coded on MatLab. Used criteria such as sensor completeness of an event and the signal-to-noise ratio of a recording initially reduced the number of earthquakes. Hence in this thesis, the final catalogue of 103 events was analysed in time- and frequency-domain after evaluating the catalogue statistically as functions of magnitude, distance, and azimuth. In the time domain, acceleration, velocity and displacement peaks were obtained and assessed individual- and group-based. Their various relations with earthquake magnitude and amplitude were also examined. In frequency-domain analyses employing modal approaches, the dependence of dominant frequencies on time, temperature, earthquake magnitude, and ground motion amplitude was investigated. Particle motions and mode shapes for the selected largest-amplitude events were identified and depicted. Finally, the existence of soil-structure interaction and the rocking vibrations in the structure were investigated.

ÖZET

İSTANBUL'DAKİ SULTAN AHMET CAMİİ'NİN DEPREMLERE BAĞLI DİNAMİK DAVRANIŞININ ÖZELLİKLERİ

İstanbul'un tarihi yarımadasında yer alan Sultan Ahmet Camii günümüz antik hipodromunun güneybatısında dört asırdır varlığını sürdürmektedir. Osmanlı devrinden günümüze erişen bu tarihi yapı, 1617'de tamamlanan inşası itibariyle Kuzey Anadolu Fayı ve özellikle fayın Marmara Denizi içerisindeki segmentlerinde meydana gelmiş hasar verici birçok depremi tecrübe etmiştir. Nitekim, camii bir kültür mirası unsuru olarak önem arz etmektedir ve bu nedenle ana strüktürel sistemi bir yapı sağlığı izleme sistemi vasıtasıyla 2012'den beri takip edilmektedir. Sultan Ahmet Camii'nde işlev gören bu sistem; dördü ana kubbede, dördü filayaklarının üst galerilerinde, biri ibadet yeri seviyesinde ve sonuncusu da bodrum zemininde bulunmak üzere on adet ivmeölçer sensörden oluşmaktadır. Her bir sensör ikisi yatay ve biri dikey olmak üzere üç bileşenlidir ve 200 Hz örnekleme hızında kayıt toplama kapasitesindedir. Ekim 2012 – Kasım 2020 aralığında toplanan ve büyüklükleri minör ölçekliden kuvvetliye değişen iki yüzün üzerinde deprem, MatLab programlama dili ile geliştirilen kodlar ile işlenerek analiz edilmiştir. Depremler başlangıçta birtakım kritere bağlı olarak indirgenmiştir; bunlar bir depremin tüm sensörlerce kayıt durumu, sinyal/gürültü oranı ve merkez üssü uzaklığıdır. Bu tez dahilinde, camiye ait deprem kataloğu deprem büyüklüğü, mesafesi ve azimutu üzerinden istatistiksel olarak incelenmiş ve ayrıca Ekim 2012'den itibaren sistemce kaydedilmiş yüzün üzerinde depremin zaman ve frekans ortamlarında analizleri gerçekleştirilmiştir. Zaman ortamında, depremlerin ivme, hız ve deplasman pik değerleri belirlenmiş ve bu değerler tekil olarak ve gruplar bazında incelenmiştir. Ayrıca, yer hareketi büyüklüğü ve genliği ile bağıntıları değerlendirilmiştir. Frekans ortamında ise, yapının belirlenmiş hâkim frekanslarının zamana, sıcaklığa, deprem büyüklüğüne ve yer hareketi genliğine bağlı olarak değişimleri irdelenmiştir. Seçilen en yüksek genlikli depremleri kullanarak yapının ana strüktürel sisteminin noktasal hareketleri ve mod şekilleri elde edilmiştir. Nihayetinde, zemin-yapı etkileşiminin ve rijit yapı titreşimlerinin yapıdaki varlığı ve etkileri araştırılmıştır.

TABLE OF CONTENTS

LIST OF FIGURES

LIST OF TABLES

LIST OF ACRONYMS\ABBREVIATIONS

FAS	Fourier Amplitude Spectrum
KOERI	Kandilli Observatory and Earthquake Research Institute
M_L	Local Magnitude
M_W	Moment Magnitude
SHM	Structural Health Monitoring
SNR	Signal-to-Noise Ratio
SSI	Soil-Structure Interaction
TF	Transfer Function

1. INTRODUCTION

Since Istanbul is in a seismically active area, preserving the cultural heritage of the city from natural disasters (especially from the most hazardous one, earthquakes) and carrying it into the future are essential yet challenging tasks. The 400-year-old Sultan Ahmet Mosque, also known as the Blue Mosque, is today one of the symbols of Istanbul, remaining from the Ottoman Empire. By using the discipline of Earthquake Engineering fundamentally and supporting the research with such fields as History and Architecture, this thesis endeavours to comprehend its dynamic response characteristics and be a pioneering step in accomplishing these ideals for the mosque.

1.1. Objective

The Sultan Ahmet Mosque, located in the historical peninsula of Istanbul, has been a source of interest since the day it was constructed. The mosque is the last example of the classical period of Ottoman architecture. The area where the mosque exists was included in UNESCO's World Heritage List as part of '*Historic Areas in Istanbul*'. It represents value for the Republic of Turkey today as wells as it did in the Ottoman period**.**

One of the most hazardous natural disasters, i.e., earthquakes, has been threatening Istanbul for centuries. By examining the earthquakes from the last 2000 years in the surrounding region of Istanbul, two significant earthquake typologies are with either moderate or high intensity; the former is expected in a 50-year period of occurrence while the latter in every 300 years (Erdik, 2013). The city is highly earthquake-prone due to the North Anatolian Fault segments within the Marmara Sea, and it is expected to face a major earthquake in the future. In this context, a major seismic event is likely to take place along the earthquake gap inactive for about 250 years, and it was predicted as an event with $M \leq 7.6$ with approximately 50% probability in upcoming decades (Bohnhoff et al., 2013; Sengor et al., 2005). When these facts highlighted are compiled onto our case, as a prominent architectural heritage in Istanbul, it is evident that the Sultan Ahmet Mosque might be at

potential risk. Thus, this study would contribute to understanding the complex nature of the structure and taking measures if necessary.

The thesis aims to reveal and evaluate the dynamic response characteristics of the Sultan Ahmet Mosque's portion of the prayer hall, which is instrumented with ten accelerometer sensors continuously recording vibrations on the critical locations of the primary structural system. Through these seismic recordings, dynamic response investigation is held in both frequency and time domains after perceiving the data set statistical-wise. In the time domain, peak acceleration, velocity and displacement values are obtained to reviewed sensor-by-sensor. The dependence of those values on earthquake magnitude and excitation amplitude is also investigated. In the frequency domain, frequencies belonging to the first two modes of the structure are identified with the aim of evaluating the change against time, seasonal temperature, earthquake magnitude and input excitation. Mode shapes belonging to identified modal frequencies are also exhibited. The impact of a tension ring installation surrounding the main dome is also assessed. In addition to those, the soil-structure interaction (SSI) and the rocking are also under consideration.

1.2. Modal Analysis

Modal analysis is a method to explain and depict the complex dynamic behaviour of a vibratory structure under specific loads by making the complexity more understandable. A structure can be described mode by mode, and its dynamic properties, such as modal frequency, damping and mode shapes, can be demonstrated. Besides its use in many scientific fields, it had been an appropriate and handy tool in civil engineering concerns. In the further understanding of historical structures, high-rise buildings, bridges, infrastructures, etc., modal analysis has become crucial and contributes to the engineering-design processes.

As seen in its history of scientific development, modal analysis is rooted in Isaac Newton's spectrum studies and the Fourier series (He and Fu, 2001). Cooley and Tukey

(1965) developed a fast Fourier transform (FFT) algorithm, and experimental modal analysis became more applicable and user-friendly. The earthquake data recorded by the Sultan Ahmet Mosque monitoring system is initially represented as acceleration series in the time domain. In order to identify dynamic response characteristics comprehensively, the data shall be examined as a function of frequency by Fourier transforms. Safak and Cakti (2014) concluded that such main parameters that belong to a structural system as modal frequencies, mode shapes, damping values, presence of soil-structure interaction (SSI) and rocking vibrations could be identified from vibration recordings by using only two tools: Fourier transforms and band-pass filters. Even though it is a task easy-to-accomplish, the analysis process requires expertise and should be carried out attentively. In this study, these approaches, which proposed by Safak and Cakti, are fundamental.

The system identification by experimental modal analysis is the basis of this thesis. Employing modal analysis methods is made using modal testing, which bridges the modal analysis and structural health monitoring.

1.3. Structural Health Monitoring

Structural Health Monitoring (SHM) is a tool for making observations on the nature of a structure to understand it at the best possible level. In the field of Civil/Earthquake Engineering, the SHM has become a primary tool to see the in-situ interaction between a structure and the dynamic factors, which mainly related to natural disasters, atmospheric effects or human-induced excitations. In other words, it can be considered as a form of communication that allows a structure to express itself, i.e., its nature.

An SHM system can be created with instruments such as accelerometers, displacement gauges, tiltmeters, thermocouples, strain gauges, load sensors and/or GPS sensors. Above all, the critical issue is to decide on suitable instruments serving the purpose. As important as the instruments used in an SHM system, two other factors, placement point and sensor layout, have critical roles in monitoring a structure. Engineering-wise, the placement points

of the sensors network should be designed to gather data efficiently: the highest possible point of a structure (main dome, roof, etc.), the base-level and/or ground-level (to record strong ground motion), specific points where mass and/or stiffness dramatically changed within a structure, and other points where significant modes with larger amplitudes are found. Therefore, the optimum data gathered by a well-designed SHM network leads to having more reliable collected data and thus results.

In the sense of preserving the heritage structures, structural characterisation through SHM systems is advantageous since it is a non-destructive tool with long service life. The main parameters of a structure can be obtained via an SHM system. Monitoring data can reveal natural frequencies and related mode shapes, damping ratios, torsion, the existence of the SSI, and rocking. In addition to those, it can also be beneficial for rapid post-earthquake structural assessment. With comprehensive instrumentation, for instance, accelerometers, GPS sensors and tiltmeters, virtual damage detection can be done.

The Sultan Ahmet Mosque SHM system was designed and installed by the Department of Earthquake Engineering of Kandilli Observatory and Earthquake Research Institute, Boğaziçi University (DEE – KOERI). The structure has been continuously monitoring by the department since 2012.

1.4. Soil-Structure Interaction and Soil Conditions

Kramer (1993) defined Soil-Structure Interaction (SSI) mechanism as '*the response of the soil influences the motion of the structure and the response of the structure influences the motion of the soil*.' SSI, particularly in our case, refers to the influence of soil flexibility surrounding the building's foundation during its vibrations under earthquake loads (Safak and Cakti, 2014).

Safak (1995) highlighted that the existence of SSI should be determined beforehand other analysis steps preliminarily since this interaction causes an alteration to the frequency content. According to the approach suggested in the same article, when we draw a comparison between Fourier amplitude spectrum (FAS) and base-to-roof transfer function (TF), we can observe whether or not the dominant frequencies overlapped. If they did, the resonance case indicates that the SSI does not exist. On the contrary, an evident frequency shift is a sign of the existence of SSI. Hence, the modal frequencies should also be identified using TF, which eliminates the effects of the soil.

General literature research was done in order also to know the local soil conditions and related earthquake hazard. Firstly, according to the report published by the Istanbul Metropolitan Municipality for the Fatih district, the soil the mosque exists over can be classified based on the value of V_{S30} (the time-averaged shear-wave velocity within the top 30 m layer of the ground), which is obtained as 350-400 m/sec (Sesetyan et al., 2020). It corresponds to the local soil group ZC (a soil profile may consist of very tight layers of sand, gravel and hard clay or cracked weak rock) in the 2018 Turkish Seismic Code (AFAD, 2018). On the other hand, the predicted earthquake hazard based on PGA-475 is 0.40 g, i.e., the largest ground acceleration for a 475-year recurrence period, which is approximately 0.60 g maximum for Istanbul (AFAD, 2018).

Some crucial findings from the land the mosque erected are given in the study of Evren et al. (2012). They used the ground penetrating radar to investigate the land, and primarily any kind of seismic source was not found. They revealed that the groundwater table level reaches 15 meters from a saturated sand and clay zone. These findings are consistent with the ground profile identified above. Between 700-950 cm, The ground layers under the prayer hall include ruins of a structure that might belong to the Eastern Roman Era. It is assumed that the minarets at the corners have foundations that reach the layer between 816 cm and 958 cm. Furthermore, the same assumption on the foundations of minarets can be made with the findings for the inner courtyard. The upper 4-meter ground of the inner courtyard consists of filling and water pipes between 192-240 cm.

1.5. Rocking

Rocking is a non-linear behaviour that is vastly governed by structural typology and earthquake parameters and hence very sensitive to changes in those (Acikgoz et al., 2012; Barthès, 2012; Yim et al., 1980). In the literature, the rocking behaviour of either a single (monolithic) or multi-block rigid body has been conceptualised by parametric studies and investigated based on several structural typologies. Priestley et al. (1978) express the rocking mechanism for a wall specimen as the state in which the overturning moment exceeds the restoring gravity moment. In their study about the rocking response of a rigid block on a rigid base, Yim et al. (1980) concluded that the sensitivity of the rocking response is proportional to such factors as size and slenderness ratio of the block. They also claimed that the vertical component of the ground motion governs the level of effectiveness of the rocking response. Rocking in slender/tower-type structures, e.g., pillars, minarets, towers, etc., have been evaluated analytically and experimentally as part of seismic response analyses in several studies (Cakti, 2016; Cakti, 2020; Konstantinidis, 2005). Even though rocking may result in overturning for a structure, an abundant number of large scale structures could rock during earthquakes without the danger of overturning (Acikgöz, 2013).

Given its theory, the vertical component of the ground motion governs the level of effectiveness of the rocking response (Yim et al., 1980). Rocking motions can be evaluated by taking vibrational characteristics of a structure into account with an approach out of the box. The state-of-the-art analysis of rocking is taking advantage of structural monitoring, which also allows us to further understand the concept by further evaluating the application of the theory. Safak and Celebi (1991) developed a technique that is based on cross-spectral evaluation of between horizontal (from the output) and vertical (from the input) recordings. If this comparison exhibits a unique dominant frequency other than modal frequencies, rocking vibrations can be isolated using narrow band-pass filtering. Since we have horizontal and vertical vibration recordings from the base (input) and the superstructure (response), reviewing the rocking response of a massive historical structure is worthwhile.

1.6. Organisation of the Thesis

This thesis is divided into six sections and organised as follows: After the introduction giving a brief overview, the second section focuses on the Sultan Ahmet Mosque in three main topics; its history, the mosque as a structure and the records of damages and repairs. In the third section, the methodology is presented: The Sultan Ahmet Mosque SHM system, the earthquake catalogue and the related data processing steps are outlined. The following two sections, the fourth and fifth, are dedicated to the analysis results. The earthquake response characteristics obtained by modal analysis, SSI, dominant frequencies, particle motions and mode shapes are given in the fourth section. Investigation of rocking response is held in the fifth section. Remarks concluding and summarising the entire thesis is provided in the last section, the sixth.

2. THE SULTAN AHMET MOSQUE

2.1. The Mosque within the Historical Context

In the early 17th century, Ahmet I (b. 1590 - d. 1617) began his reign as the fourteenth sultan of the Ottoman Empire after his father, Sultan Mehmed III (b. 1595 - d. 1603). The young sultan had a strong ambition to build a new imperial mosque (Selâtin Camii) into the hearth of the capital, and he gave this critical mission to the chief imperial architect, Sedefkâr Mehmed Agha (b. the 1540s - d.?). Mehmed Agha's intriguing occupational background includes many titles like a guard, an empire officer, a musician, a mother-of-pearl artist (sedefkâr), and finally an architect. When he eventually became the chief imperial architect in 1606, he had spent approximately forty years in education and training on the architecture field (Nayır, 1975). Thus, two leading factors that created this monument were the enthusiasm of Sultan Ahmet I and the skills of Sedefkâr Mehmed Agha as an architect.

The historical conditions that formed the Sultan Ahmet Mosque mainly were related to the Ottoman Empire's long effort to create a new religious identity in Istanbul. After the period between the conquest of Constantinople in the middle of the 15th century and the early 17th century, the construction of the mosque was the last step in the development of this identity for the capital through building imperial mosques that have many prominent examples, such as Fatih (1462-69), Bayezid (1501-06), Sehzade (1543-48), Süleymaniye (1551-57), Valide Sultan (1597-1665). In terms of Ottoman architecture, the mosque was the last significant religious structure of the classical era (Figure 2.1). In choosing land where the complex would be implemented, the sultan and the architect agreed on the area lying along the southern side of the ancient hippodrome and also corresponding to the western façade of Hagia Sophia, which has been an extremely important monument for the city. Hence, the creation process of the mosque was influenced not only by the previous great imperial mosques built in Istanbul but also by its convenient location, making the mosque comparable with Hagia Sophia directly.

Consequently, another massive imperial mosque was going to contribute to the silhouette of the first hill of İstanbul. The construction process of the Sultan Ahmet Mosque started in 1609 fall after buying and demolishing several pasha palaces and buildings which were already in the area. In October of the same year, the excavation process began and proceeded until February 1610 (Nayır, 1975). Soil from the excavation was used to fill the ancient hippodrome, and its ground level was raised by roughly five meters (Müller-Wiener, 2016). After a seven-year intensive construction programme, the first stage of the complex was finally completed, including the mosque, the sultan's pavilion, exterior courtyard walls, and bazaar (arasta). The dome-closing ceremony of the Sultan Ahmet Mosque was held on June 9, 1617 (Rüstem, 2016). The construction of the whole Sultan Ahmet Complex eventually finalised in 1620 with additional buildings.

Figure 2.1. The copper engraving of the Sultan Ahmet Mosque in 1804 by Luigi Mayer. (Mayer, 1810)

2.2. Description of the Structure

The complex of Sultan Ahmet is situated with a layout scattered due to the inappropriate site it was built in the historic peninsula of Istanbul. When completed in 1620, it comprised buildings such as a bazaar (arasta), a hospice (darüşşifa), a madrasah (medrese), a public kitchen (imaret), a public bath (hamam), a primary school (sıbyan mektebi), the sultan's pavilion (hünkar kasrı), the mausoleum of the sultan and the mosque (Figure 2.2). Besides religious usage, Sultan Ahmet Complex also had a public-service mission like other former imperial mosques did. Throughout the thesis, the focused portion of the complex is the mosque, especially the prayer hall.

The unique feature of the mosque arises from its six minarets that appeared for the very first time in Ottoman architecture. Minarets located at four corners of the prayer hall have three balconies each, and two other minarets at the corners of the northern courtyard wall have two balconies. An outer courtyard surrounds the mosque in three directions except for the southern. A U-shaped portico and a last-prayer hall quadratically frame the inner courtyard by thirty small domes, and an ablution fountain is located in the centre of the inner courtyard. The prayer hall and the inner courtyard have roughly the same plan dimensions.

Figure 2.3 exhibits the primary structural system of the mosque in detail. From top to ground, the structural system of the prayer hall is crowned by the main dome reaching 43 m in height, and it is 23,5 m in diameter. The circular area created by four main arches and four pendentives is where the windowed drum (tambour) of the main dome sits on. Four pairs of small buttresses support the drum. Hence, the main dome is symmetrically supported by four pendentives, four main arches, and four semi-domes in each direction. Octagonal and hollow weight towers rise at the joints of the main arches, and a pair of buttresses perpendicular to each other support each tower and main pillar from outward. Three exedras lie under the level of each windowed drum of the eastern, western and northern semi-domes. However, the semi-dome over the qibla wall has only two exedras. Four small corner domes exist in the area between the perpendicular buttresses of each weight tower. Four enormous pillars, also defined as elephant-foot (filayağı) as load-bearing elements, are the source of attention

because of their extraordinary size. Goodwin (2012) criticises this issue and relates it to the engineering-wise incompetence of the chief architect. Nevertheless, this should be further analysed using analytical methods. Thus, from the upper structure to the side walls where buttresses embedded, the upper structure is supported by the elements such as main pillars, buttresses, exedras, secondary arches and secondary colonnade system.

Structural materials used during the construction are as follows: elements constructed by cut-stone units usually made of limestone (küfeki) are minarets, pillars, columns, arches and sidewalls. On the other hand, domes are of brick units and covered by lead (Sayin, 1999; Erdogan et al., 2019). Joists, tie beams and clamps were made of iron (Nayır, 1975). Marmara marble was used for colonnade systems. Also, various kinds of marbles mainly were used for decorative purposes.

The interior of the prayer hall can be defined as a nearly square area inside the sidewalls that has dimensions of 53.50 m by 49.47 m (Nayır, 1975). Three galleries lie all along the three sides, which are northern, eastern and western. The richly coloured Iznik tiles with floral patterns create the aesthetic impact of the interior design of the mosque, and the artistic value of the mosque fundamentally arises from here. Moreover, this is the reason why the mosque is well-known as the Blue Mosque. Other artworks such as muqarnas, decorative pen-works, and Islamic calligraphies receive the secondary concentration of the interior atmosphere.

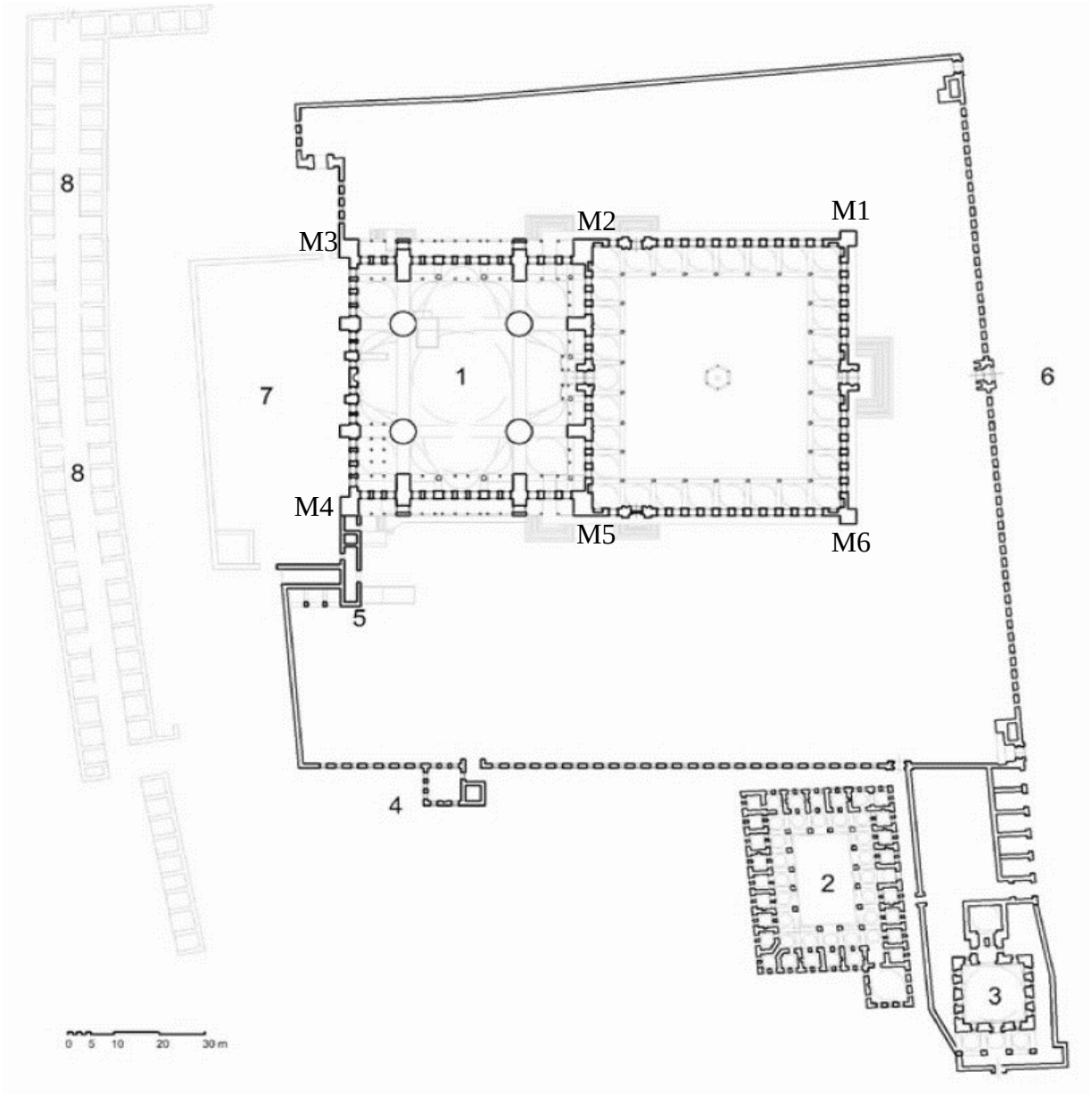

Figure 2.2. Plan view of the Sultan Ahmet Complex: 1) The mosque; 2) Madrasah; 3) Mausoleum of the sultan; 4) Primary school; 5) Sultan's Pavilion; 6) Ancient Hippodrome; 7) Backyard; 8) Bazaar (Arasta), and six minarets (M1-M6) are also shown (Modified from Rüstem, 2016. Drawing: Arben N. Arapi. Courtesy of Gülru Necipoğlu and Ünver Rüstem).

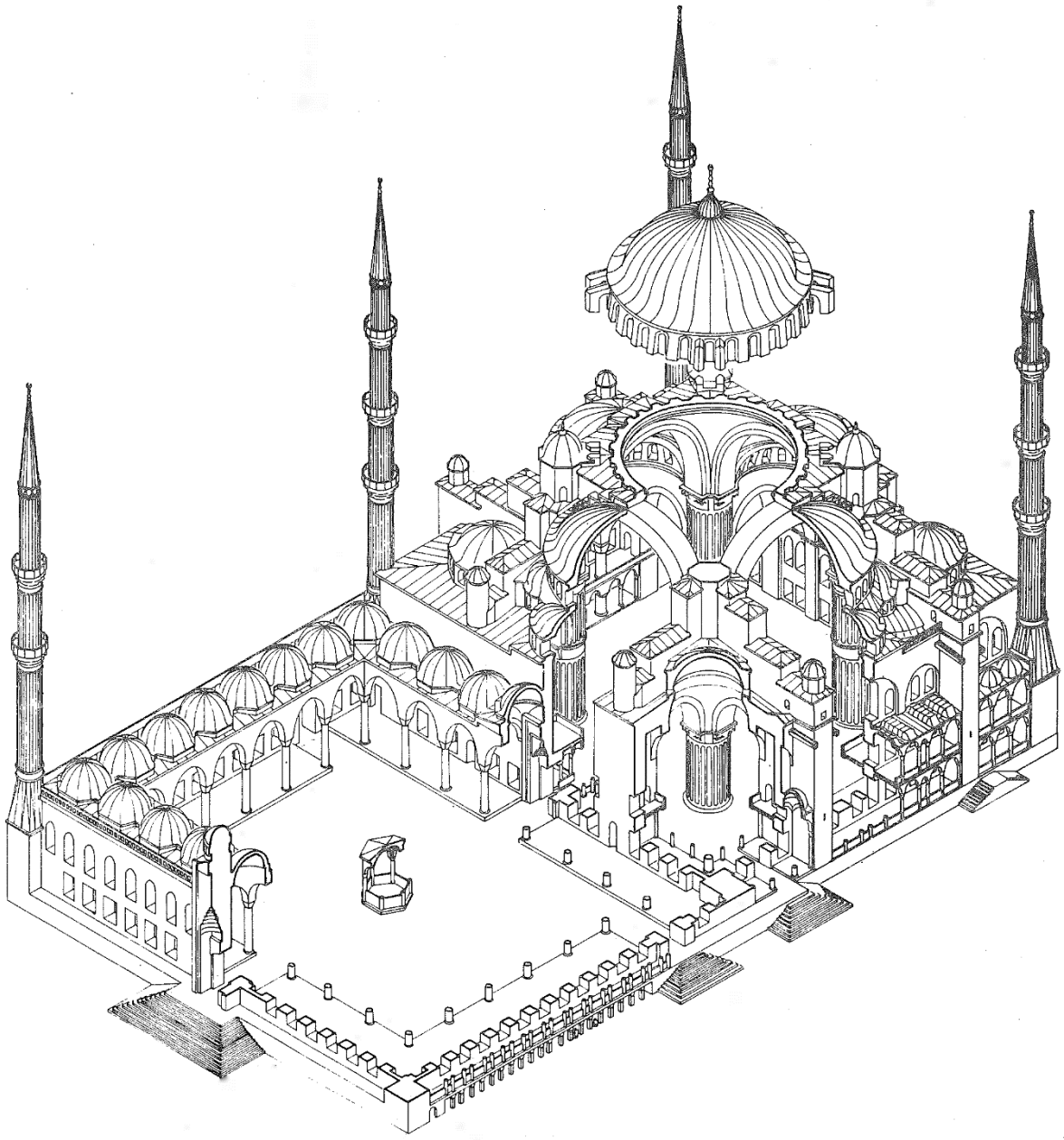

Figure 2.3. Axonometric view of the Sultan Ahmet Mosque (Nayır, 1975. Drawing: Kâni Kuzucular)

2.3. Chronological List of Structural Damages and Repairs for the Mosque

This section aims to demonstrate the recordings of structural damages, and damage-dependent repairs and other applied repairs within the several restoration processes for the Sultan Ahmet Mosque. The list focuses specifically on a portion consisting of the prayer hall and its four minarets and the other two minarets at the corners of the northern courtyard wall. From the point of view presented in Ambraseys and Finkel's study (1991), monuments that have been subjected to a number of destructive earthquakes have partly or wholly survived through a process of natural selection, and they represent today a small sample of the best final design and construction. The mosque experienced many large magnitude earthquakes that occurred in the Marmara region or its surrounding area (Figure 2.4). In this context, the list based on a literature survey has a substantial role in understanding the survival story of the 400-year-old Sultan Ahmet Mosque by investigating the primary supporting system and six minarets.

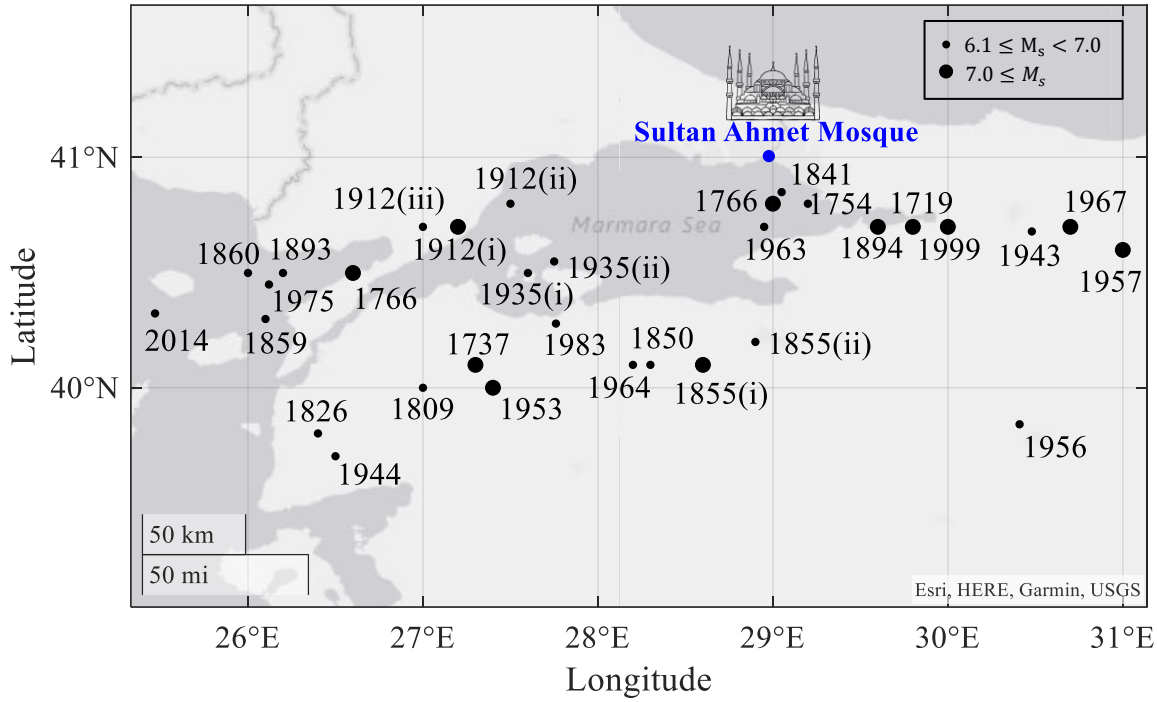

Figure 2.4. Major historical earthquakes with magnitude larger than 6.0 around the Marmara region since the Sultan Ahmet Mosque was constructed; 1617-2014 (Earthquake locations and magnitudes are based on the study of Ambraseys and Jackson (2000). The M_W6.8 2014 Aegean Sea earthquake added afterwards).

When the literature research was done, any information could not be found from the 17th Century. Thus, the list begins with the earliest considerable seismic event, which is in 1766, based on written historical sources.

(i) 18th Century

In this century, earthquakes in 1766 were significant. The May 22, 1766 earthquake, with the estimated epicentre in the Marmara Sea offshore, caused damage to a non-specified minaret (Ambraseys and Finkel, 1991). Further detailed information, such as earthquake-based damage and the resultative repair process completed in 1767, can be gained from Mazlum's book written in light of the Ottoman archival documents. According to this study, the mosque was severely damaged by the May 22 event, and the current amount of damage increased due to the event on August 5. The main dome was slightly damaged during the May 22 event in that there were several cracks then filled with gypsum. The repairs to partial cracks on four semi-domes, exedras, small corner domes, and main arches were also applied. Four massive pillars were restored but not necessitated any strengthening or repair. Additionally, all the six minarets of the mosque were damaged, but most importantly, 'minaret 3' at the southwest corner (as figure 2.2 indicates). Ambraseys (2009) also confirms Mazlum's argument, indicating a fallen minaret. Its upper body part (petek) above the third balcony collapsed over the three small domes of the outer portico below and caused them to collapse, either. Both the upper body part and the three small domes reconstructed. Reconstruction was also reported for the upper body part of 'minaret 2'. In addition to the restored spire (külah) of the 'minaret 1', its finial (alem) was repaired and replaced. On-site repairs were applied to the spire of the 'minaret 6'. Both the finial and the spire of the 'minaret 5' renewed. The last one, 'minaret 4', was in a moderate situation when compared to others.

Other than earthquake damage, it is known that both in the 17th and 18th centuries, the mosque and its complex had been affected slightly by the several citywide fires owing to its separate location, and it is understood that any considerable structural damage did not emerge (Müller-Wiener, 2016).

(ii) 19th Century

The Marmara Sea earthquake on July 10, 1894 was the significant event in the century, and it is stated in the Ottoman archival documents as the reason for some ruined parts of the mosque (Özkılıç, 2015). Finkel and Ambraseys (1997) also reported that the mosque and minarets were damaged due to the event. Mazlum (2011) predicts that restored minarets in the decade were damaged because of the 1894 event; moreover, this conjecture and Figure 2.5 support each other. (Figure 2.5 shows renovation works for the two minarets on the west edge of the prayer hall were proceeding. Although uncertain, the prediction that the photograph belongs to the decade of the 1890s would not be wrong because it is known that restoration for the mosque was held in 1883 (Ordu, 2019). However, the artist signature on the photograph had been used since 1885 (Casaretto, 2019). Consequently, the photograph could be taken while the ongoing restoration after the 1894 event.)

Figure 2.5. The general appearance of the mosque and scaffoldings rising on the top balconies (minarets 2 and 3) in the 1890s (?). Photograph by Sébah & Joaillier (from Fabrizio Casaretto collection).

(iii) 20th Century

Müller-Wiener (2016) indicates that the minaret located in the northeast, the minaret 5, was repaired in 1955. Eyice (1963) adds that the whole minaret defined as *'the minaret at the left corner of the qibla wall'* (estimated as the 'minaret 3' by Mazlum (2011)) reconstructed in 1955. The 'minaret 2' was also repaired in this century. It is also known that none of the six minarets and the mosque itself had any major damage reported due to the devastating 1999 Kocaeli or Duzce earthquakes (Erdogan et al., 2019).

(iv) 21st Century

The mosque overcame the danger of a bombing attack on January 12, 2016 in Sultanahmet Square, and the blast did not cause any visible structural damage. After that, when the earthquake of September 26, 2019 occurred, inner plaster cracks were detected on two peripheral domes of the courtyard. It is indicated that the event was strongly felt by the renovation workers at the minaret 1. Nothing else was detected beyond the given information (Aktas, 2019). The 'minaret 1', having slight instability, was partially renovated between 2014 and 2016. After that, the mosque has been undergoing the most extensive restoration in its history, which began on July 7, 2017 (Figure 2.6). In the structural aspect of this ongoing process, plaster applications made with cement before were detected and scraped on the main dome. Furthermore, the main dome strengthened with a tension ring. Minarets, other than the one reconstructed in 2014, have been overhauling by reconstructing and strengthening (Alyanak, 2019).

Ultimately, knowledge of damages and repairs in the history of the mosque would reflect as strong and weak points in its survival story, which could be helpful to associate those with results gained by structural monitoring. Hence, these clues would be valuable in the evaluation and interpretation of outcomes in this thesis.

Figure 2.6. A look at the ongoing restoration for ‘minaret 3’ and ‘minaret 6’ (December 19, 2019).

3. METHODOLOGY

3.1. The Sultan Ahmet Mosque Structural Health Monitoring System

The Sultan Ahmet Mosque Structural Health Monitoring System has been operating by Boğaziçi University, Kandilli Observatory and Earthquake Research Institute, Department of Earthquake Engineering, Structural Health Monitoring Laboratory since October 2012.

The system consists of three-component accelerometers placed in structurally critical locations that make structural behaviour capable of being investigated. There are ten accelerometer sensors (type: GURALP CMG-5T) monitoring the primary structural system of the Sultan Ahmet Mosque. Each accelerometer has three channels working separately in three directions: horizontal north-south (X) and east-west (Y) components, and the Z component functioning vertically. Thus, thirty acceleration recordings can be collected during an event. These ten sensors were placed at four levels of height, i.e., four sensors at the main dome level (KUB1, 2, 3, 4), four sensors on galleries of each pillar (GAL1, 2, 3, 4), another one at ground level (MUMA) and finally the other at the basement (HAMU). The placement layouts of sensors are displayed in figures Figure 3.1, Figure 3.2 and Figure 3.3.

Since the deployment, the system has recorded many earthquakes with magnitudes varying from 2.1 to 6.6 on Richter's magnitude scale. Additionally, three explosions that occurred in 2016 were recorded by the system (namely: 12 January, Sultanahmet Square; 7 June, Saraçhane Square; 11 December, Dolmabahçe area). Nevertheless, it is known that several interruptions in the real-time recording were happened due to some unexpected technical reasons, especially during the ongoing comprehensive restoration that began in 2017.

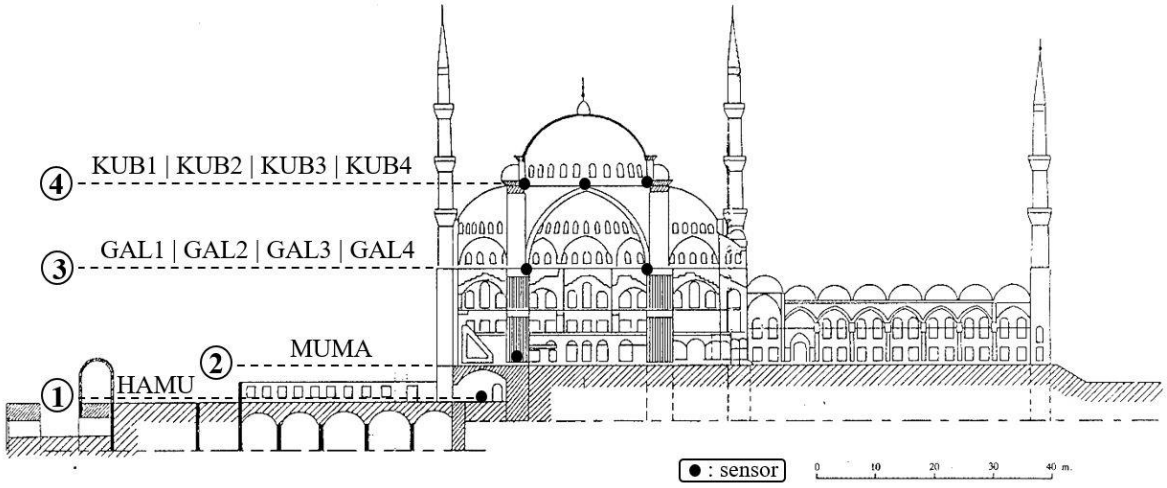

Figure 3.1. The section view from the eastern façade. Sensor groups' layout at four levels of height (Modified from Sayin, 1999).

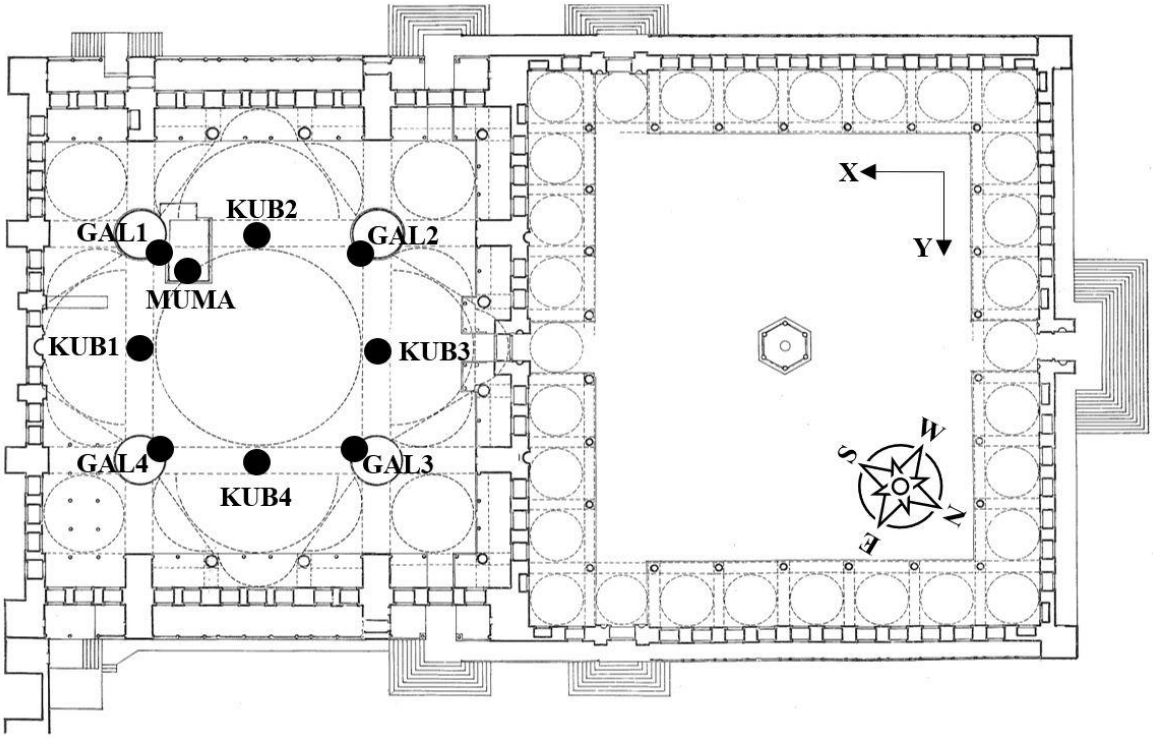

Figure 3.2. Sensors at dome-level, pillar-level and ground-level in the plan view (Modified from Nayır, 1975).

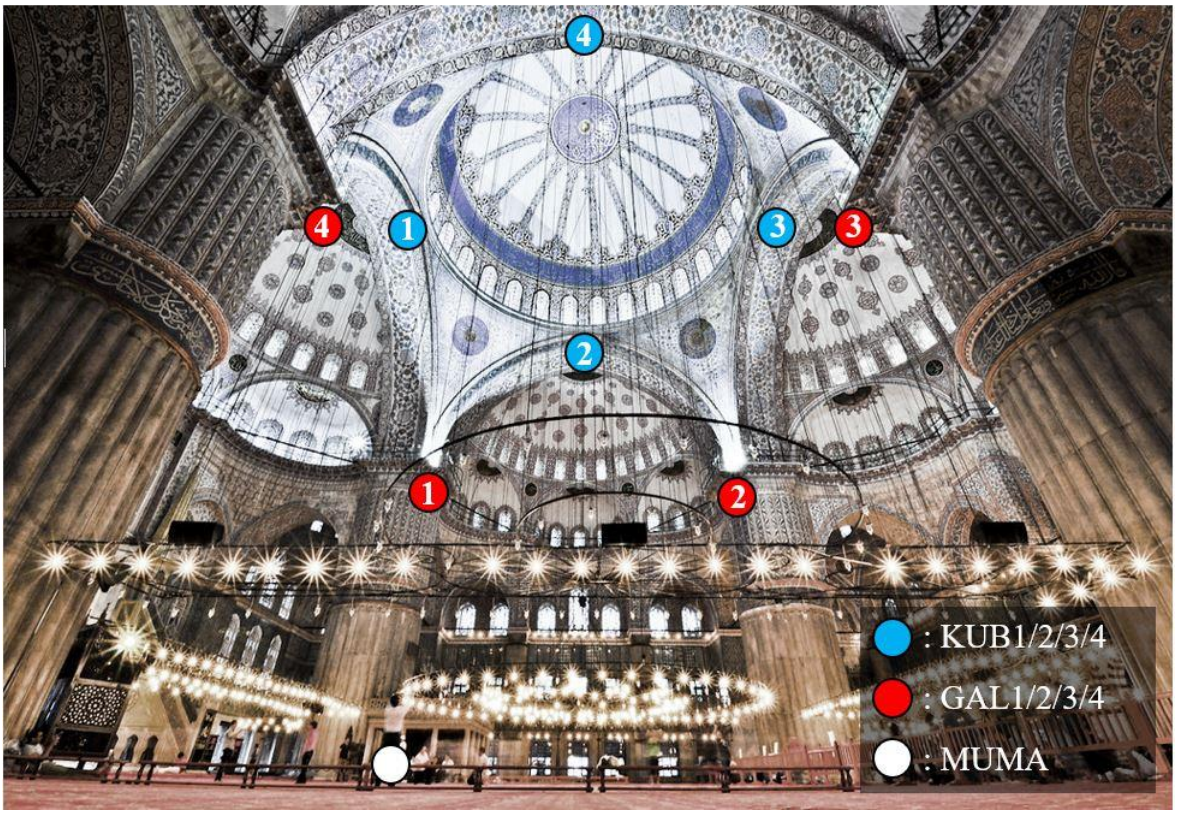

Figure 3.3. The mosque's interior view. The instrumentation layout exhibiting sensors at levels; dome, gallery and ground. (Taken and modified from KayYen's Flickr archive, July 2012)

A crucial operational change made should be highlighted. The sampling frequency was initially at 100 Hz, and then this was changed to 200 Hz in March 2014 (Kafadar, 2020). This change was taken into account throughout the steps of the analysis, and necessary adjustments were made.

3.2. Data Processing

The main approaches and techniques employed to process and analyse the data are explained in this section. The software program used was MATLAB (version R2019b).

In most cases, the collected raw data set for an earthquake is not ready-to-use in that noise-driven unrealistic or misleading results that do not represent the actual response of the

structure could be gathered. Avoiding this is possible when the signal is processed. After examining the Signal-to-Noise ratio (SNR), earthquakes with satisfactory ratios were included in the analyses. In this study, the first step was always the baseline correction of the recordings to remove mean values. Then, datasets were filtered by using 4^{th} order band-pass filters of Butterworth type. These processed acceleration recordings were the basis of the study in that they were used for both time-domain and frequency-domain analyses. In the time domain, acceleration recordings were integrated once to velocities and twice to displacements to gather their time histories. The maximum absolute values of each component (typically, 30 recordings for each earthquake) were obtained. Recorded signals in the time domain were transformed into frequency-domain data through the Fourier method. Transformed data were smoothed with a predetermined window length. In subsections from 3.2.1 to 3.2.4, the fundamental steps given above are explained in detail.

3.2.1. Signal Quality

The fundamental approach for SNR examination was checking the square root of the ratio of signal + noise window to the noise window. Acceleration recordings evaluated within specific time windows varying from 3 seconds to 6 seconds as manually identified integers proportional to the earthquake duration, magnitude and distance. Two inputs are the numerator as windowed signal + noise and the denominator as windowed noise. The noise portion was selected from the pre-event. On the other hand, the noise included signal portion has been beginning at the s-wave arrival time, which is inevitably picked as a consequence of manual reviews. When the whole dataset was evaluated through SNR examination, the obtained signal-to-noise ratios from HAMU and MUMA sensors were dramatically low as a most common observation. This observation can be predicated on the whereabouts of these two sensors since they are functioning on ground-level (MUMA), where the sensor is directly open to environmental noise, and basement-level (HAMU). Another common and expected observation was that the SNR levels for up-down components were significantly lower than for horizontal counterparts.

3.2.2. Filtering

The band-pass filtering technique provides a basis for examining the vibration recording within a specific frequency range, and it should be determined as an earthquake-specific tool. In order to keep the phase content of the original signal as it is, either zero-phase filters or forward-backward double filtering technique needed to be used (Safak and Cakti, 2014). In our case, 4^{th} order Butterworth type filters were applied, i.e., the recordings were filtered first forward and then backwards. The low-pass frequency was selected as 25 Hz as a constant for each earthquake. There are several rules to consider while choosing that range appropriately. The high-pass frequency can be suitably obtained after investigating displacement-time history series, which is more able to reflect noise-induced errors since it is a double-integrated version of acceleration. In this context, one of the five main high-pass filtering frequencies (0.1-0.5 Hz) was selected after a component-by-component examination of acceleration/velocity/displacement-time histories to avoid common errors, such as erroneous baselines, spikes or any unreliable physical values in the series. Whether or not displacement time histories were satisfactory was visually checked. It is a considered and also an observed relation that main earthquake-based properties, i.e., earthquake magnitude, epicentral distance, and acceleration levels observed at the sensors, may govern the necessitated high-pass filter. It can be said based on an empirical observation that the high-pass frequency value was inversely proportional to magnitude and acceleration levels; on the contrary, it is proportional to the epicentral distance. After all, with a constant low-pass filter of 25 Hz, 0.1 Hz of an initial value for high-pass frequency is set. It is increased up to 0.5 Hz as long as the recordings of an event are required.

3.2.3. Transform into the Frequency Domain

Baseline corrected and filtered recordings in the time domain were represented in the frequency domain with discrete Fourier transforms. Obtained FAS and TF, i.e., Fourier-based spectral ratios, smoothed as they were necessitated. Modal frequencies can finally be identified by investigating amplitude peaks in spectra, and this manual visual-check technique is peak-picking. By using FAS and TF, we can identify the presence of SSI, as in

subsection 4.2.2. Accordingly, whether the SSI is consistent, we can decide that modal frequencies of the structure are represented by either FAS or TF. In our case, TF is more reliable due to the SSI consistency, so TF-based modal frequencies and their corresponding shapes eventually can be gained, as in subsection 4.2.3. Consequently, the rocking frequency of rigid-body vibrations, i.e., rocking vibrations, can also be evaluated by comparing the horizontal components of output with the vertical components of input in the frequency domain, as in the 5th section.

3.2.4. Smoothing

Noise-induced spectral errors can be minimised by smoothing the content in the frequency domain. To properly achieve this, the optimum smoothing window length should be selected. In our case, the approach Safak proposed in 1997 was carried out based on two main assumptions. The first is that the noise in the signals is of additive type and uncorrelated with signals, and the second is that the true amplification is a smooth function of frequency (Safak, 1997). Thus, the change of the area under the Fourier-amplitudes squared was evaluated with increasing smoothing window lengths (odd numbers between 3 and 41). The optimum window length can be defined as a point where the line extension of the initial linear part of the curve intersects with the line extension of the curve that becomes linear again. In other words, it is where the change rate of the curve slowed down. It should be noted that, in such cases that the optimum window length cannot smooth the spectrum, smoothing window length carefully increased.

3.3. Earthquake Catalogue of the Sultan Ahmet Mosque

The Sultan Ahmet Mosque SHM system has been producing an earthquake database since October 2012. A final catalogue of this database consisting of more than 100 seismic events is generated in order to decide on main seismic events that could be used in modal analysis. Furthermore, the entire catalogue plays a role statistically, i.e., magnitude, epicentral distance and azimuth histograms, and scatterplots for sensor-by-sensor evaluation of

acceleration, velocity and displacement peak values. Scatterplots concerning M_W and ground-level strong excitations are also created. Long story short, all these allow us to see the big picture during the mosque's eight-year recording history (October 2012 – 2020).

The catalogue was initially consisting of 209 earthquakes with local magnitudes varying from 2.1 to 6.5 and with epicentral distances between 13.5 km the nearest and 947.4 km the farthest. After performing a selection procedure, the ultimate version of the catalogue was created. Generally, this procedure is based on earthquake usability, which is related to the signal quality (signal-to-noise ratio, SNR), the method of which is explained in subsection 3.2.1, and to the event record-status, i.e., whether or not the event was recorded by all KUB or GAL sensors. The first criterion of the selection procedure was the event record status. Seismic events that all the sensors had properly recorded took account in the next step: assessing the SNR level, and others were excluded (54 events). Secondly, if any channel rates a lower SNR than 5, the related earthquake was excluded from the catalogue (51 events). However, if outstanding accelerations observed during the earthquake, the event got involved for analyses without considering this criterion.

Another criterion was the epicentral distance of the event; it is limited to 350 km in that three distance away events excluded. On the other hand, no criterion was applied related to the earthquake magnitude. From late 2020, two earthquakes (24.09.2020 M_W4.1 Marmara Sea and 30.10.2020 M_W6.9 Aegean Sea) were included in the catalogue since they are of particular importance with their magnitudes and acceleration levels observed at the mosque. The catalogue was completed with 103 earthquakes overall.

The last step was the conversion of local magnitudes into moment magnitudes. Most of the moment magnitudes replaced with local magnitudes were taken from the KOERI's earthquake catalogue (BOUN-KOERI, 2021). The rest was converted by using a relationship, which is $M_W = (2/3)M_L + 1.15$, generated based on earthquakes from the Alto Tiberina fault area (Munafò et al., 2016). Most of the catalogue, about 80%, consists of earthquakes in the range of 3.0-4.9. While earthquakes with $M_W \geq 6.0$ are rare (approximately 3%), M_W2.0-2.9 and M_W5.0-5.9 rated about 10% and 7%, respectively.

As it is displayed in figures Figure 3.4 and Figure 3.5, a sufficient final catalogue was gained. According to this distribution map and histogram, a specific magnitude range was only limited within a particular distance. While distance-far earthquakes were mostly $M_W \geq 4.5$, minor and/or light earthquakes were recorded if the event takes place within a limited distance. For instance, earthquakes with $M_W \leq 2.9$ were found only in an area framed around the Marmara Sea. The sensitivity of the recording system is hence evident.

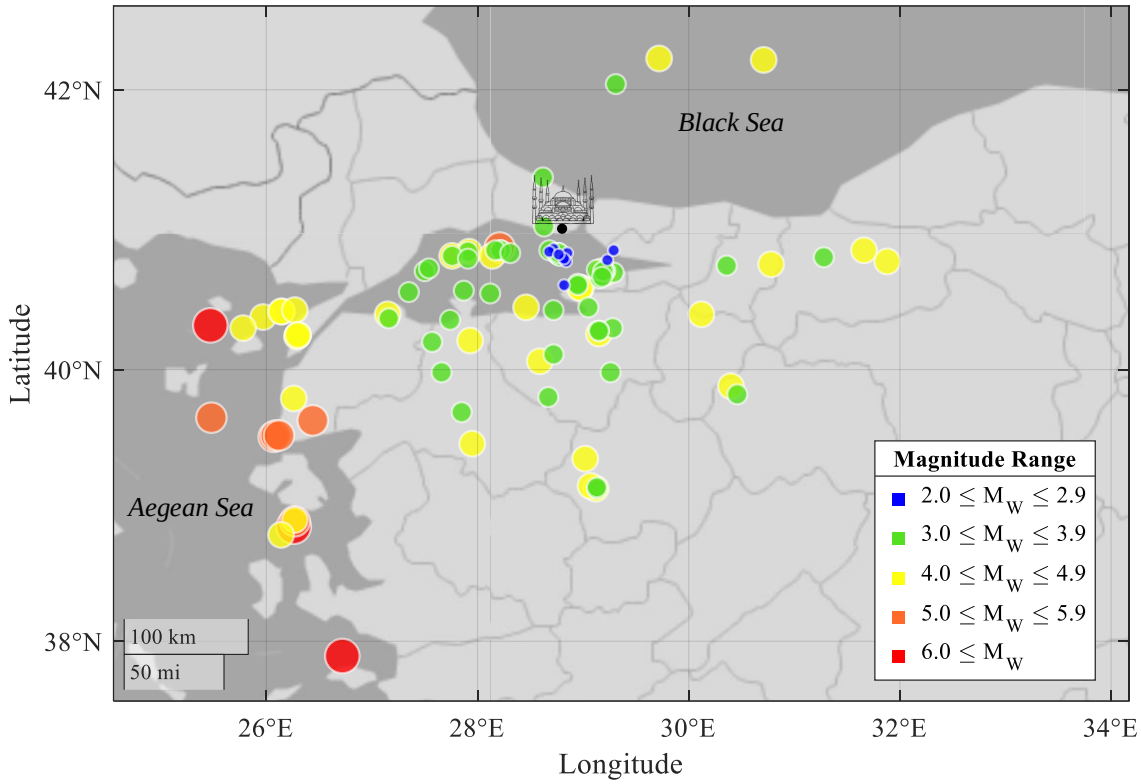

Figure 3.4. Locations of earthquakes in the catalogue.

Arrival directions of earthquakes to the mosque were indicated with azimuthal property in Figure 3.6. Considering the mosque as the centre, a majority of events occurred between the degrees 180º and 270°, which corresponds to the portion between the general south and west (67 events). Approximately 30% of the events occurred in the quarter between 90º and 180°, corresponding to the southeast portion of the mosque. On the other hand, a far fewer number of earthquakes originated from northerly, north-easterly and north-westerly to the mosque (only five events). It should be highlighted that the sensor direction X acts through southeast-northwest directions while direction Y does southwest-northeast.

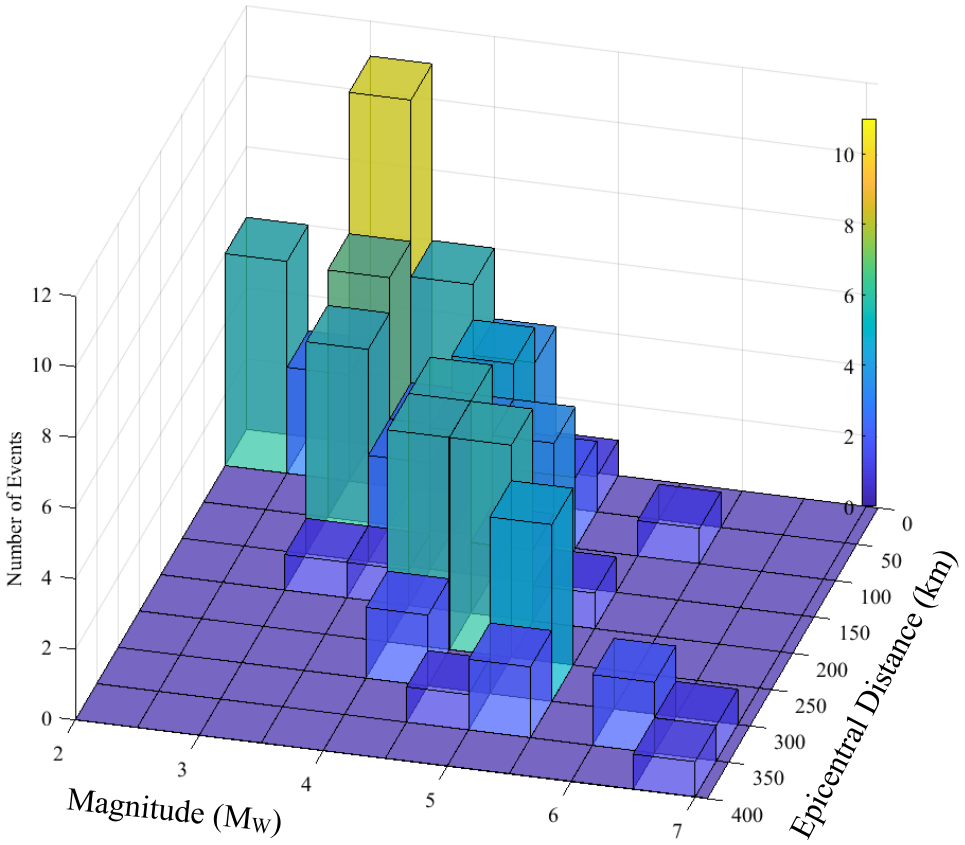

Figure 3.5. Bivariate 3D coloured histogram of magnitude and epicentral distance.

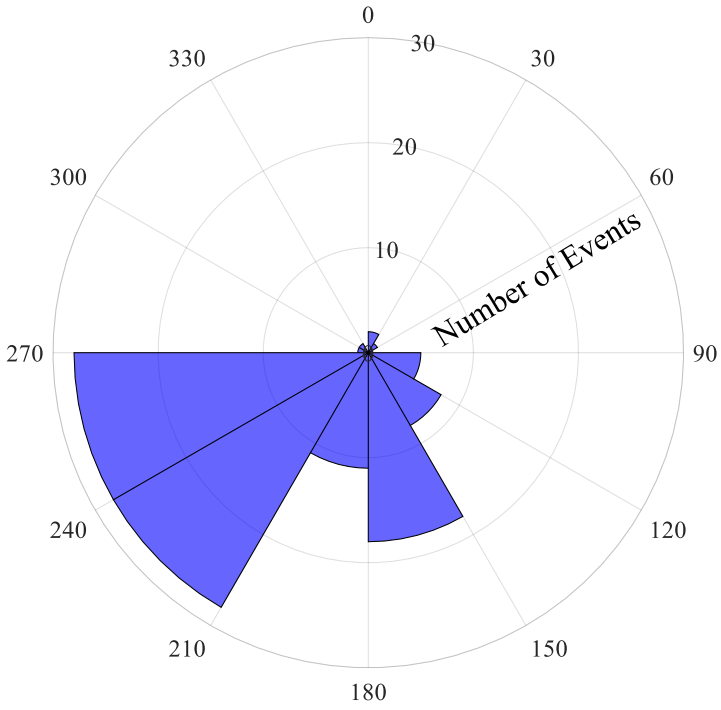

Figure 3.6. Azimuthal polar rose diagram of earthquakes.

The final catalogue is exhibited chronologically in tables from Table 3.1 to Table 3.4. In this list, eight significant events with the highest acceleration amplitudes indicated between the star icons, all of which are fundamentals for the analyses. Foundation-level peak ground accelerations of three components are provided based on basement-level sensor HAMU. Instead, ground-level sensor MUMA is given if the HAMU did not record the earthquake, and these values are highlighted in red.

Table 3.1. Earthquakes recorded by the Sultan Ahmet Mosque SHM system (Oct 2012 – Jul 2014).

NO	Event Date (dd.mm.yyyy)	Local Time (hh:mm:ss)	Coordinates		Depth (km)	Epicentral Location	Magnitude (M_W)	Distance (km)	Azimuth (degree)	Acceleration (cm/sec^2)		
			Lon	Lat						X	Y	Z
1	19.10.2012	11:17:24	28.63	41.03	13.20	Buyukcekmece (Istanbul)	3.7	29.65	275.48	0.829	1.063	0.724
2	26.10.2012	06:37:36	28.72	40.43	7.60	Gulf of Gemlik	3.8	67.99	198.77	0.115	0.117	0.063
3	30.10.2012	02:12:35	29.13	39.13	10.70	Simav (Kutahya)	3.8	209.38	176.37	0.048	0.032	0.013
4	8.01.2013	16:16:06	25.48	39.65	8.40	★Aegean Sea★	5.7	332.45	244.19	1.946	2.279	0.808
5	22.02.2013	05:07:58	29.26	39.98	6.50	Keles (Bursa)	3.4	117.01	168.05	0.033	0.030	0.034
6	9.04.2013	14:42:23	28.12	40.55	5.00	Balikesir Offshore	3.4	87.60	235.22	0.099	0.092	0.072
7	11.04.2013	00:40:29	29.28	40.30	5.40	Gursu (Bursa)	3	82.41	161.84	0.036	0.023	0.019
8	23.04.2013	18:19:56	30.36	40.75	6.30	Serdivan (Sakarya)	3.3	119.72	103.27	0.054	0.037	0.033
9	5.06.2013	16:03:16	27.57	40.20	8.00	Gonen (Balikesir)	3.4	148.67	233.44	0.070	0.069	0.025
10	12.07.2013	03:36:57	25.97	40.38	13.20	Gulf of Saros	4.2	263.14	255.64	0.066	0.056	0.021
11	30.07.2013	08:33:08	25.78	40.30	9.80	Gokceada (Canakkale)	4.9	280.69	254.83	0.443	0.585	0.162
12	3.10.2013	13:26:07	28.72	40.11	2.30	Nilufer (Bursa)	3.6	101.51	192.38	0.088	0.057	0.042
13	3.11.2013	12:46:38	27.16	40.37	5.80	Biga (Canakkale)	3.3	168.40	245.83	0.032	0.028	0.013
14	24.11.2013	22:49:37	31.88	40.78	8.00	Ulumescit (Bolu)	4.6	244.91	94.91	0.138	0.120	0.054
15	27.11.2013	06:13:37	27.92	40.85	9.60	Tekirdag Offshore	4.6	90.44	259.33	0.628	0.681	0.456
16	27.11.2013	06:21:35	27.91	40.85	7.40	Tekirdag Offshore	3.8	91.13	259.44	0.259	0.341	0.142
17	10.01.2014	09:20:46	27.95	39.46	10.30	Akcakoy (Balıkesir)	4.1	192.79	207.23	0.102	0.100	0.030
18	21.01.2014	03:34:03	29.23	40.79	5.30	Tuzla (Istanbul)	2.9	31.92	138.30	0.081	0.038	0.069
19	5.02.2014	03:56:43	28.62	41.38	16.00	Arnavutkoy (Istanbul)	3.8	50.86	324.49	0.935	0.492	0.620
20	7.04.2014	04:25:45	28.72	40.87	20.70	Avcilar (Istanbul)	2.8	26.22	235.17	0.028	0.024	0.088
21	17.04.2014	12:55:27	27.76	40.82	11.10	Marmara Sea	3.3	104.03	259.00	0.035	0.037	0.027
22	24.05.2014	12:25:01	25.47	40.32	23.30	★Aegean Sea★	6.8	305.41	256.70	7.896	7.501	2.231
23	25.05.2014	14:38:38	26.15	40.42	13.00	Gulf of Saros	4.9	246.83	255.64	0.542	0.583	0.167
24	28.05.2014	06:59:51	26.14	40.42	13.30	Gulf of Saros	4.3	247.73	255.70	0.146	0.124	0.030
25	3.07.2014	08:04:46	27.93	40.21	12.10	Lake Manyas	4.3	125.27	225.32	0.468	0.648	0.233
26	10.07.2014	02:45:02	26.27	40.43	14.90	Gulf of Saros	4.0	237.23	255.22	0.048	0.064	0.021

Table 3.2. Earthquakes recorded by the Sultan Ahmet Mosque SHM system (Oct 2014 – Sep 2015).

NO	Event Date (dd.mm.yyyy)	Local Time (hh:mm:ss)	Coordinates		Depth (km)	Epicentral Location	Magnitude (M_W)	Distance (km)	Azimuth (degree)	Acceleration (cm/sec^2)		
			Lon	Lat						X	Y	Z
27	22.10.2014	20:11:05	30.12	40.40	7.60	Geyve (Sakarya)	4.5	117.17	124.56	0.794	0.525	0.230
28	28.11.2014	04:30:06	29.02	39.35	5.30	Simav (Kutahya)	4.6	183.97	178.84	0.179	0.157	0.048
29	6.12.2014	03:45:06	26.27	38.89	12.40	Aegean Sea	5.1	328.99	225.33	0.257	0.232	0.081
30	6.12.2014	08:20:53	26.27	38.90	13.40	Aegean Sea	4.9	329.07	225.46	0.147	0.195	0.050
31	20.12.2014	00:56:00	28.82	40.81	5.40	Marmara Sea	2.7	25.21	211.29	0.027	0.046	0.020
32	24.12.2014	02:21:18	27.74	40.36	6.90	Erdek Gulf	3.3	126.23	235.87	0.043	0.048	0.016
33	30.12.2014	01:25:59	28.85	40.84	10.90	Marmara Sea	2.7	20.79	210.12	0.049	0.035	0.025
34	17.01.2015	02:42:34	30.40	39.88	5.50	Tepebasi (Eskisehir)	4.2	173.02	135.63	0.078	0.068	0.033
35	19.01.2015	13:10:43	28.68	40.86	16.00	Marmara Sea	3.2	29.52	237.14	0.097	0.103	0.208
36	23.01.2015	12:19:42	28.59	40.06	5.00	Mustafakemalpasa (Bursa)	4.2	109.67	197.40	0.861	0.626	0.115
37	1.02.2015	12:46:31	27.50	40.71	6.00	Tekirdag Offshore	3.4	128.61	255.67	0.067	0.052	0.032
38	6.02.2015	01:41:22	29.16	40.66	11.60	Cinarcik (Yalova)	3	41.19	158.07	0.178	0.101	0.108
39	6.02.2015	13:32:10	29.13	40.72	9.80	Cinarcik (Yalova)	3	34.54	157.85	0.265	0.184	0.093
40	22.03.2015	21:48:21	28.68	40.85	8.10	Marmara Sea	2.7	30.58	235.38	0.044	0.039	0.031
41	29.04.2015	07:40:53	29.31	42.04	14.10	Black Sea	3.9	118.22	13.45	0.287	0.293	0.344
42	20.05.2015	01:47:16	28.84	40.78	5.40	Marmara Sea	2.9	27.53	204.69	0.082	0.087	0.057
43	20.05.2015	03:14:10	28.82	40.80	6.80	Marmara Sea	2.7	26.64	210.04	0.036	0.028	0.027
44	3.07.2015	01:22:26	27.85	39.69	5.40	Kabakdere (Balikesir)	3.8	174.99	213.50	0.124	0.081	0.020
45	7.07.2015	08:08:29	31.28	40.81	5.00	Yesilcam (Duzce)	3.7	194.63	95.65	0.073	0.083	0.032
46	24.07.2015	04:26:00	26.30	40.25	11.60	Eceabat (Canakkale)	4.1	241.30	250.48	0.126	0.086	0.036
47	24.07.2015	05:39:42	26.29	40.24	10.50	Eceabat (Canakkale)	4.8	242.16	250.31	0.261	0.183	0.076
48	24.07.2015	09:54:09	26.30	40.25	11.30	Eceabat (Canakkale)	4.2	240.73	250.48	0.115	0.118	0.040
49	13.08.2015	04:01:28	29.29	40.70	10.60	Yalova Offshore	3.7	43.14	142.10	0.870	0.670	0.275
50	3.09.2015	11:23:19	29.12	39.13	10.90	Simav (Kutahya)	4.0	208.84	176.61	0.077	0.044	0.023
51	10.09.2015	11:12:45	26.14	38.79	5.00	Chios Island	4.7	345.38	225.41	0.237	0.162	0.040
52	19.09.2015	01:30:28	30.46	39.82	5.40	Tepebasi (Eskisehir)	3.7	182.40	135.91	0.066	0.070	0.027

Table 3.3. Earthquakes recorded by the Sultan Ahmet Mosque SHM system (Sep 2015 – Sep 2016).

NO	Event Date (dd.mm.yyyy)	Local Time (hh:mm:ss)	Coordinates		Depth (km)	Epicentral Location	Magnitude (M_W)	Distance (km)	Azimuth (degree)	Acceleration (cm/sec^2)		
			Lon	Lat						X	Y	Z
53	22.09.2015	09:25:04	29.13	39.14	10.10	Simav (Kutahya)	3.7	207.67	176.35	0.106	0.065	0.030
54	14.10.2015	02:18:10	29.07	39.15	4.60	Simav (Kutahya)	4.2	206.37	177.77	0.088	0.079	0.030
55	26.10.2015	23:07:59	26.26	39.79	6.00	Ezine (Canakkale)	4.6	267.08	240.45	0.114	0.110	0.021
56	28.10.2015	19:20:02	27.76	40.82	12.70	Marmara Sea	4.3	103.90	259.00	0.664	0.425	0.294
57	16.11.2015	17:45:43	28.76	40.83	7.70	★Marmara Sea★	3.9	27.09	223.12	1.234	2.332	0.513
58	16.11.2015	18:36:24	28.76	40.84	11.10	Marmara Sea	3.2	26.34	224.79	0.164	0.214	0.278
59	16.11.2015	19:04:12	28.77	40.83	14.40	Marmara Sea	3.4	26.03	221.77	0.216	0.243	0.164
60	16.11.2015	19:20:15	28.77	40.83	10.70	Marmara Sea	2.8	26.74	221.77	0.051	0.064	0.082
61	17.11.2015	06:36:23	28.75	40.84	6.80	Marmara Sea	3.1	26.60	226.09	0.238	0.391	0.303
62	18.11.2015	14:52:11	28.78	40.82	9.20	Marmara Sea	3.1	26.46	218.80	0.125	0.148	0.247
63	5.12.2015	22:53:51	29.05	40.45	4.30	Gulf of Gemlik	3.6	62.33	174.27	0.149	0.120	0.127
64	15.12.2015	03:13:38	29.72	42.22	10.20	Black Sea	4.0	148.10	24.34	0.402	0.214	0.163
65	11.02.2016	03:53:24	27.35	40.56	7.10	Tekirdag Offshore	3.4	145.75	250.65	0.046	0.043	0.024
66	28.03.2016	20:23:46	27.54	40.73	6.20	Marmara Sea	3.7	124.50	256.25	0.187	0.132	0.042
67	1.06.2016	00:14:10	28.22	40.86	13.20	Silivri Offshore (Istanbul)	3.3	65.84	255.98	0.091	0.108	0.048
68	7.06.2016	07:09:45	29.15	40.26	11.50	★Kazikli-Gürsu (Bursa)★	4.3	83.81	169.94	2.145	0.927	0.675
69	7.06.2016	11:02:15	29.15	40.28	5.20	Osmangazi (Bursa)	3.6	81.91	169.67	0.140	0.068	0.048
70	7.06.2016	11:05:11	29.15	40.28	5.20	Osmangazi (Bursa)	3.4	81.83	169.67	0.081	0.043	0.040
71	10.06.2016	00:08:58	29.29	40.86	5.40	Pendik (Istanbul)	2.7	30.93	121.47	0.062	0.053	0.122
72	15.06.2016	08:20:57	28.22	40.86	8.90	Silivri Offshore (Istanbul)	3.3	65.54	255.98	0.082	0.119	0.048
73	23.06.2016	02:35:59	29.21	40.71	9.90	Yalova Offshore	3.7	38.74	149.08	0.439	0.336	0.258
74	25.06.2016	08:40:11	29.21	40.70	6.80	★Yalova Offshore★	4.4	39.11	149.91	1.883	2.046	0.761
75	9.07.2016	17:20:51	29.20	40.71	6.80	Yalova Offshore	3.8	38.10	150.18	0.210	0.158	0.119
76	9.07.2016	20:28:19	29.19	40.71	11.30	Yalova Offshore	3.4	37.85	151.30	0.296	0.251	0.228
77	17.07.2016	11:55:41	29.18	40.71	7.40	Yalova Offshore	4.1	36.85	152.45	1.657	1.023	0.339
78	30.09.2016	07:40:05	28.77	40.84	9.30	Marmara Sea	3.1	25.63	223.44	0.188	0.339	0.108

Table 3.4. Earthquakes recorded by the Sultan Ahmet Mosque SHM system (Sep 2016 – Oct 2020).

NO	Event Date (dd.mm.yyyy)	Local Time (hh:mm:ss)	Coordinates		Depth (km)	Epicentral Location	Magnitude (M_W)	Distance (km)	Azimuth (degree)	Acceleration (cm/sec^2)		
			Lon	Lat						X	Y	Z
79	30.09.2016	17:09:43	29.18	40.67	4.50	Cinarcik (Yalova)	3.6	41.49	155.31	0.898	0.587	0.236
80	9.10.2016	02:02:46	28.95	40.62	5.60	Cinarcik (Yalova)	3.7	43.46	183.02	0.496	0.261	0.084
81	12.10.2016	02:42:43	28.95	40.61	5.40	Cinarcik (Yalova)	3.4	44.00	182.95	0.119	0.073	0.035
82	15.10.2016	11:18:32	30.71	42.21	11.40	Black Sea	4.8	196.66	46.52	0.805	0.901	0.239
83	25.10.2016	00:04:47	28.67	39.80	8.00	Mustafakemalpasa (Bursa)	3.9	137.07	191.07	0.103	0.101	0.071
84	20.12.2016	15:06:17	28.17	40.86	2.60	Marmara Sea	3.3	70.02	256.85	0.074	0.060	0.050
85	6.02.2016	13:58:00	26.07	39.51	6.80	Ayvacık (Canakkale)	5.1	297.13	236.96	0.351	0.370	0.113
86	7.02.2016	05:24:02	26.09	39.52	5.00	Ayvacık (Canakkale)	5.2	295.52	236.95	0.369	0.532	0.122
87	12.02.2016	16:48:15	26.12	39.52	11.10	Ayvacık (Canakkale)	5.2	293.73	236.66	0.471	0.494	0.112
88	8.03.2017	23:09:58	27.66	39.98	7.00	Gonen (Balikesir)	3.8	159.84	224.75	0.331	0.243	0.082
89	11.04.2017	20:27:51	28.31	40.84	6.60	Marmara Sea	3.2	59.15	252.04	0.177	0.191	0.185
90	12.06.2017	15:28:38	26.26	38.85	20.70	★Aegean Sea★	6.1	333.30	224.91	1.513	1.554	0.567
91	31.12.2017	23:12:02	27.87	40.57	12.40	Erdek Offshore (Balikesir)	3.8	105.59	242.91	0.381	0.430	0.419
92	8.04.2018	00:16:31	31.66	40.86	5.80	Yesilcele (Bolu)	4.6	226.17	93.22	0.221	0.263	0.087
93	7.07.2018	01:06:51	28.82	40.61	8.70	Yalova Offshore	2.7	46.13	196.76	0.086	0.049	0.055
94	30.11.2018	05:36:34	28.98	40.59	6.90	★Cinarcik (Yalova)★	4.0	46.06	179.66	1.484	1.735	0.652
95	20.12.2018	06:34:24	28.97	40.59	12.47	Cinarcik (Yalova)	4.4	45.77	180.71	1.097	0.993	0.517
96	15.02.2019	19:14:27	27.91	40.80	8.90	Marmara Sea	3.8	92.72	256.06	0.311	0.435	0.220
97	20.02.2019	00:33:54	27.15	40.40	9.00	Biga (Canakkale)	4.1	168.15	246.99	0.083	0.084	0.053
98	20.02.2019	21:23:27	26.44	39.63	7.60	Ayvacık (Canakkale)	5.0	264.24	235.41	0.696	0.798	0.295
99	5.03.2019	00:07:27	28.46	40.45	11.30	Bayramdere Offshore	4.0	75.84	215.36	0.168	0.133	0.121
100	2.06.2019	16:08:47	30.78	40.76	9.50	Hendek (Sakarya)	4.4	153.66	99.61	0.714	0.653	0.184
101	26.09.2019	13:59:24	28.21	40.88	12.30	★Silivri Offshore★	5.7	65.88	258.04	22.18	47.85	14.75
102	24.09.2020	16:38:31	28.14	40.82	14.4	Marmara Sea	4.1	73.27	253.93	3.107	3.305	1.240
103	30.10.2020	14:51:24	26.72	37.89	13.1	Aegean Sea	6.9	396.89	209.94	0.730	1.173	0.433

4. DYNAMIC RESPONSE CHARACTERISTICS

In this section, the response of the mosque to 103 earthquakes in the final catalogue is analysed and assessed in time and frequency domains distinctively.

Dynamic response of the mosque, i.e., prayer hall, in the literature are compiled in three main works. The first systematic study on the response investigation for the Sultan Ahmet Mosque was carried out in 1999 by Sayin. In performed analytical (finite element model) and experimental (ambient vibration tests) models, the first two natural frequencies of the corresponding modes identified as 1.84 Hz and 2 Hz from the numerical model, and the experimental one resulted in 1.83 Hz and 1.93 Hz for the first two modes, respectively. In the analytical model, it is indicated that the author had to make assumptions due to the limited technical and geometrical information, e.g., uncertainties about the dimensions of elements. However, the entire primary structural system was modelled and involved in the analysis, and there is an acceptable consistency of dominant frequencies between models, i.e., analytical and experimental. The outcomes hence are worth mentioning. The finite element model of the mosque was evaluated statically and dynamically. In the former, it was found out that the mosque is under-stressed. The latter, dynamic analysis, gives the first five modal frequencies and corresponding shapes: 1. Translational (1.84 Hz), 2. Translational (2 Hz), 3. Squeezing (2.17 Hz), 4. Squeezing (2.88 Hz) and 5. Breathing (3.05 Hz). It should be noted that the author could not obtain modes other than the first two from the ambient vibration survey.

As mentioned previously, the Sultan Ahmet Mosque SHM system recorded three explosions that occurred in 2016. This unique dataset was evaluated in a paper by Yenihayat and Çaktı (2017). In addition to the dynamic response investigation of explosion records, authors also reported results for a specific earthquake, which is M_W6.8 Aegean Sea (Gökçeada) event in 2016 and the obtained FAS results are 2.31 Hz (X-direction) for the 1st mode and 2.46 Hz (Y-direction) for the 2nd mode.

The latest study examining the relationship between frequency and environmental effects was carried out by Dar and Cakti (2018). The authors analysed long-term vibration recordings and revealed a low correlation between the first two modal frequencies and air temperature. Also, it was comprehended that humidity ratio and atmospheric pressure reversely and partially influence the frequencies. Other atmospheric actions, such as precipitation, soil temperature and wind, have no frequency-domain impact on the structure.

4.1. Time-Domain Analyses

Fundamental three quantities, i.e., acceleration, velocity and displacement, of earthquake recordings are assessed in the time domain. Sensor-by-sensor evaluation of three types of histories is held by obtaining maximum absolute values recorded in each sensor component. Time histories belonging to selected three earthquakes (two events with the largest amplitudes and an additional moderate magnitude event) are instanced in figures between 4.1 to 4.9. Acceleration- (Figure 4.1/Figure 4.4/Figure 4.7), velocity- (Figure 4.2/Figure 4.5/Figure 4.8) and displacement-time (Figure Figure 4.3/Figure 4.6/Figure 4.9) histories of these events are selected.

Among recorded acceleration amplitudes of 103 earthquakes, two earthquakes stand out. M_W5.7 Silivri Earthquake (2019) is the most important one in the catalogue because it resulted in the largest acceleration amplitudes in the history of the SHM system. Although there were two sensors nonfunctioning during the event, the event must be included because of its particular importance. The M_W6.8 Aegean Sea earthquake that occurred at the north of the sea in 2014 has the second-largest amplitude. It had differed from the rest of the catalogue, as well. In addition, it is deemed appropriate to present an earthquake with a moderate M_W for the sake of the depiction of a broader range of the catalogue.

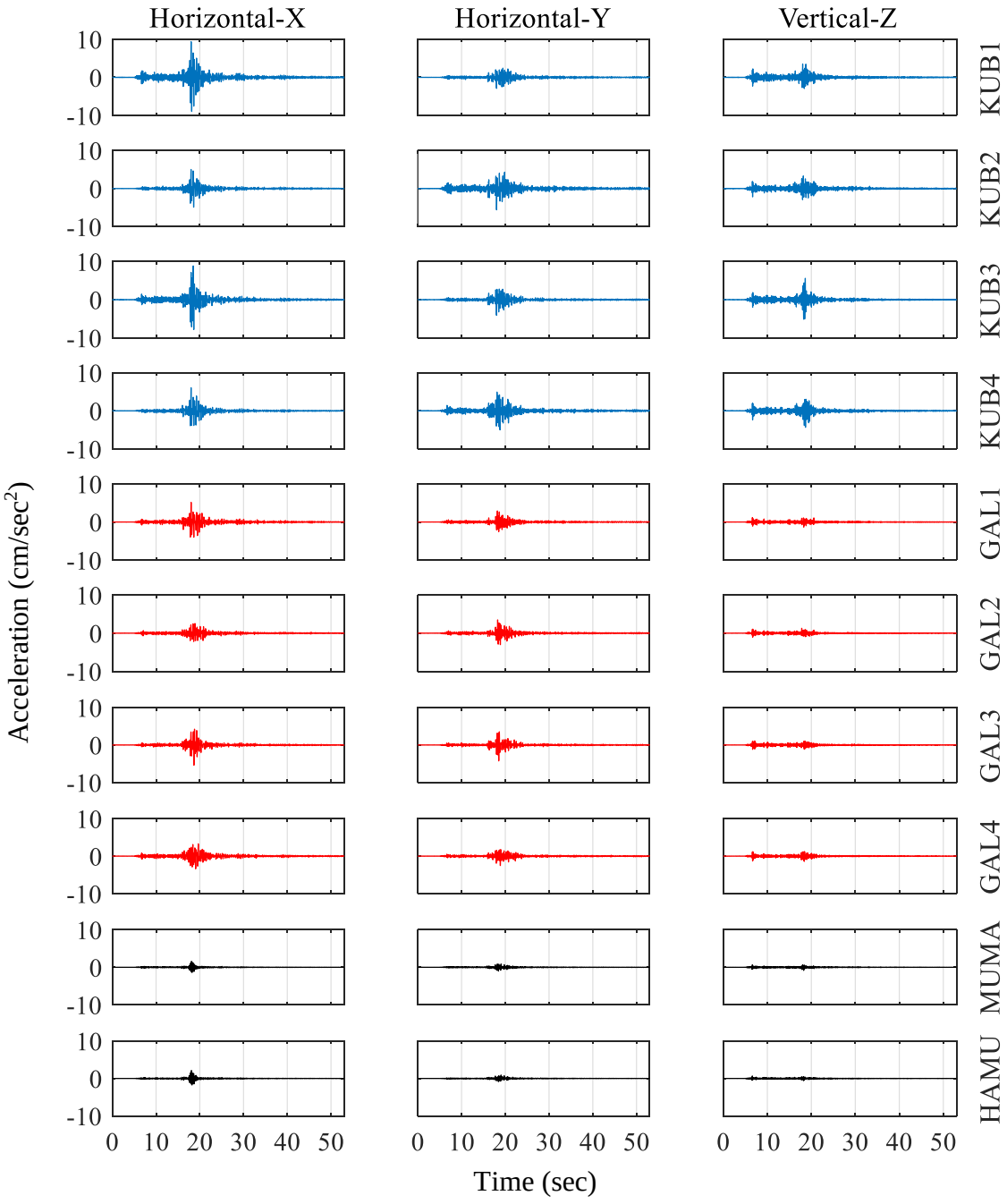

Figure 4.1. Acceleration time history of the M_W4.3 (06.2016) Kazikli/Gursu event.

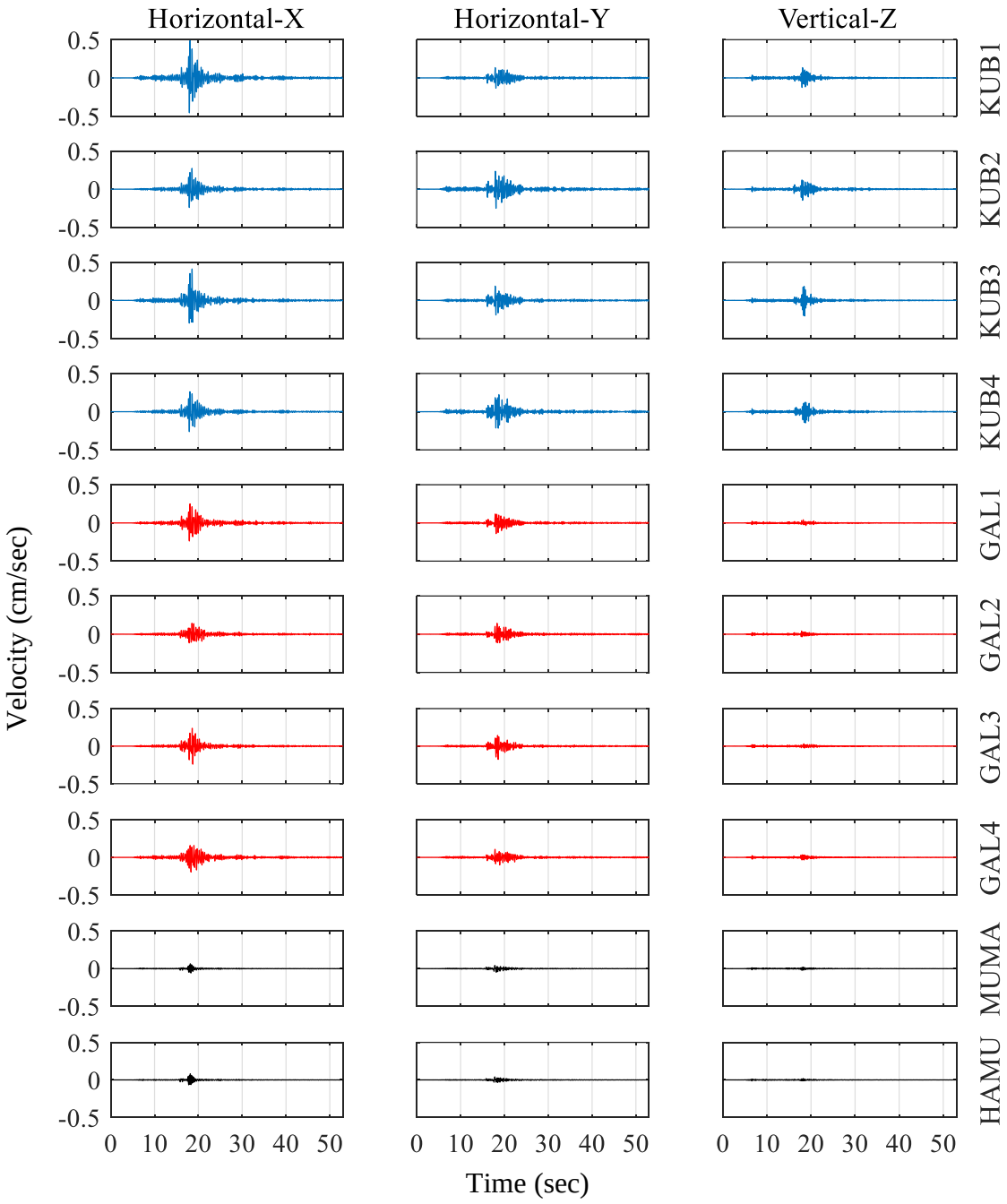

Figure 4.2. Velocity time history of the M_W4.3 (06.2016) Kazikli/Gursu event.

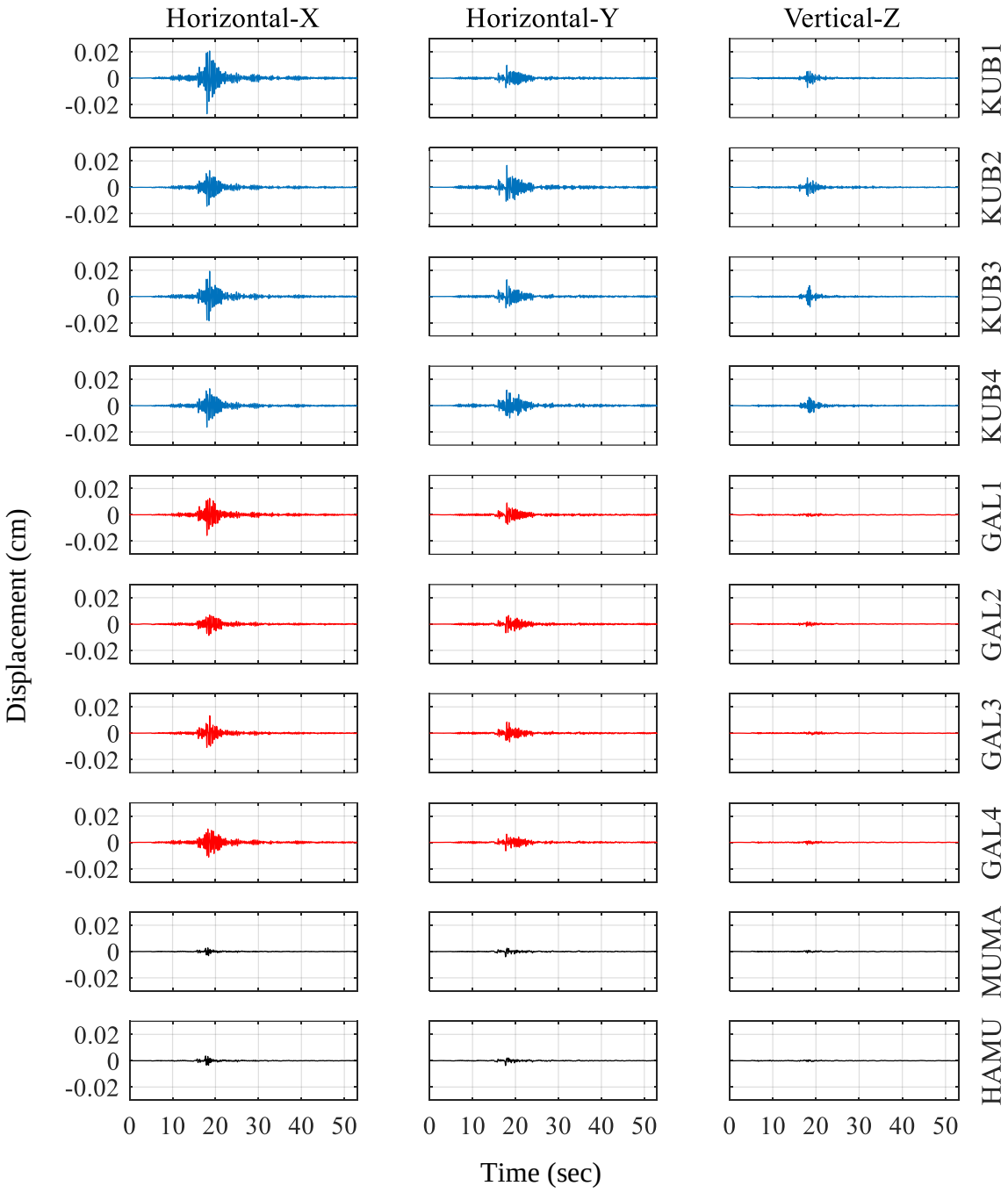

Figure 4.3. Displacement time history of the M_W4.3 (06.2016) Kazikli/Gursu event.

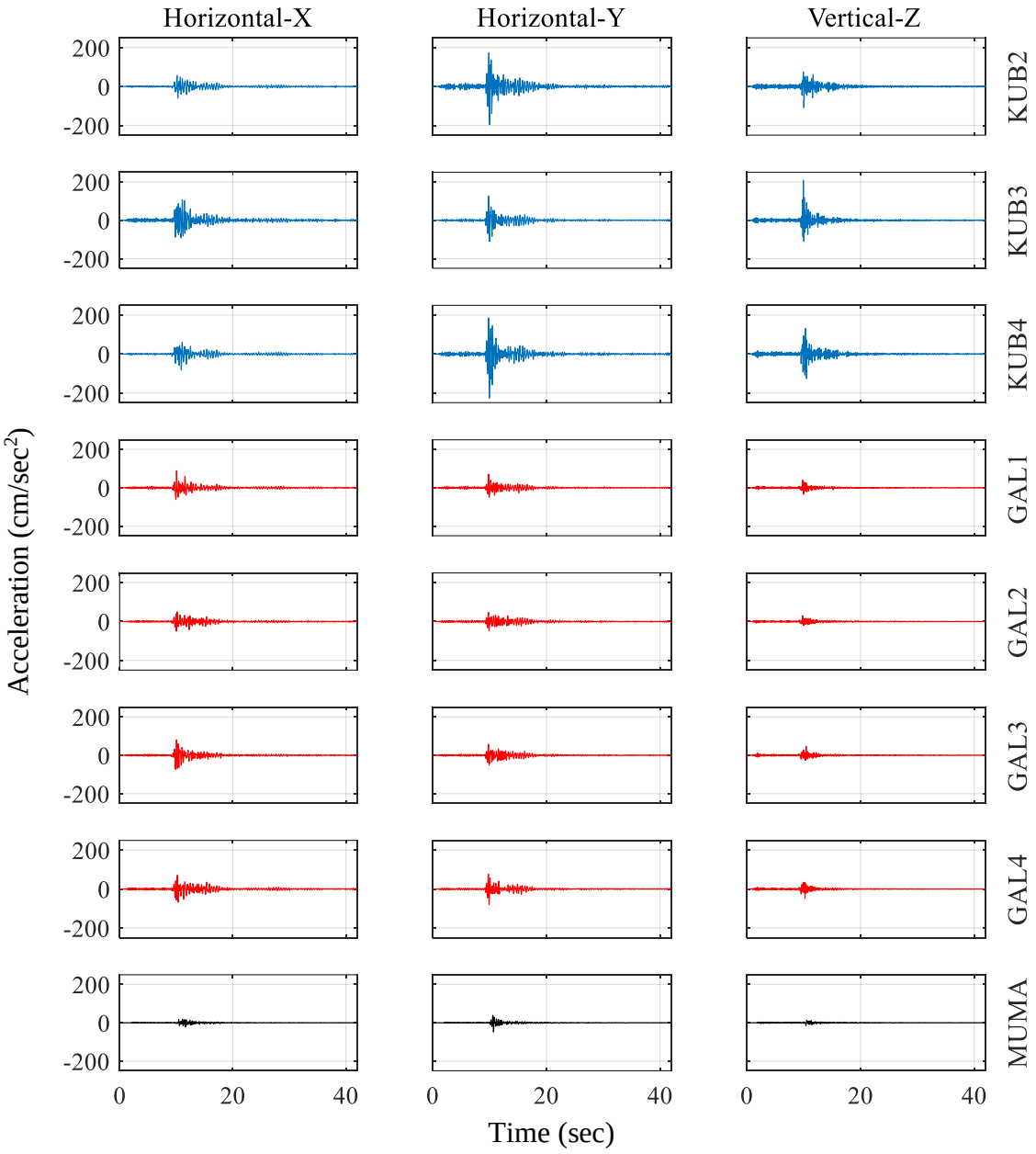

Figure 4.4. Acceleration time history of the M_W5.7 (09.2019) Silivri Offshore event.

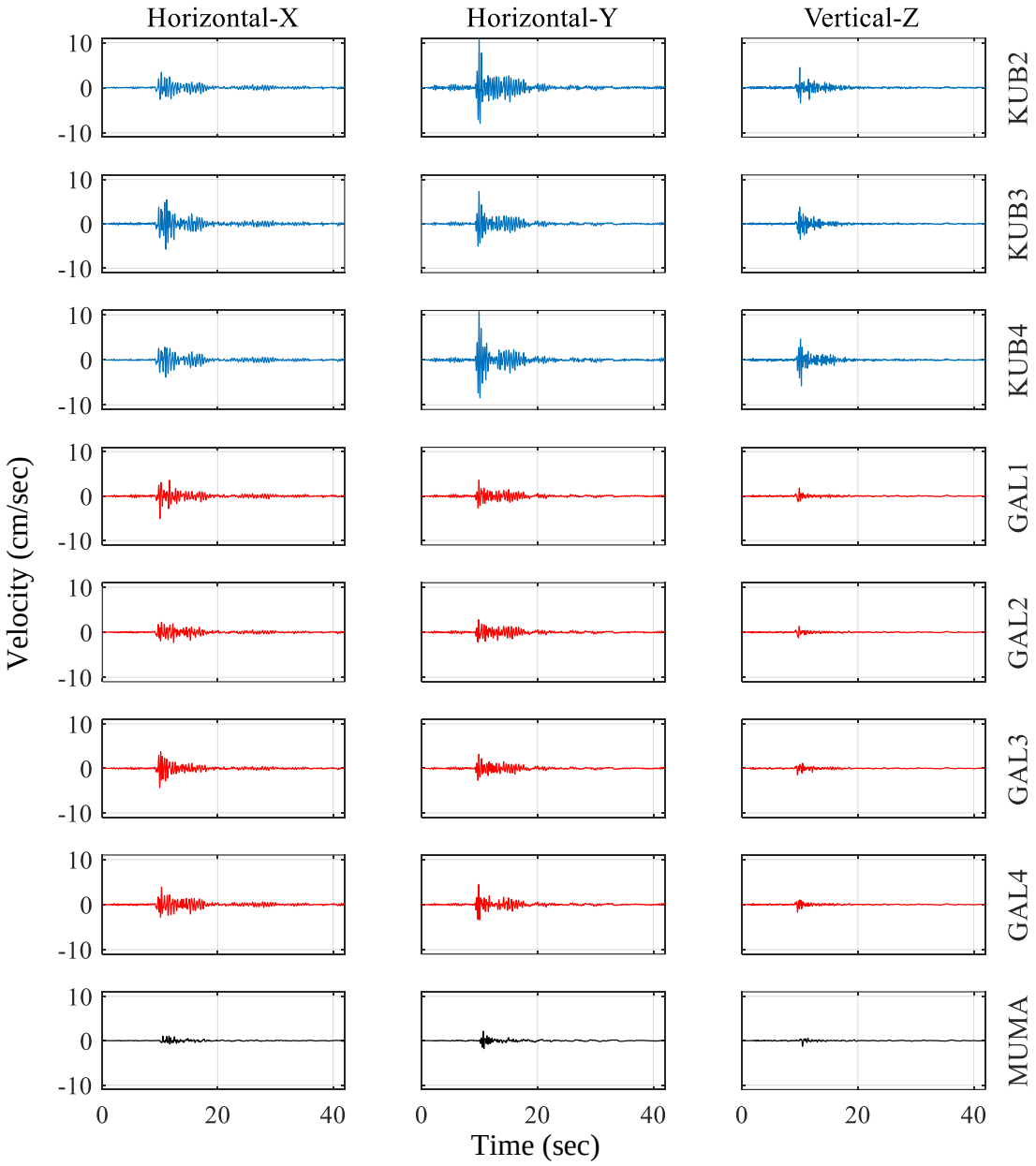

Figure 4.5. Velocity time history of the M_W5.7 (09.2019) Silivri Offshore event.

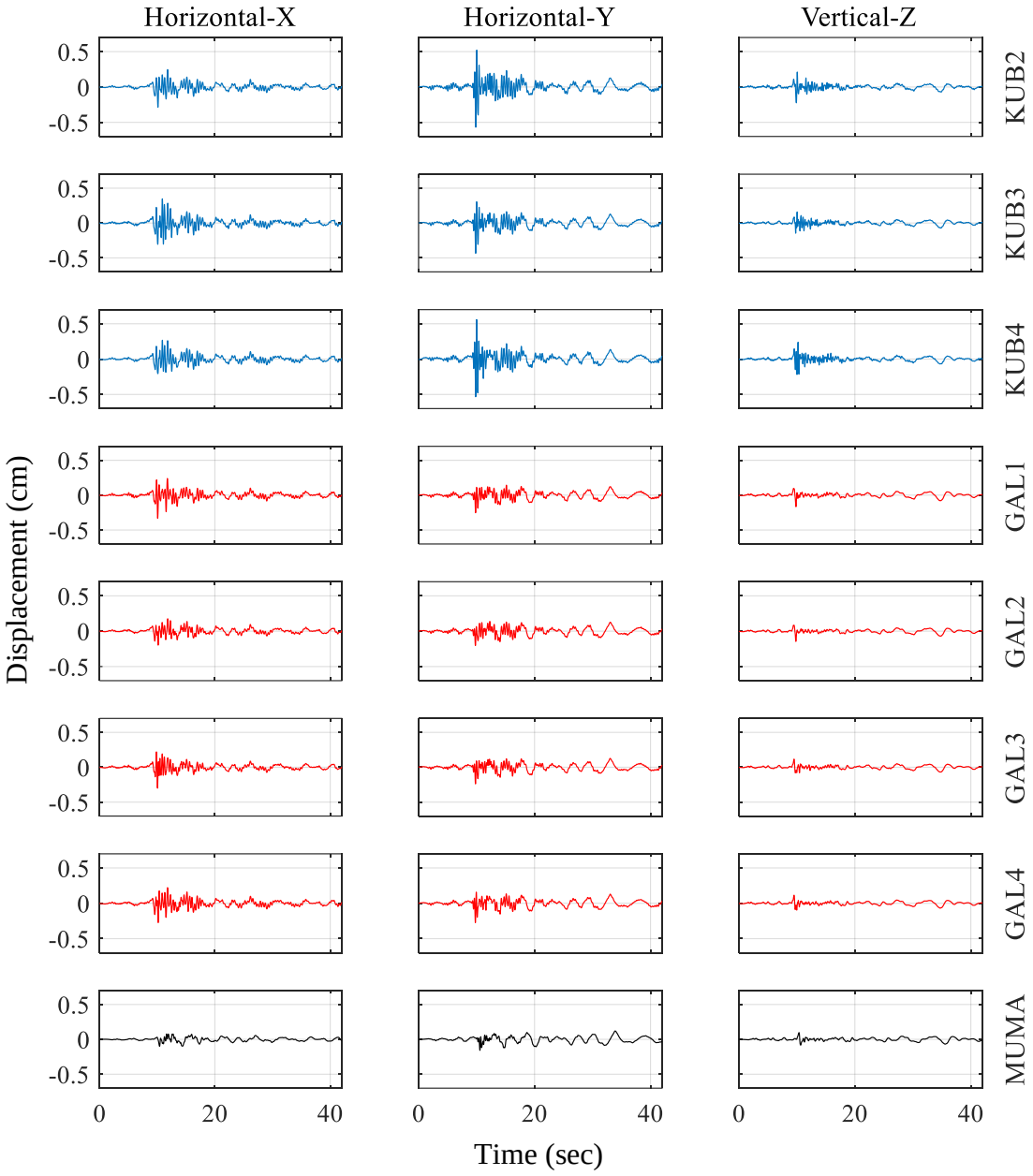

Figure 4.6. Displacement time history of the M_W5.7 (09.2019) Silivri Offshore event.

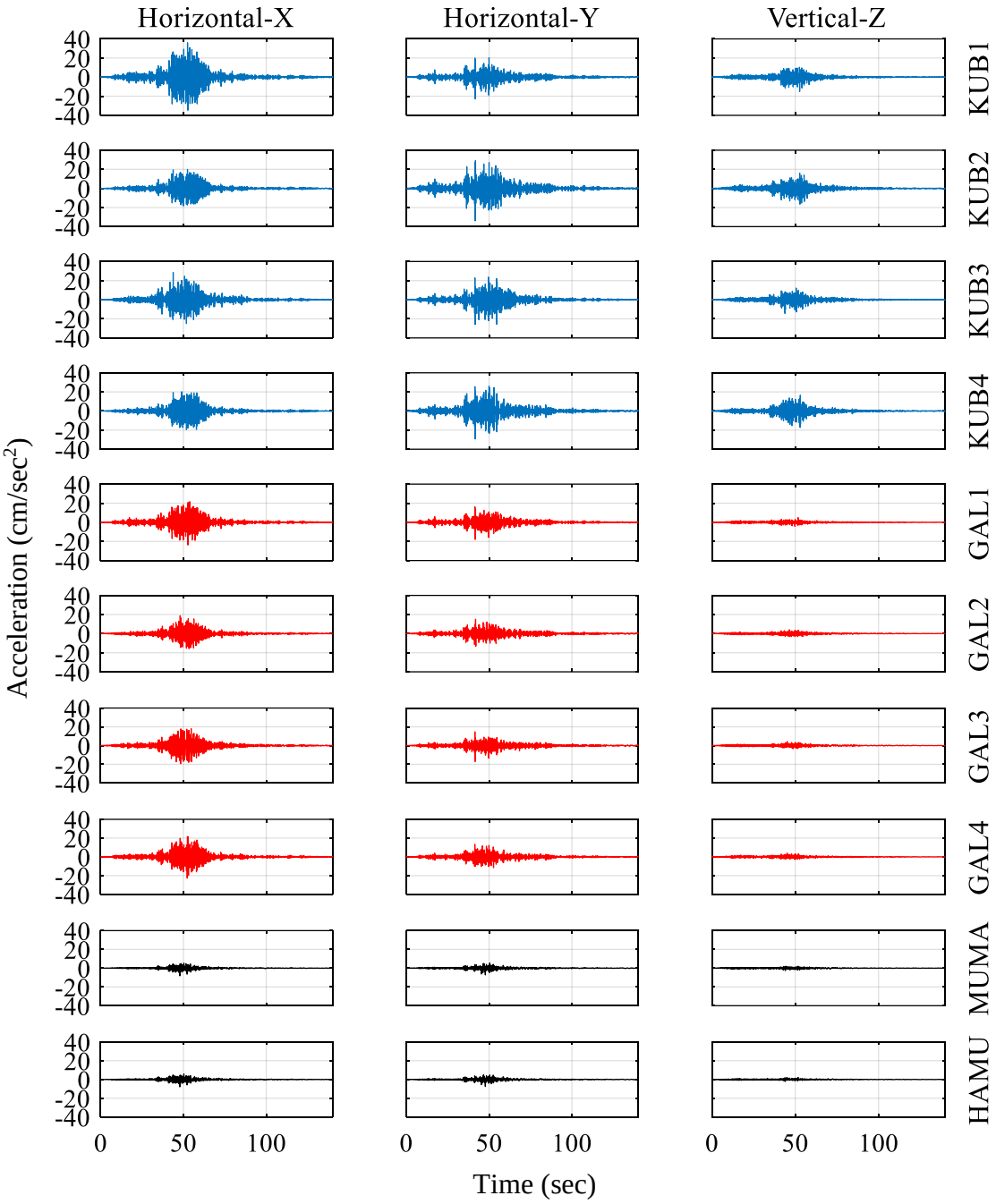

Figure 4.7. Acceleration time history of the M_W6.8 (05.2014) Aegean Sea event.

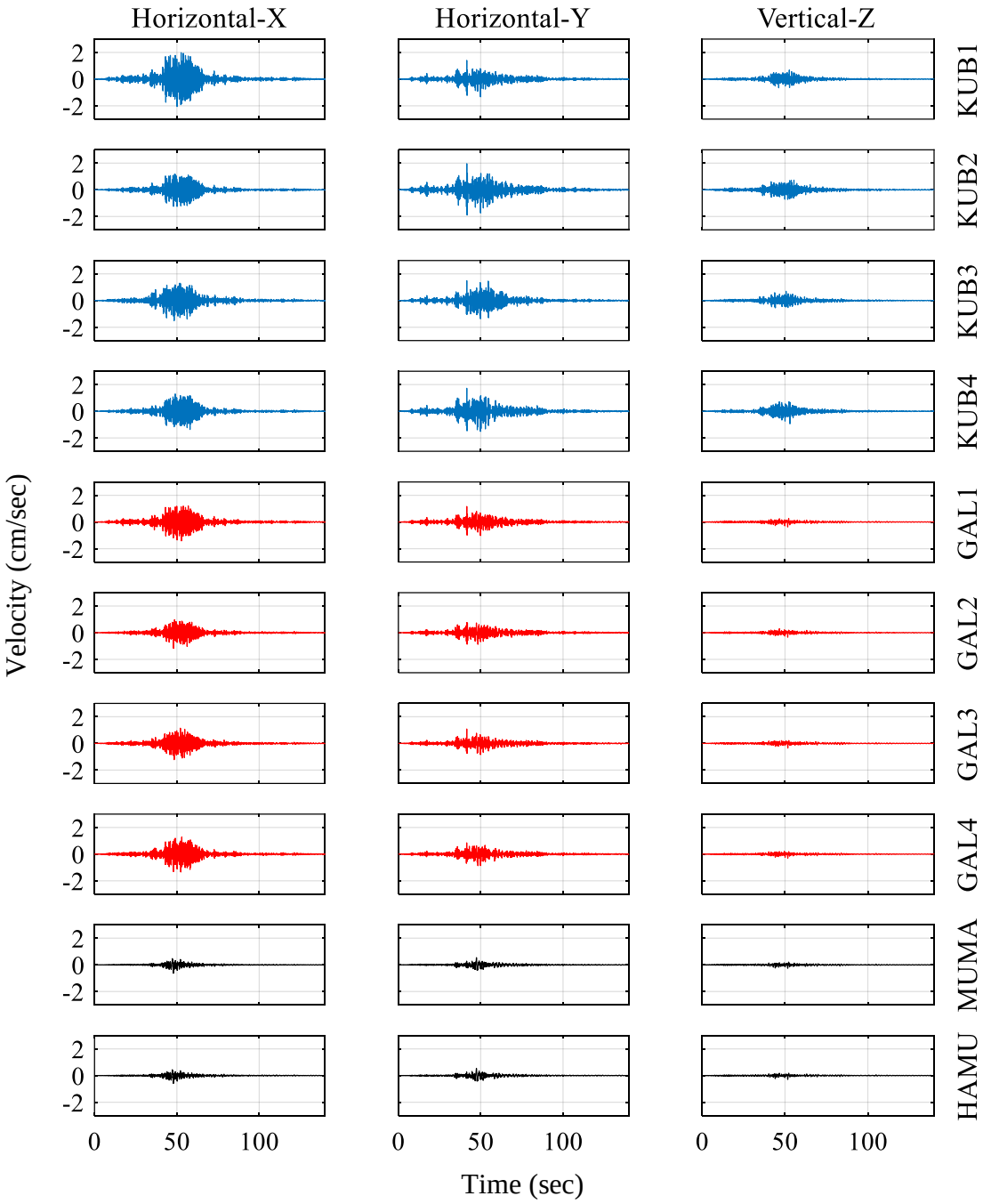

Figure 4.8. Velocity time history of the M_W6.8 (05.2014) Aegean Sea event.

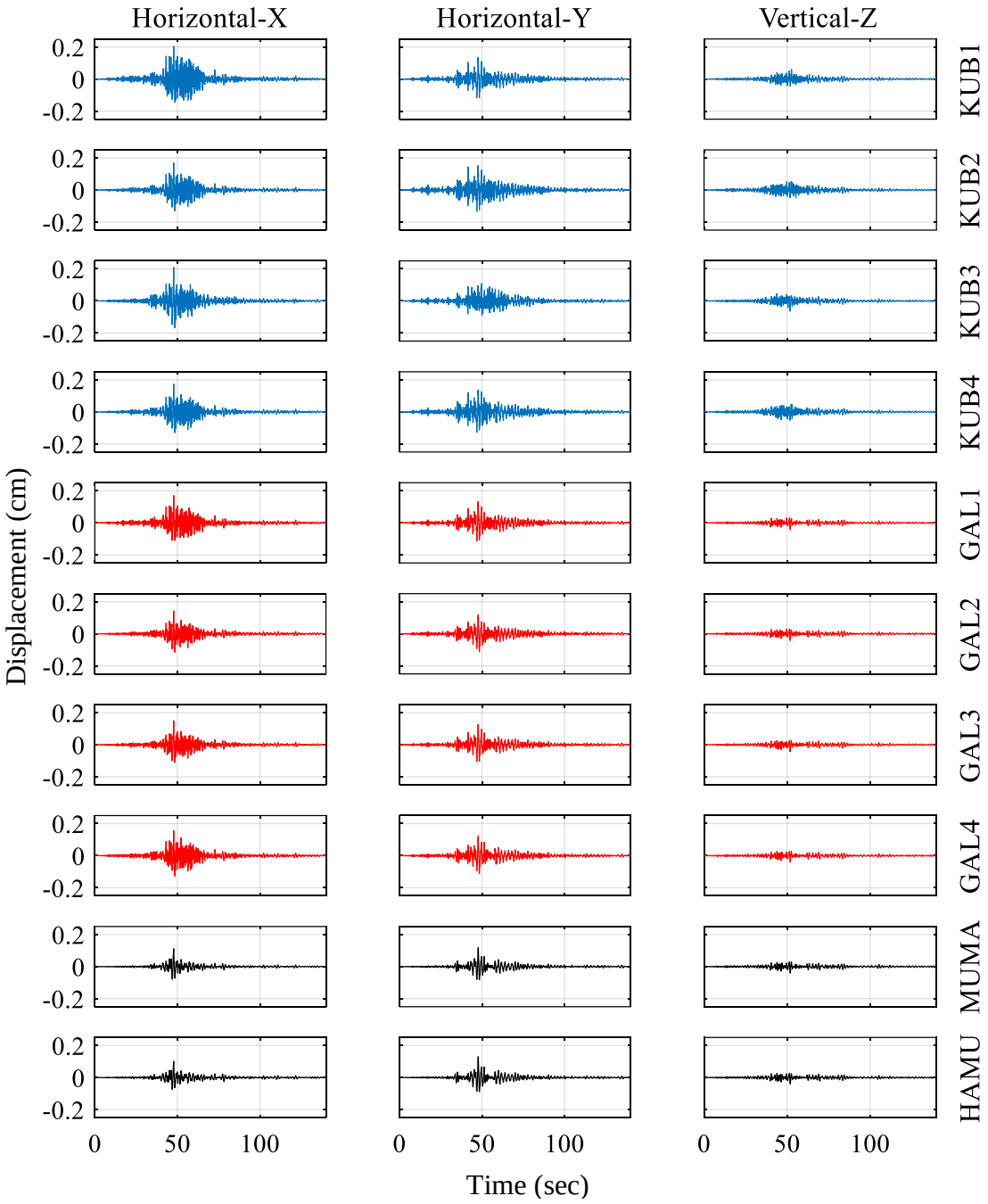

Figure 4.9. Displacement time history of the M_W6.8 (05.2014) Aegean Sea event.

In each type of peak, i.e., acceleration, velocity and displacement, a comparison is drawn among components X, Y and Z (Figure 4.10, Figure 4.11 and Figure 4.12). First of all, when horizontal (directions X and Y) and vertical (Z) vibrations are evaluated distinctively, it is seen that the structure vibrates vertically with amplitudes consistently smaller than its horizontal counterparts; however, the exception of this observation is the M_W5.7 Silivri event. Vertical response at the crowns of the arches, i.e., the base of the main dome, reached or exceeded the limits of the horizontal vibrations during this strong excitation. On the other hand, the upper structure of the mosque is ideally pure symmetrical along the X-axis line. Considering the Y-axis line, it has a similar geometry. Thus, vibrations in two horizontal directions are expected to change in a specific limited range. When both time histories and corresponding peaks are evaluated, it is revealed that the symmetry the mosque has does not provide a constant similarity of the behaviour or response throughout two horizontal directions perpendicular to each other. This could be related to various matters of fact, e.g., material non-linearity, concealed structural damage, and different characteristics of earthquakes like the azimuthal inhomogeneity.

Secondly, ten sensors are grouped within four different structural levels, i.e., basement, ground, pillar-to-arch springings and the main dome. The reflection of these different levels in the structural response is noticeable easily in the figures. In each earthquake, vibration amplitudes also varied within level-groups and decrease from top to bottom group-by-group. Lastly, some findings related to the main arches and pillars can be revealed. Each plane of four main arches behaves in a natural manner; in-plane and out-of-plane vibrations at their crowns are evidence. Out-of-plane amplitudes (please refer to KUB1&3 in Horizontal-X and KUB2&4 in Horizontal-Y) exceed their perpendicular in-plane counterpart constantly (please refer to KUB2&4 in Horizontal-X and KUB1&3 in Horizontal-Y). Under the southeastern portion of the prayer hall, there is a basement floor along the qibla wall. Among four pillars, the couple in the southern part has longer extensions reaching deeper. These two pillars on the qibla wall side have galleries where the sensors GAL1 and GAL4 function, and the other two has been monitoring by sensors GAL2 and GAL4. The difference in amplitudes between these two couples can be attributed to this.

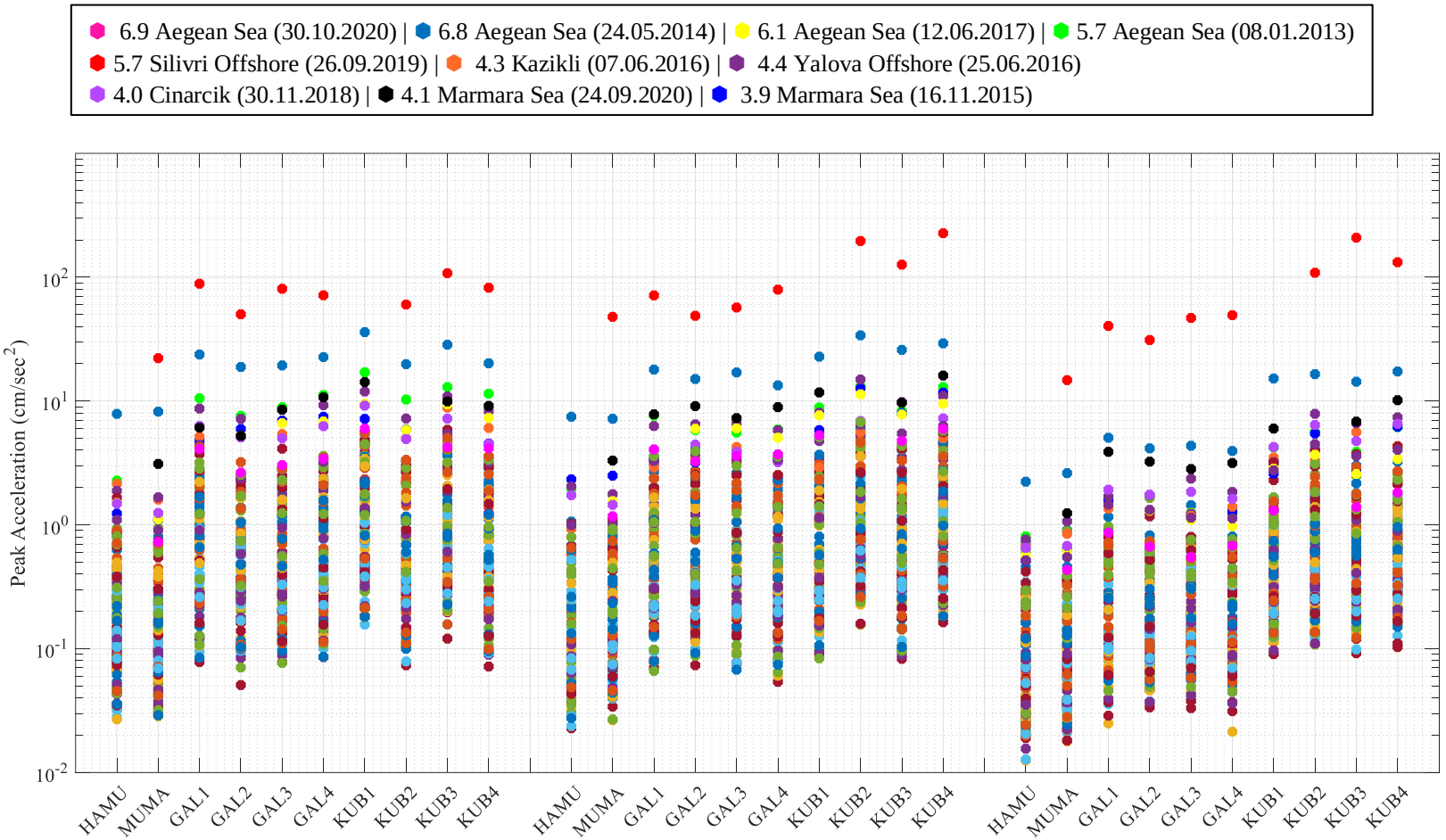

Figure 4.10. Peak horizontal accelerations from earthquakes in the catalogue.

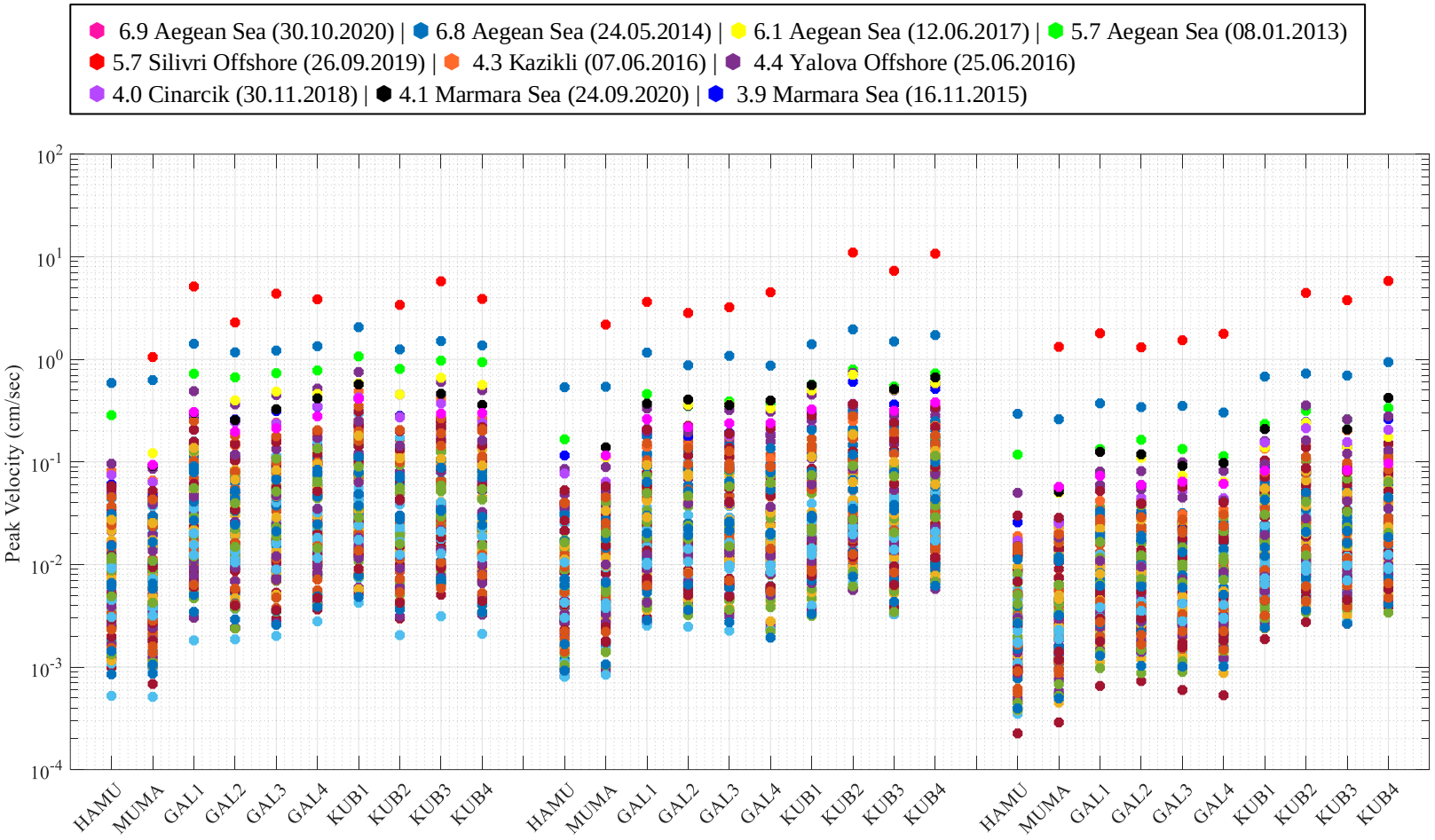

Figure 4.11. Peak horizontal velocities from earthquakes in the catalogue.

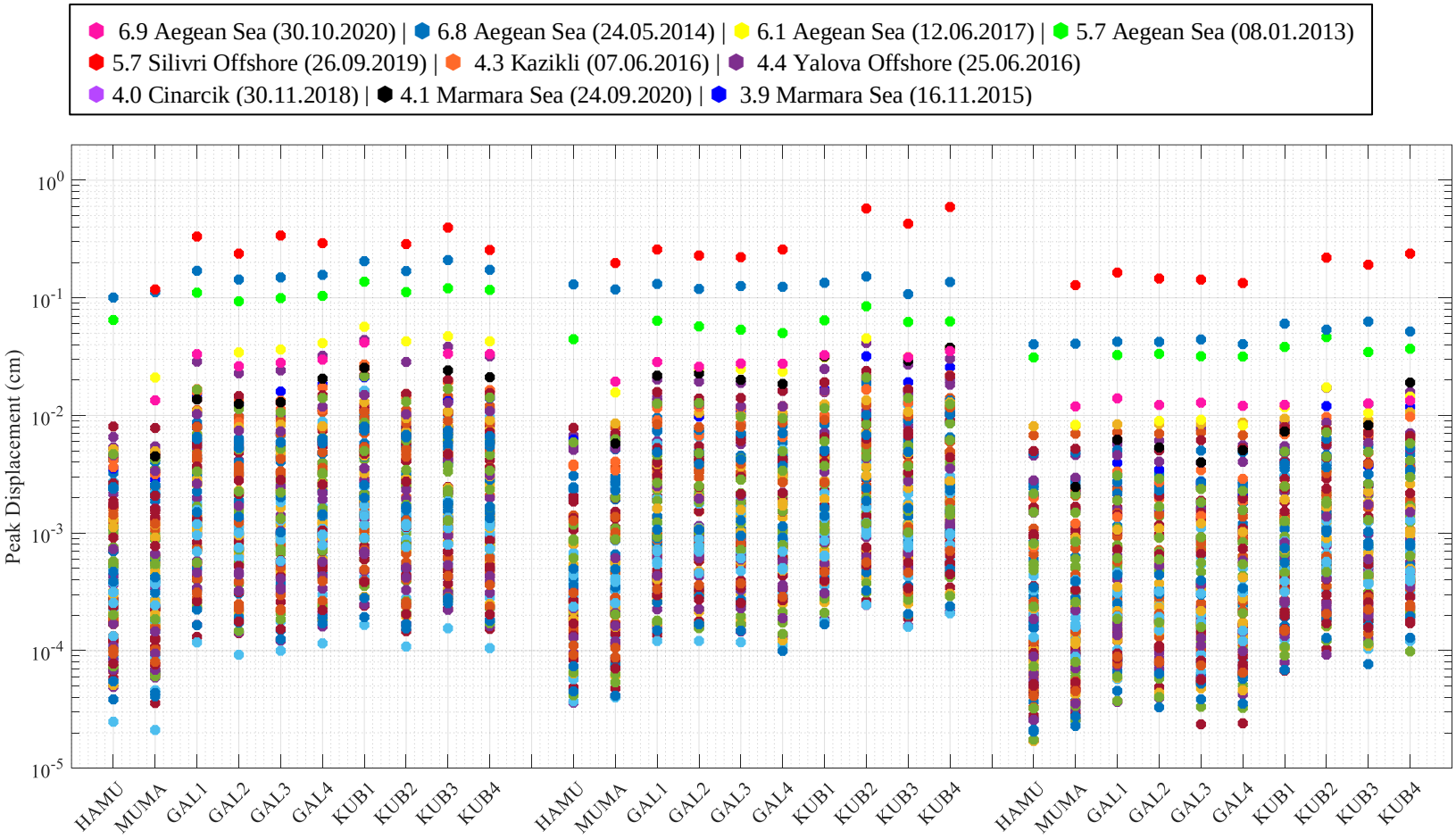

Figure 4.12. Peak horizontal displacements from earthquakes in the catalogue.

Amplitudes are also assessed as a function of earthquake magnitude. Figures Figure 4.13, Figure 4.14 and Figure 4.15 show the relationship between the moment magnitude and geometric means of acceleration, velocity and displacement in two horizontal components, namely X and Y. In general, the data set of the Sultan Ahmet Mosque covering a moment magnitude range of 2.1-6.9, suggests a positive correlation between amplitudes and magnitude. Besides, from acceleration to displacement, the area amplitudes scattered becomes narrower, and amplitudes vertically fit in a more limited variation; hence, the correlation becomes sharper. Despite this, the vertical variations in different earthquakes with the same magnitude in the data set necessitate a new comparison that allows a more proper scaling, i.e., logarithmic.

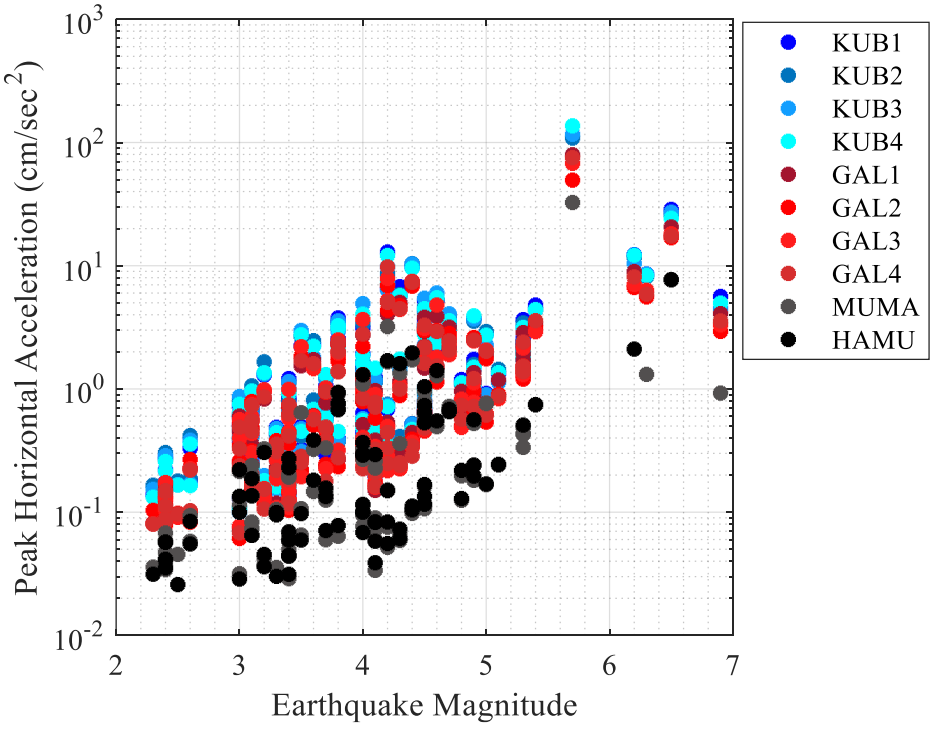

Figure 4.13. The variation of the peak accelerations with earthquake magnitude.

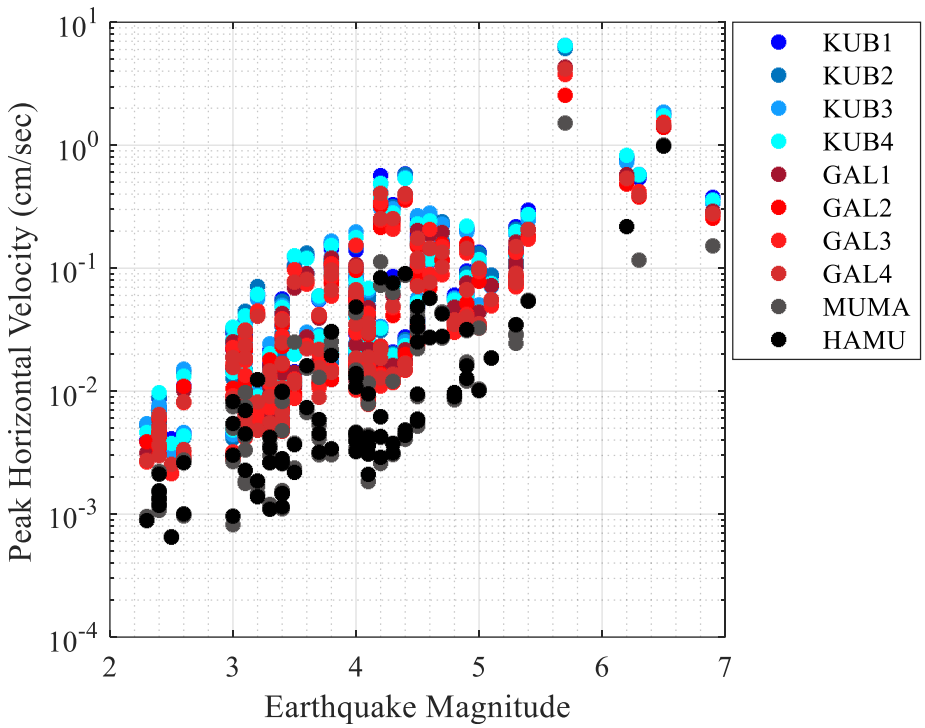

Figure 4.14. The variation of the peak velocities with earthquake magnitude.

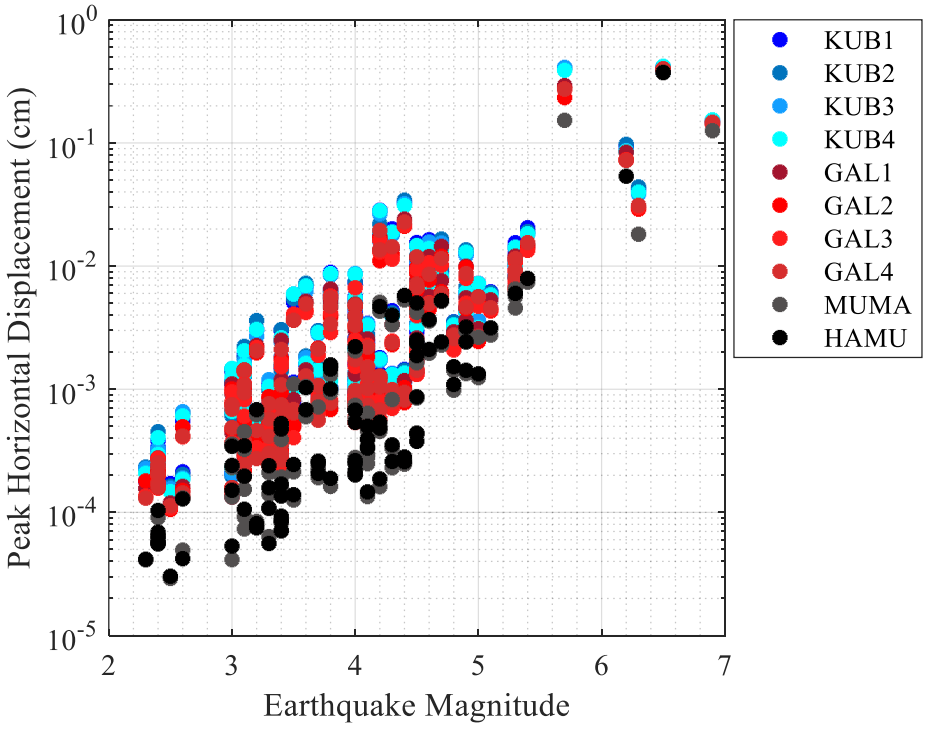

Figure 4.15. The variation of the peak displacements with earthquake magnitude.

In a log-log scaled graph, the dependence of amplitudes at dome-level, pillar-level and ground-level to the input excitation at the basement-level (HAMU) is given. Since the HAMU was out of service during several crucial earthquakes in the catalogue, e.g., during the M_W5.7 Silivri event, MUMA at the ground level is also used as the input. In Figure 4.16, the change of accelerations at the ground level with respect to those at the basement level scattered throughout the diagonal of the square graph. The data set is in a smooth and considerable correlation with the input acceleration. Figure 4.17 plots the MUMA as input acceleration and suggests the continuity of the same relationship with additional input earthquakes with high amplitudes. The relationship between the input excitation and displacement output is also investigated (Figure 4.18 and Figure 4.19). These correlations are promising within the data set boundaries. Once the seismic excitation that the mosque exposed is known, a reliable prediction for how specific structural elements (main arches, top of main pillars, base of the main dome, or pendentives) would vibrate can be made. In this context, using tools based on statistics and/or machine learning would be very efficient.

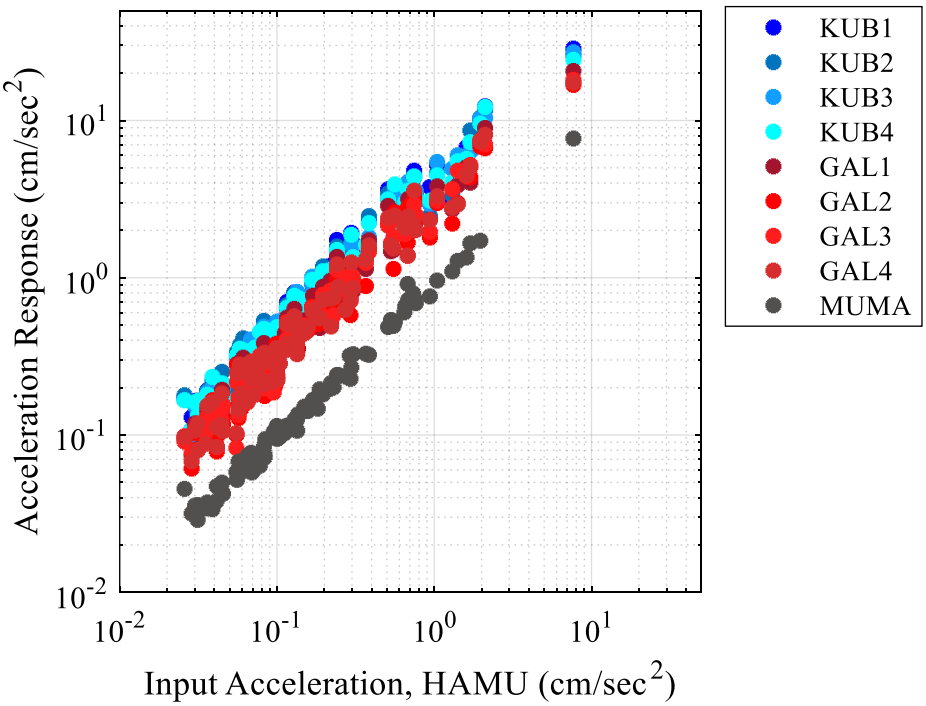

Figure 4.16. Response of the structure to basement-level acceleration amplitudes.

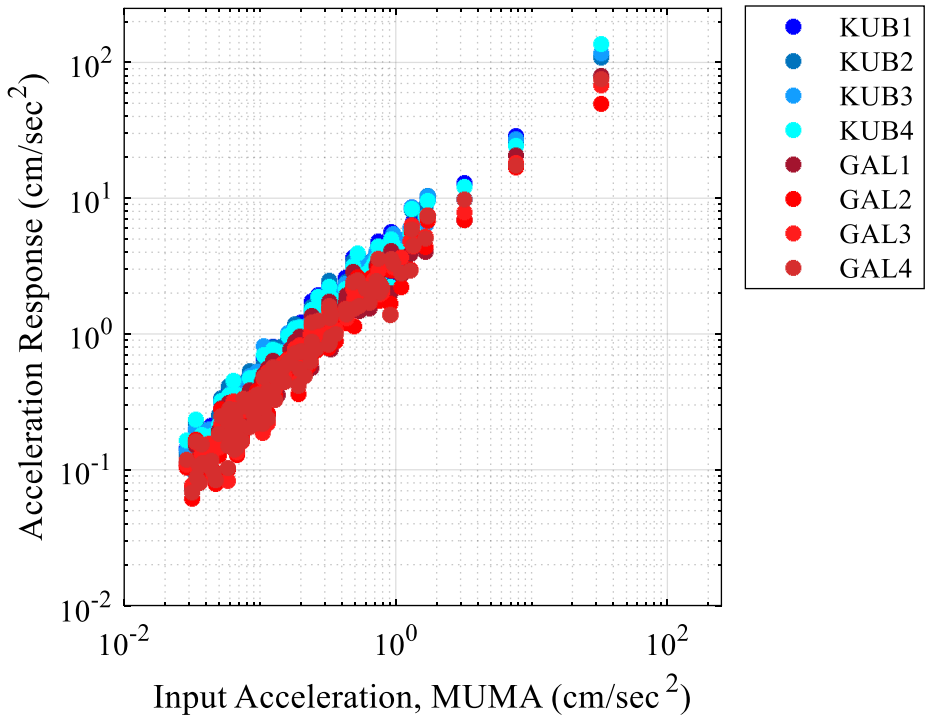

Figure 4.17. Response of the structure to ground-level acceleration amplitudes.

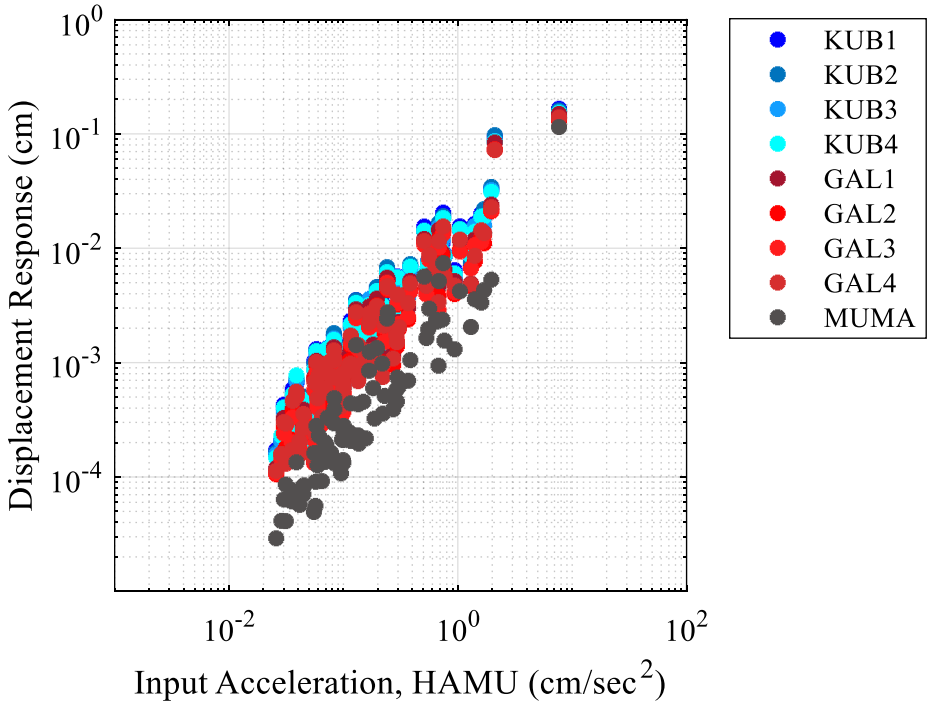

Figure 4.18. Change in displacements with basement-level acceleration amplitudes.

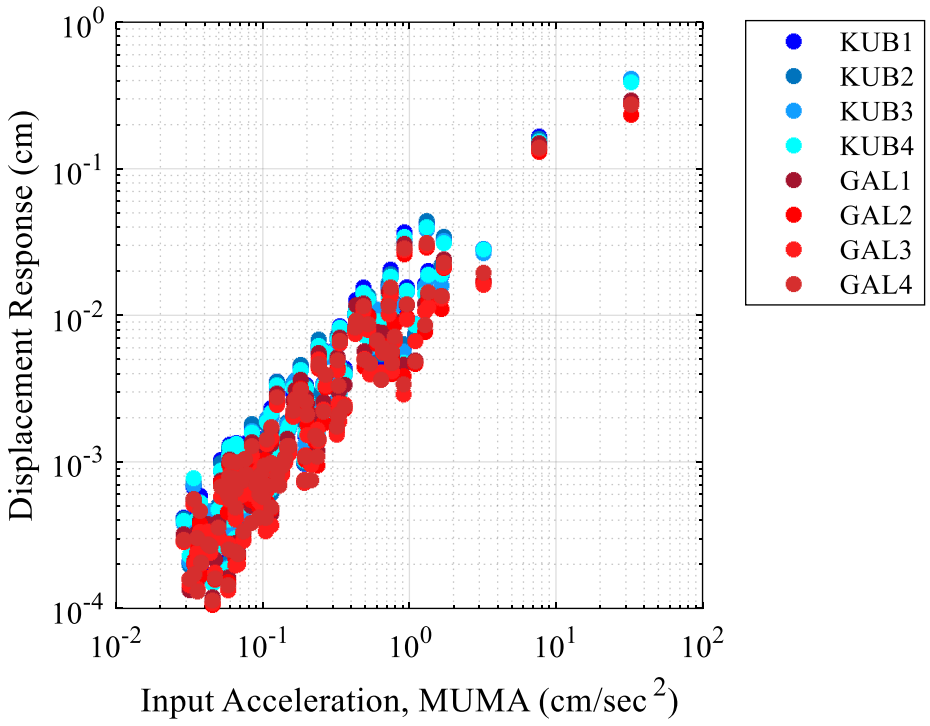

Figure 4.19. Change in displacements with ground-level acceleration amplitudes.

4.2. Frequency-Domain Analyses

This section aims to investigate whether the modal frequencies identified by spectral evaluations using FAS and TF depend on time, earthquake magnitude, seasonal temperature, or ground-level seismic excitation. If yes, the relationship between specific parameters is going to be further explained. The method used to assess the SSI is one carried out in the frequency domain. So, this section also involves SSI investigation in light of identified frequencies from the spectra of FAS and TF. On the other hand, the question of how the primary structural system of mosque vibrated, i.e., displaced, during earthquakes with large amplitudes is fulfilled by plotting particle motions. This thus leads us to understand the responsiveness of the system under strong dynamic excitation. Finally, significant mode shapes, one of the essentials of modal analysis, are obtained.

4.2.1. Analysis on Modal Frequency

In this study, the Fourier transform is used to represent the series in the frequency domain. Baseline corrected and band-pass filtered data set was transformed and smoothed. Spectral evaluation in the frequency domain is performed with the help of Fourier amplitude spectra and base-to-dome transfer functions. Both types of spectra are sampled for significant events, and these samples can be found in subsection Soil-Structure Interaction. The first two modal frequencies of the mosque are in X and Y directions, respectively.

In both horizontal directions, it was detected that the M_W5.7 Silivri event resulted in a sharp frequency drop, and this necessitated a more detailed frequency-domain analysis to see post-earthquake circumstances of the mosque in terms of its modal frequencies. Eleven additional earthquakes that occurred in the following period of the main event of the M_W5.7 were included in the catalogue. However, their transfer functions can be generated using the sensor MUMA at the ground level because the basement-level sensor HAMU was failed to function during these eleven events. After all, when the change of modal frequencies within time was investigated in the period from October 2012 to late 2020, the most crucial finding was that the frequency drop that is detected during the main event of M_W5.7 was recovered in that the modal frequencies individually in both directions approached its previous levels (Figure 4.20 and Figure 4.21). A permanent frequency drop would be a sign of structural damage. In our case, the recovery can also be supported by in-situ structural investigation provided by the crew from ongoing restoration works (Aktas, 2019). No visible structural damage was found in any structural element.

Figures Figure 4.22 and Figure 4.23 plot all the identified frequencies in the annual base to investigate their seasonal dependence, i.e., whether or not modal frequencies could be affected by seasonal temperature. It can be concluded that seasonal weather seemingly does not affect the characteristics of the mosque in the frequency domain. In the study of Dar and Cakti (2018), long-term ambient recordings were used to check the dependence of natural frequency on atmospheric conditions, and it was found that there is a positive yet small correlation between temperature and natural frequencies. In our case, solely the seismic

activity signals were used, and modal frequency during excitation was found independent of seasonal temperature changes in both horizontal directions.

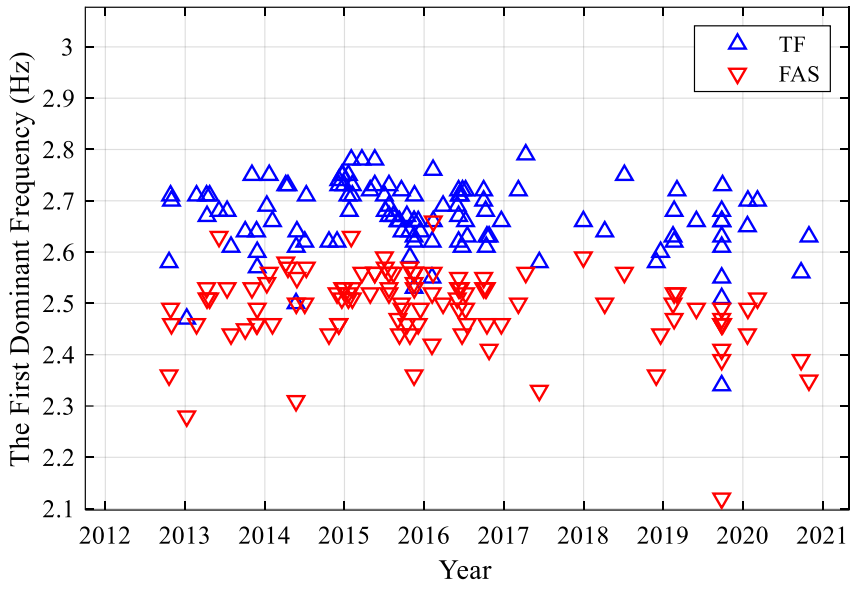

Figure 4.20. Variation of the 1st modal frequencies in horizontal-X over time.

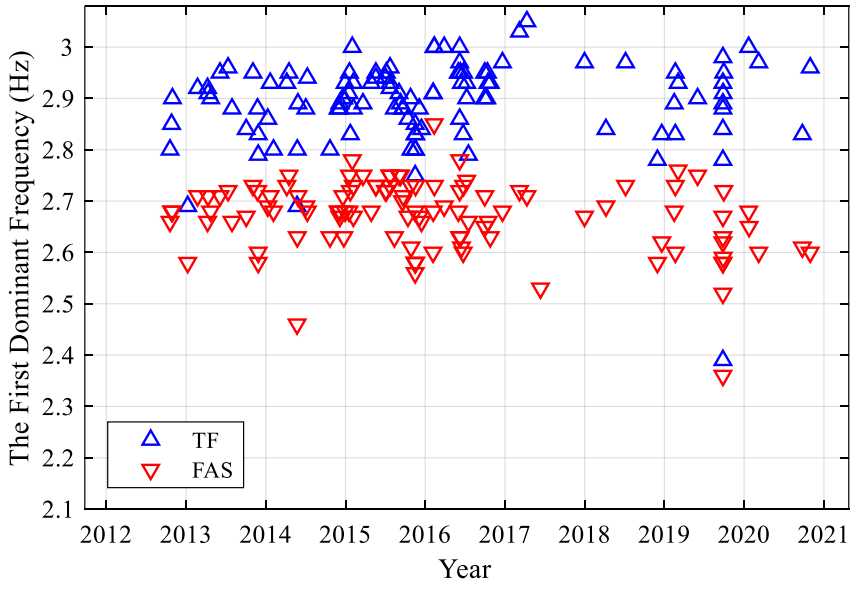

Figure 4.21. Variation of the 2nd modal frequencies in horizontal-Y over time.

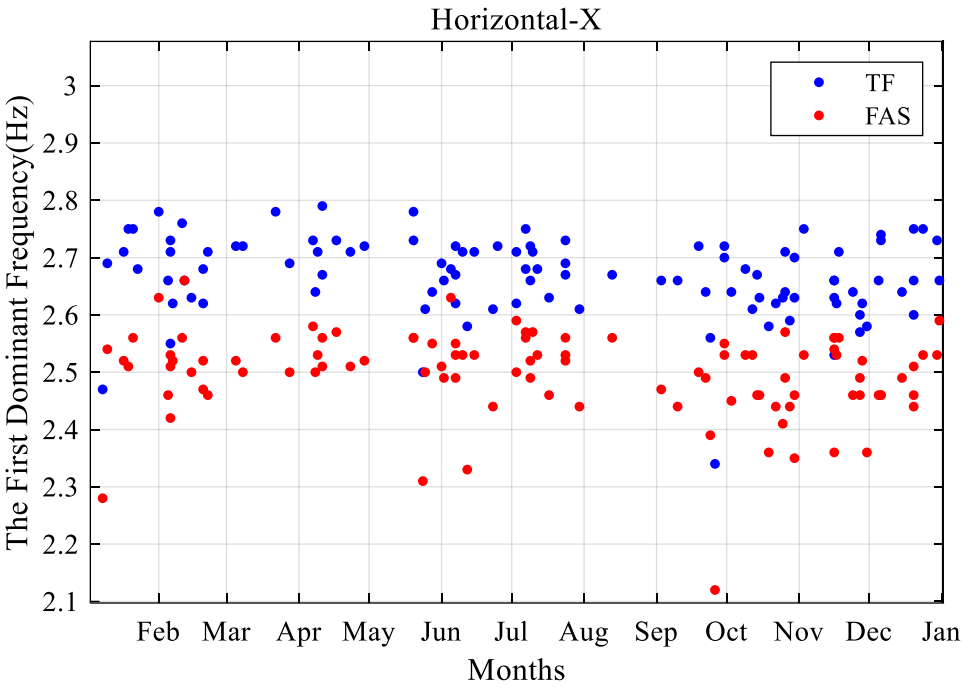

Figure 4.22. The variation of the 1st modal frequencies in annual-base.

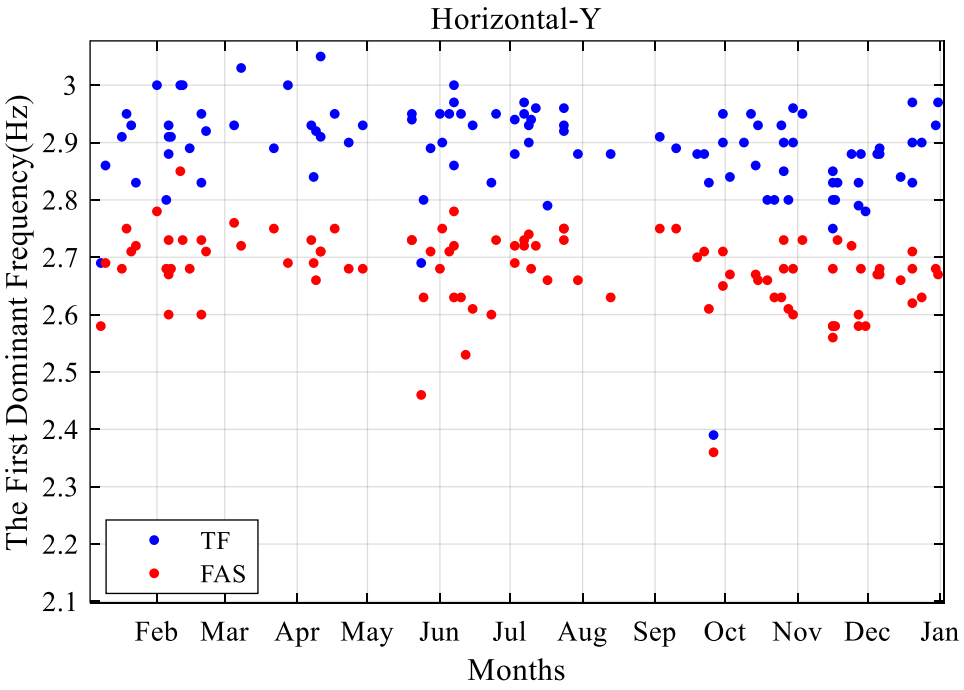

Figure 4.23. The variation of the 2nd modal frequencies in annual-base.

The variation of the modal frequency with increasing input excitation (again, considering both sensors at the basement and ground levels) is evaluated. In our structure, the acceleration levels of the input can be a decisive factor characterising the vibrational frequencies. We can benefit from two diverse sensors as inputs. Nevertheless, one of them (HAMU) dysfunctioned during several significant earthquakes, e.g., the M_W5.7 Silivri event, and the input acceleration level is limited to <10 cm/sec^2. On the other hand, the ground-level sensor MUMA can be evaluated into a broader frame since acceleration levels reach 40 cm/sec^2. Taking advantage of a higher number of large-amplitude earthquakes, the sensor MUMA exhibits a more evident relationship (Figure 4.24 and Figure 4.25). This relationship between dominant frequencies of vibration and increasing amplitude becomes distinctive when a threshold of about 1 cm/sec^2 was exceeded. Although its data set is limited and results hence are less obvious, both figures Figure 4.26 and Figure 4.27 belonging to the sensor HAMU also show the same relationship.

As mentioned, during the strong ground motion of the M_W5.7 Silivri earthquake in 2019, the modal frequencies of the structure dramatically dropped. It is understood that the frequency levels were recovered in the following period that earthquakes with moderate magnitudes occurred. However, time-frequency analyses, which are by short-time Fourier transforms, were carried out for the sensor KUB4 in order to comprehend the recovery mechanism. The vibration recording was processed within 5-second-long (1000 points) portions with an overlapping window of 4.5 seconds (900 points). The number of points specified for the discrete Fourier transform was 1024. Figure 4.28 shows the sharp frequency drop that occurred in the portion corresponding to body waves. In the context of acceleration amplitudes, it is also evident that the frequency content became broader and complex during the most substantial part of this seismic event. In the period corresponding surface-wave part of the signal, the recovery of the dominant frequency began. Between 60-210 second, the frequency content got narrower into its fundamental frequency, alteration of which can be seen as a positively-sloped curve.

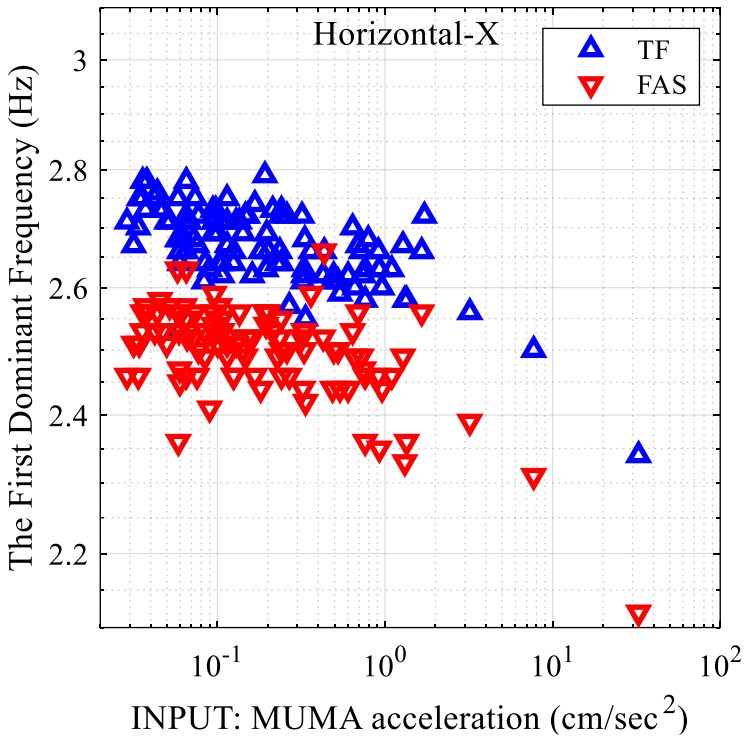

Figure 4.24. The change of the 1st modal frequency with mean accelerations of MUMA.

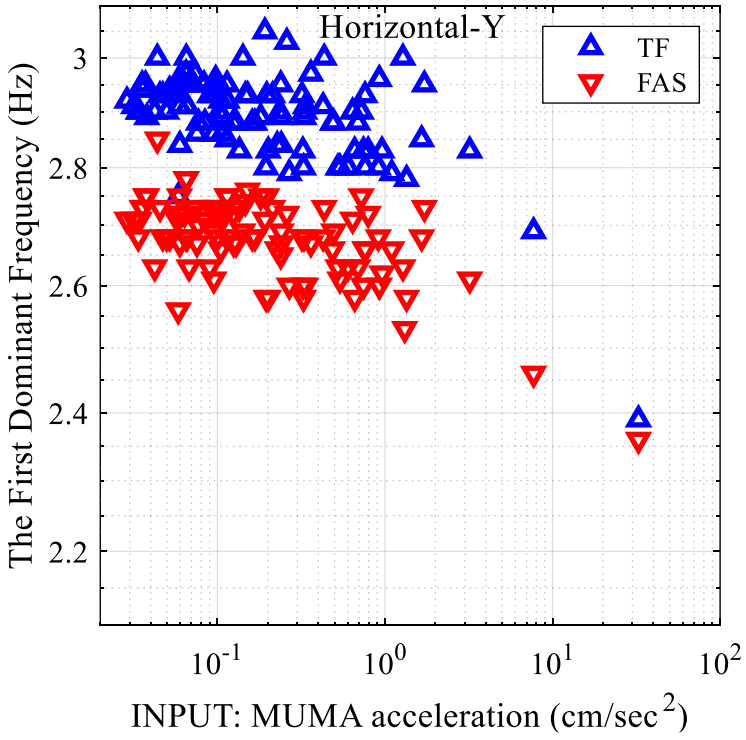

Figure 4.25. The change of the 2nd modal frequency with mean accelerations of MUMA.

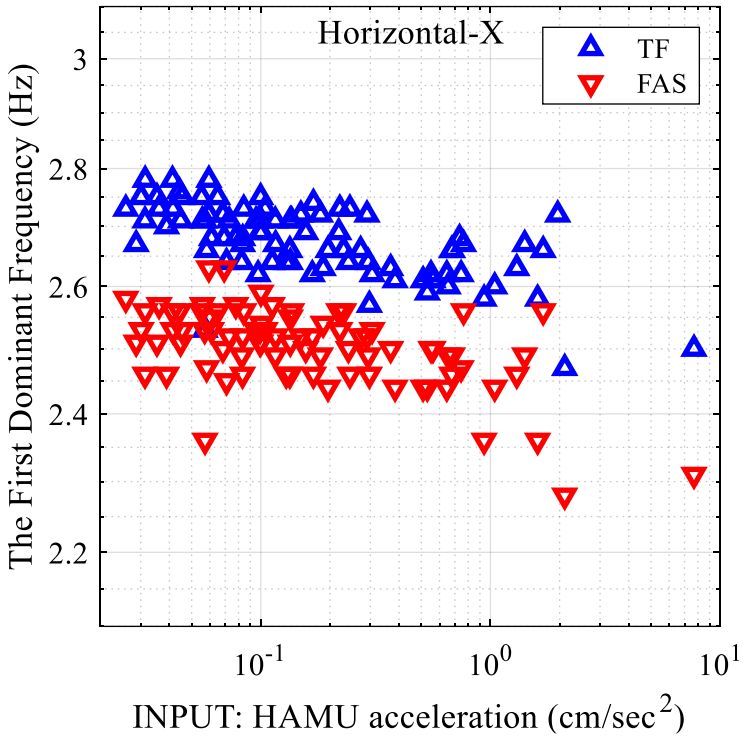

Figure 4.26. The change of the 1st modal frequency with mean accelerations of HAMU.

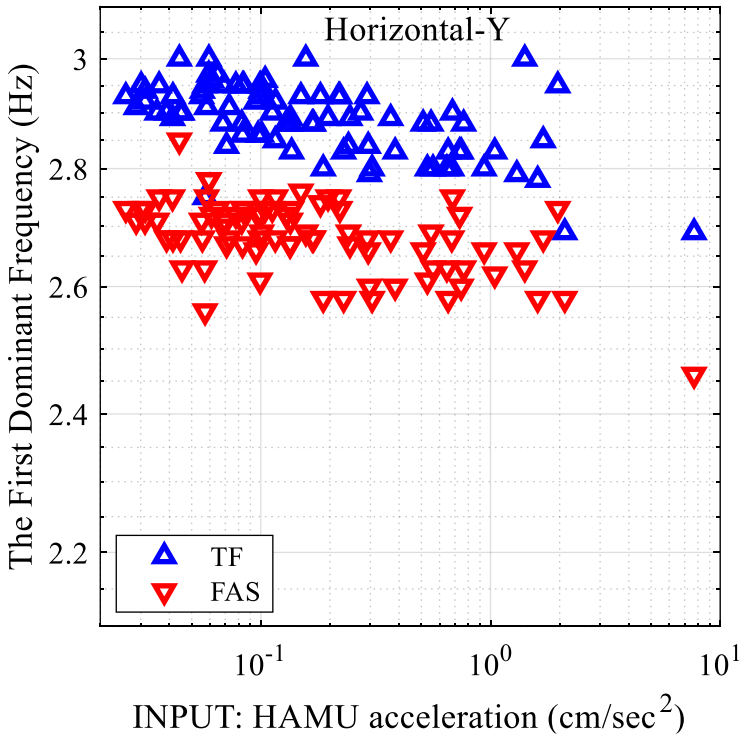

Figure 4.27. The change of the 2nd modal frequency with mean accelerations of HAMU.

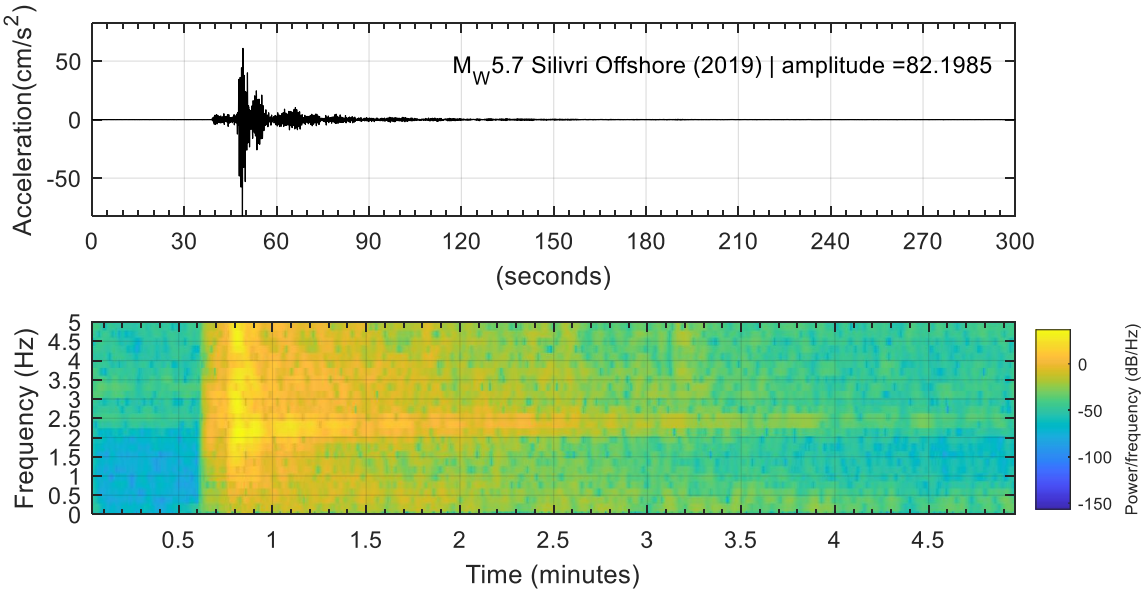

Figure 4.28. Time-frequency analysis of sensor KUB4 (X).

4.2.2. Soil-Structure Interaction

The results of the SSI investigation using the eight fundamental events are provided through this subsection. The epicentral locations of examined events are exhibited in Figure 4.29, all of which with magnitudes ranging from moderate to strong (M_W3.9-6.8) took place with epicentral distances from 27.1 km the nearest and 333.4 km the farthest.

The technique proposed by Safak and Cakti (2014) is applied to the mosque. SSI-case results in smaller frequency than those obtained from fixed-base systems. In each horizontal direction, both FAS and TF spectra of these events are displayed in the figures from Figure 4.30 to Figure 4.61. In each direction, the frequency shift between TF, i.e., a fixed-base approach that eliminating the effects of the underlying soil, and FAS values are evidence to observe the SSI existence.

Identified the first (X-axis) and second (Y-axis) dominant frequencies of FAS and TF are given in Table 4.1. Dominant frequencies identified by TF approximately rated 10% and 15% larger than those of FAS in X- and Y-direction, respectively. Consequently, a consistent SSI effect in the mosque is detected.

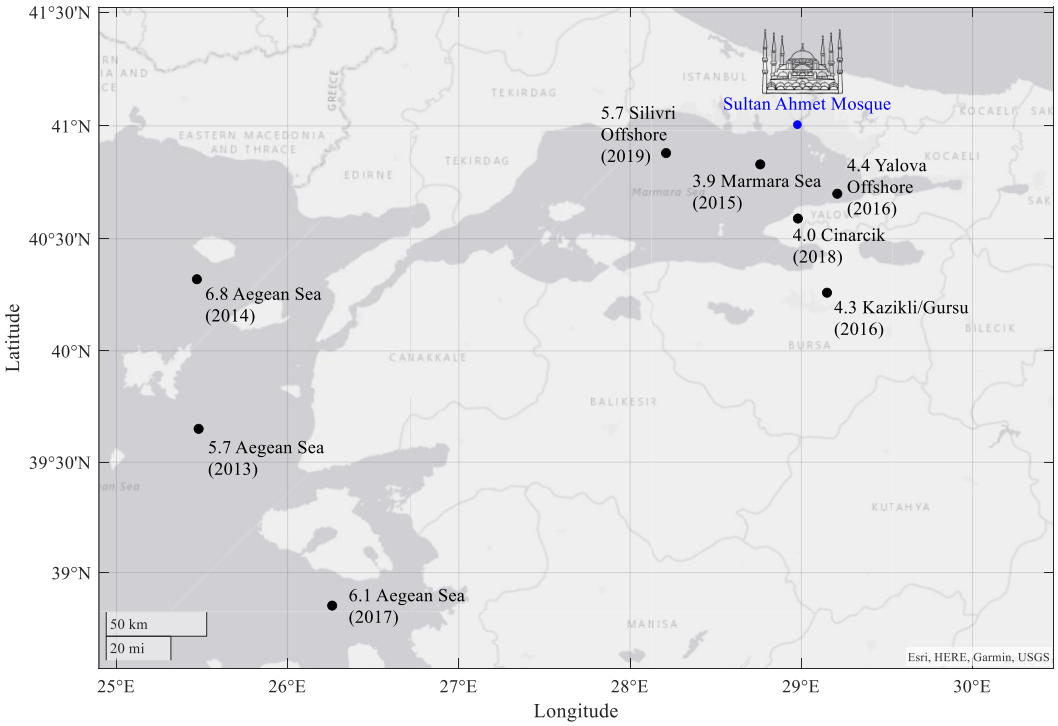

Figure 4.29. Map of earthquakes, of which FAS and TF displayed.

Table 4.1. Identified modal frequencies from earthquakes examined for SSI.

Earthquake:	Frequency (Hz)			
	X-axis		Y-axis	
	FAS	TF	FAS	TF
M_W6.8 Aegean Sea	2.31	2.50	2.55	2.75
M_W6.1 Aegean Sea	2.52	2.60	2.57	2.97
M_W5.7 Silivri Offshore	2.12	2.34	2.36	2.36
M_W5.7 Aegean Sea	2.29	2.53	2.56	2.69
M_W4.4 Yalova	2.46	2.59	2.56	2.79
M_W4.3 Kazikli	2.44	2.61	2.60	2.83
M_W4.0 Cinarcik	2.36	2.58	2.58	2.78
M_W3.9 Marmara Sea	2.46	2.58	2.56	2.75

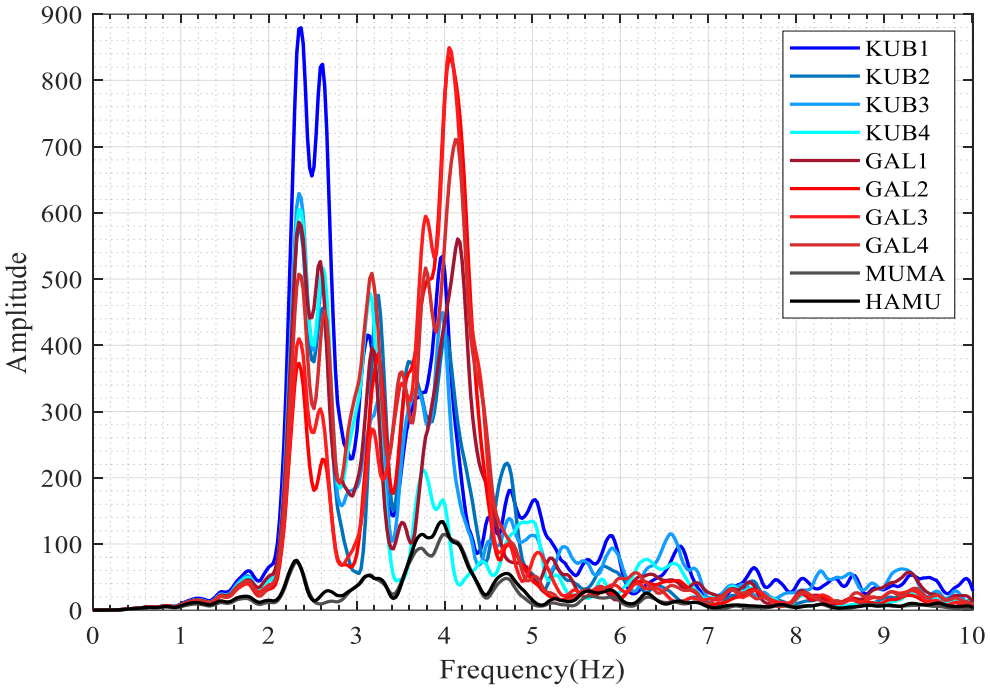

Figure 4.30. Horizontal-X: FAS of the M_W3.9 Marmara Sea earthquake.

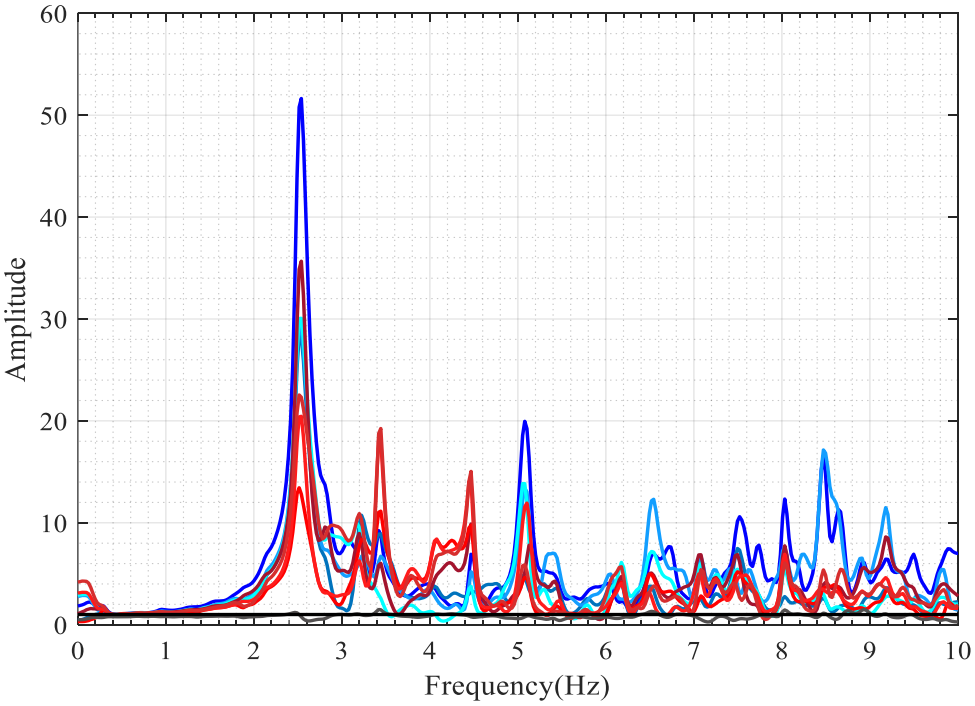

Figure 4.31. Horizontal-X: TF of the M_W3.9 Marmara Sea earthquake.

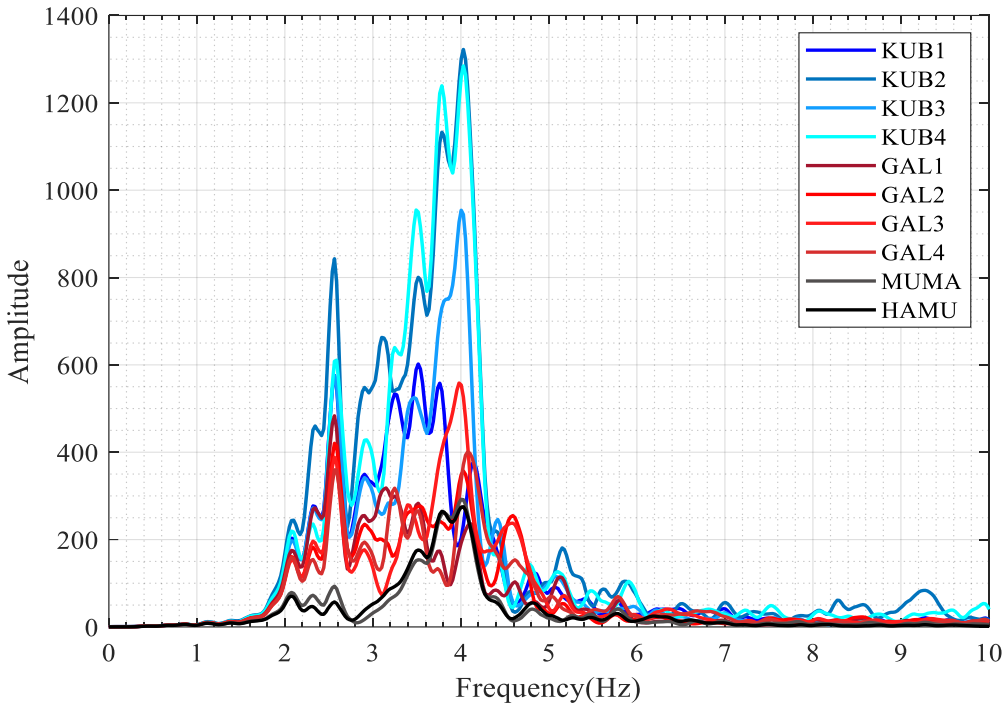

Figure 4.32. Horizontal-Y: FAS of the M_W3.9 Marmara Sea earthquake.

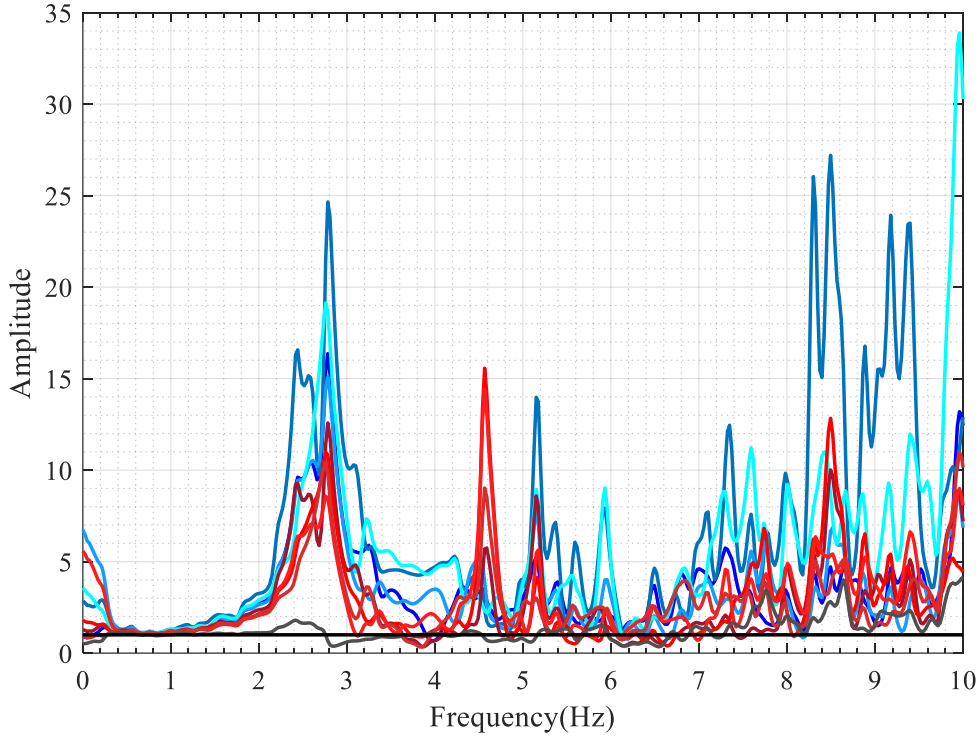

Figure 4.33. Horizontal-Y: TF of the M_W3.9 Marmara Sea earthquake.

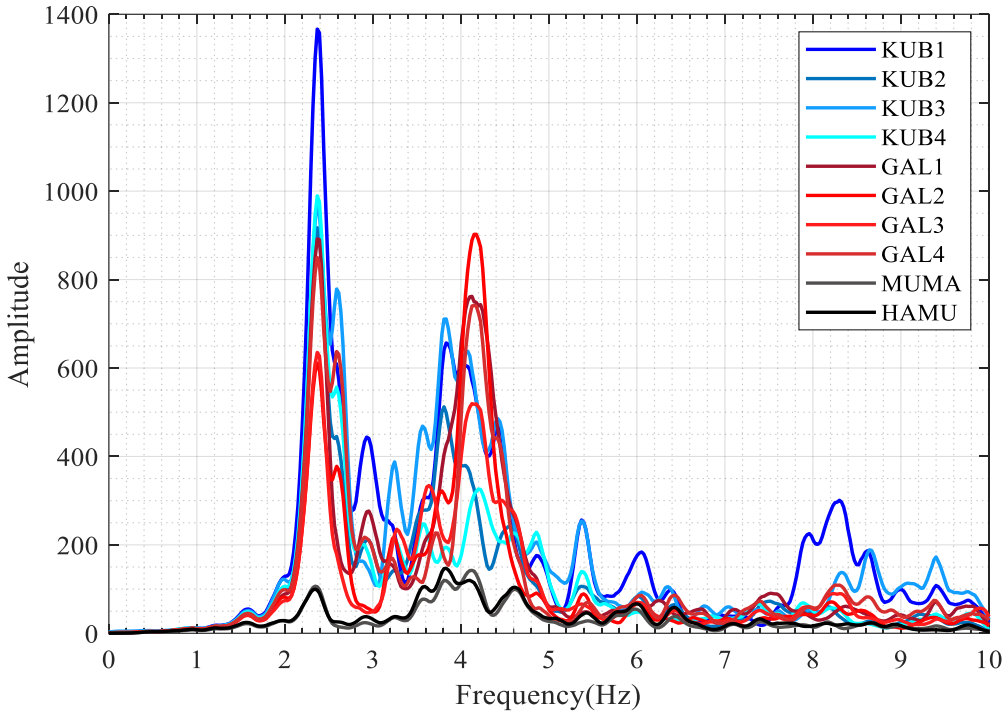

Figure 4.34. Horizontal-X: FAS of the M_W4.0 Cinarcik earthquake.

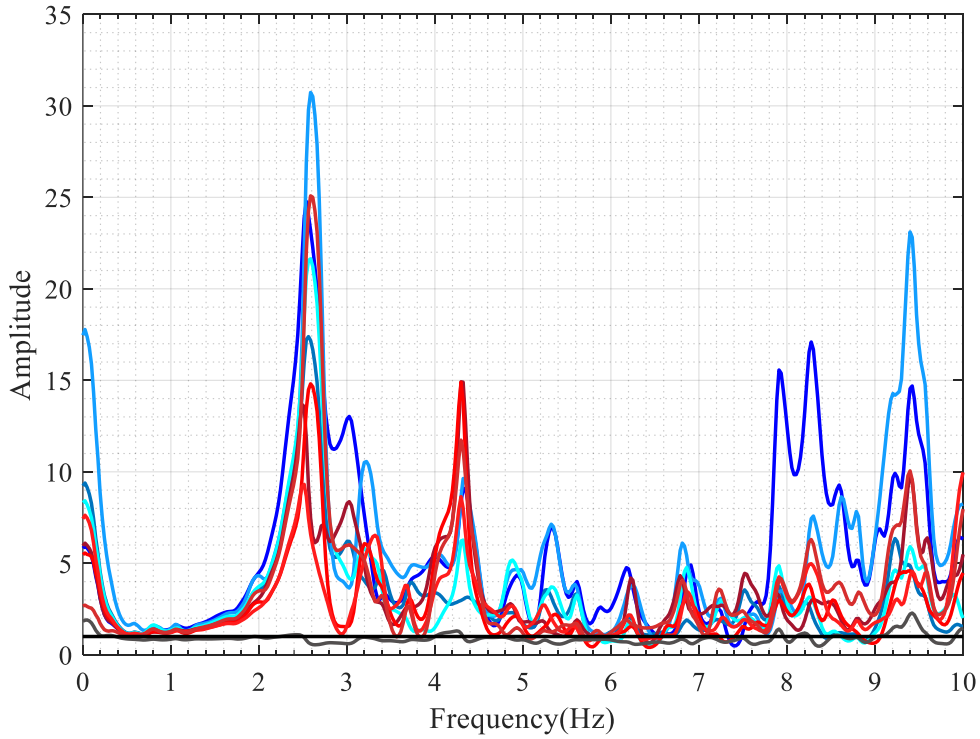

Figure 4.35. Horizontal-X: TF of the M_W4.0 Cinarcik earthquake.

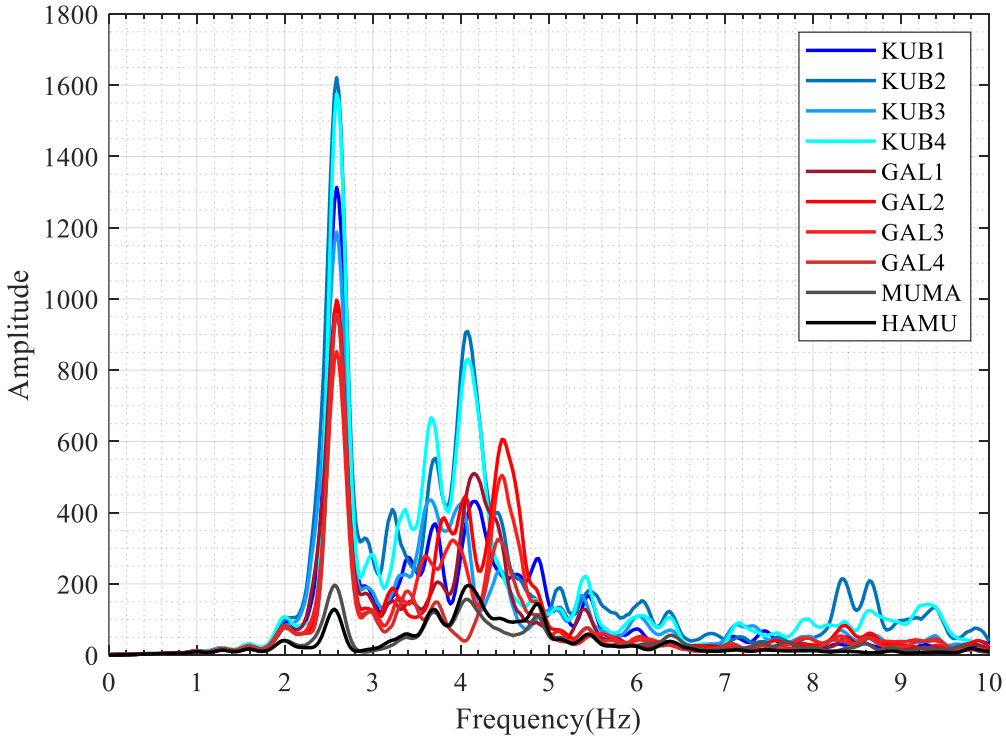

Figure 4.36. Horizontal-Y: FAS of the M_W4.0 Cinarcik earthquake.

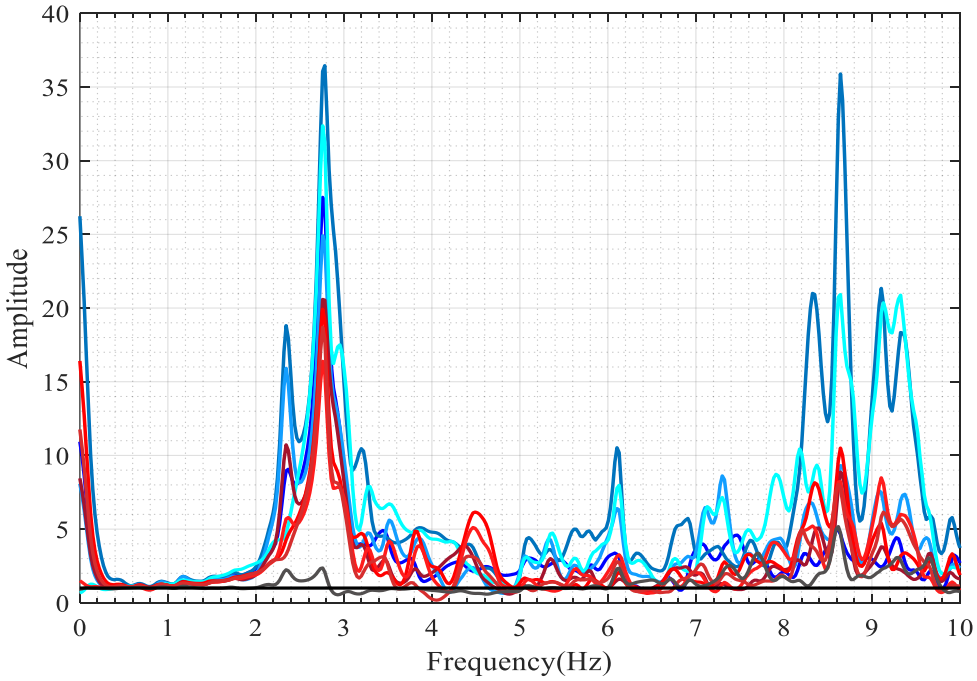

Figure 4.37. Horizontal-Y: TF of the M_W4.0 Cinarcik earthquake.

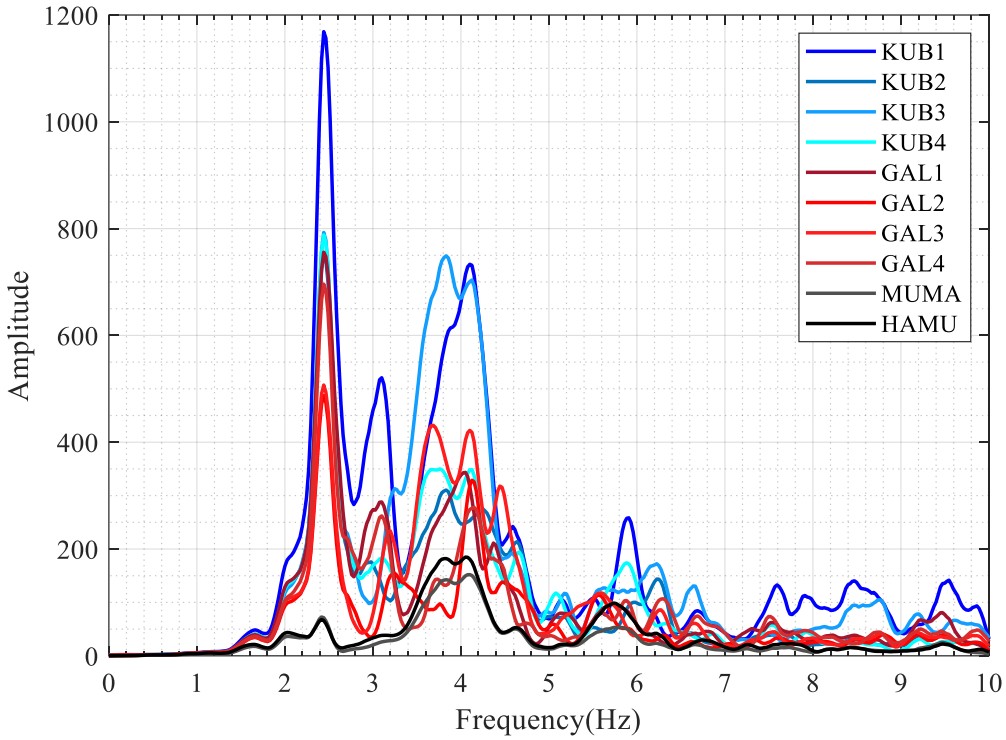

Figure 4.38. Horizontal-X: FAS of the M_W4.3 Kazikli earthquake.

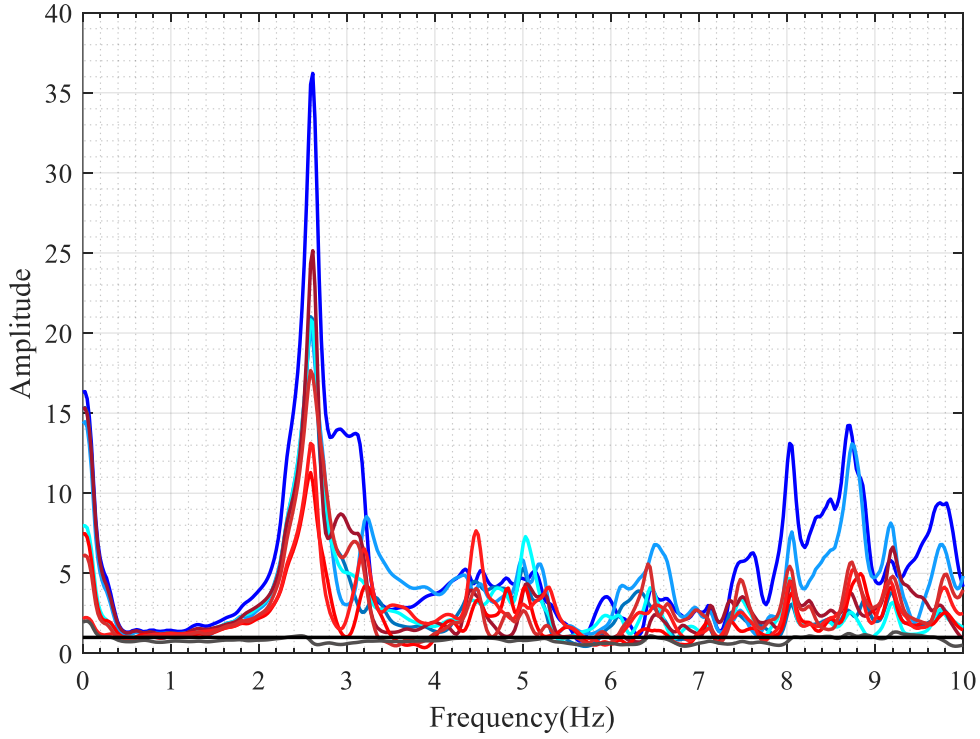

Figure 4.39. Horizontal-X: TF of the M_W4.3 Kazikli earthquake.

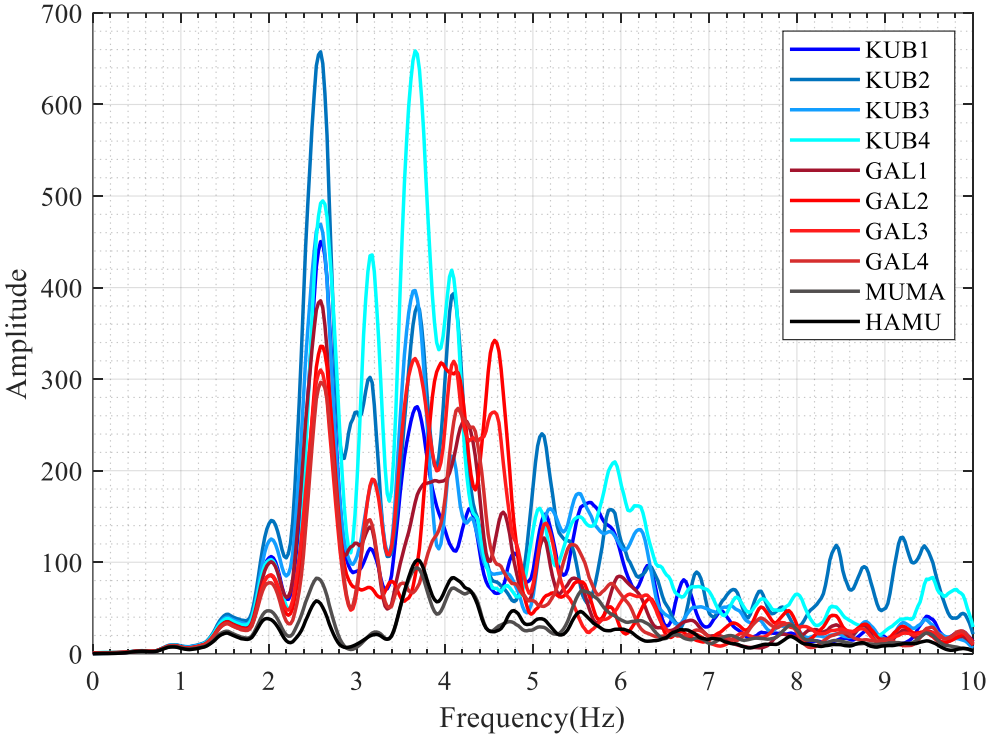

Figure 4.40. Horizontal-Y: FAS of the M_W4.3 Kazikli earthquake.

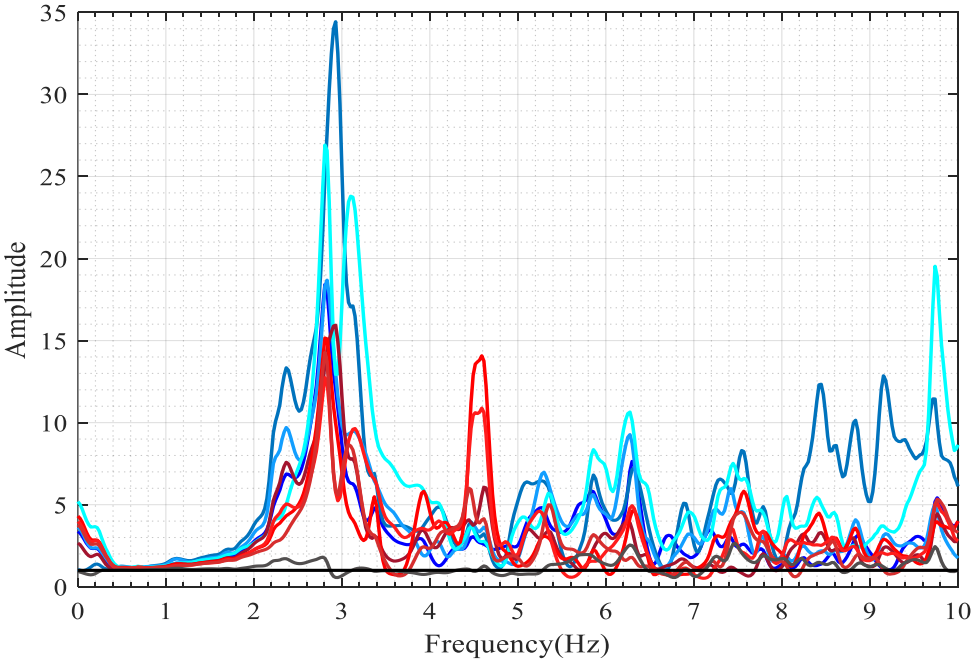

Figure 4.41. Horizontal-Y: TF of the M_W4.3 Kazikli earthquake.

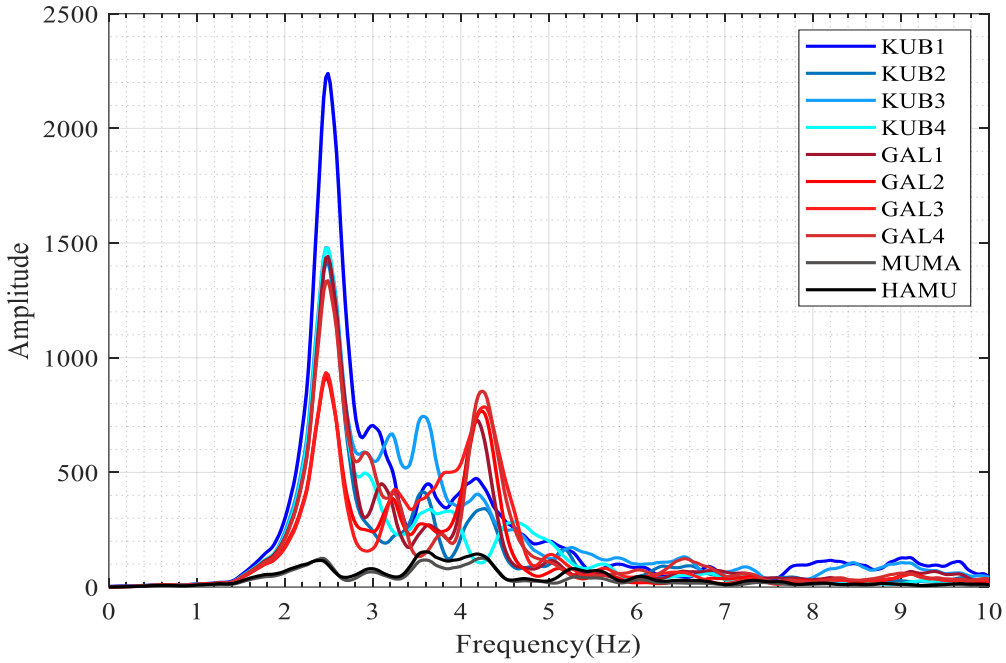

Figure 4.42. Horizontal-X: FAS of the M_W4.4 Yalova earthquake.

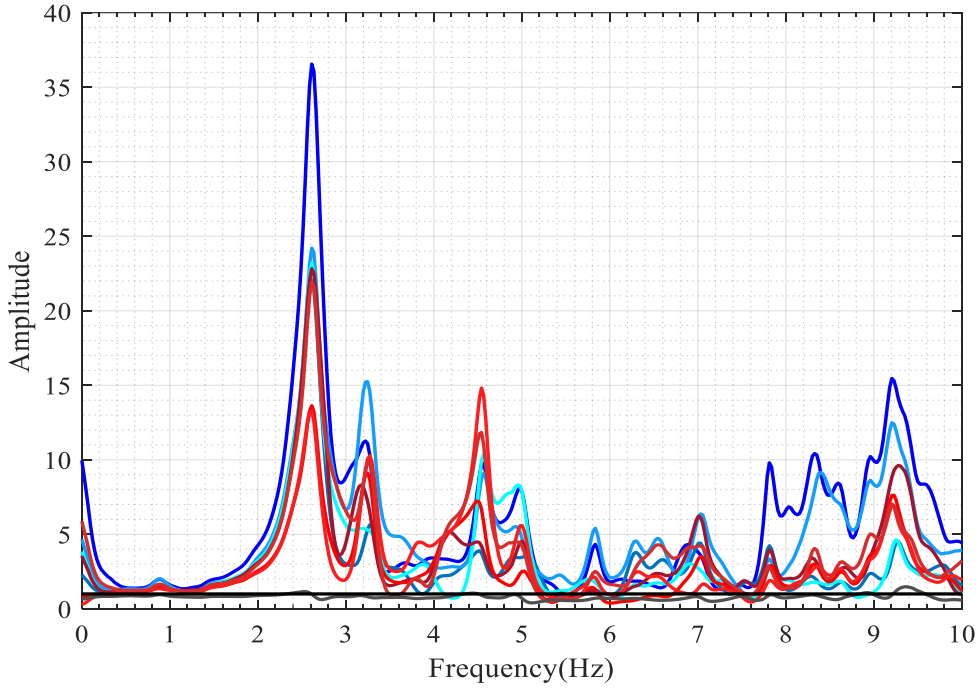

Figure 4.43. Horizontal-X: TF of the M_W4.4 Yalova earthquake.

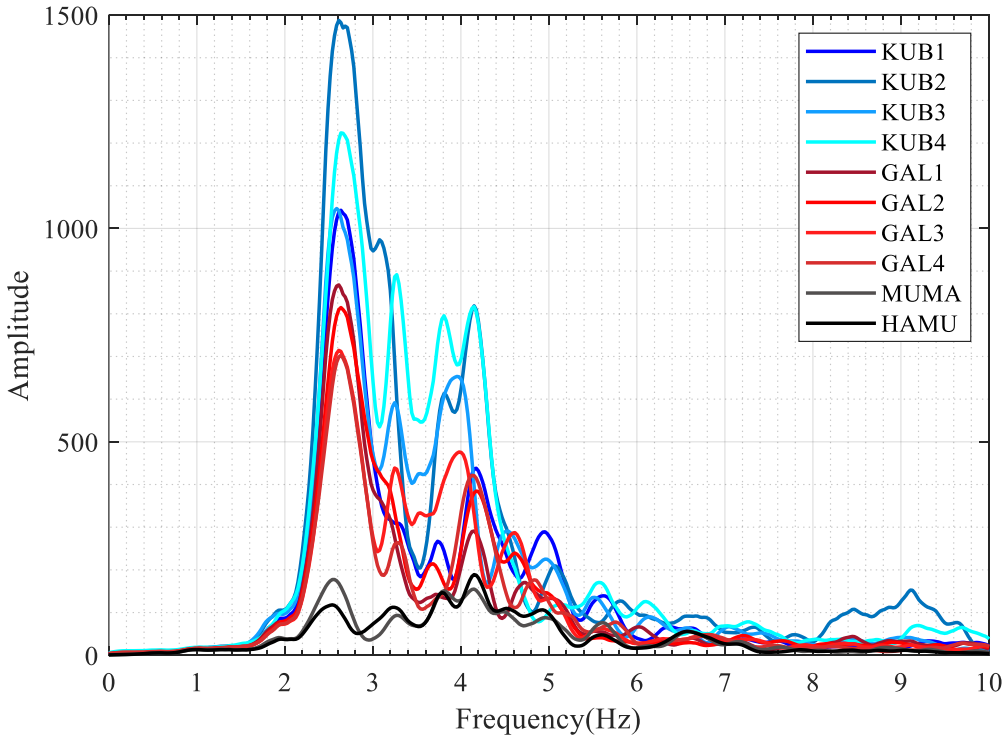

Figure 4.44. Horizontal-Y: FAS of the M_W4.4 Yalova earthquake.

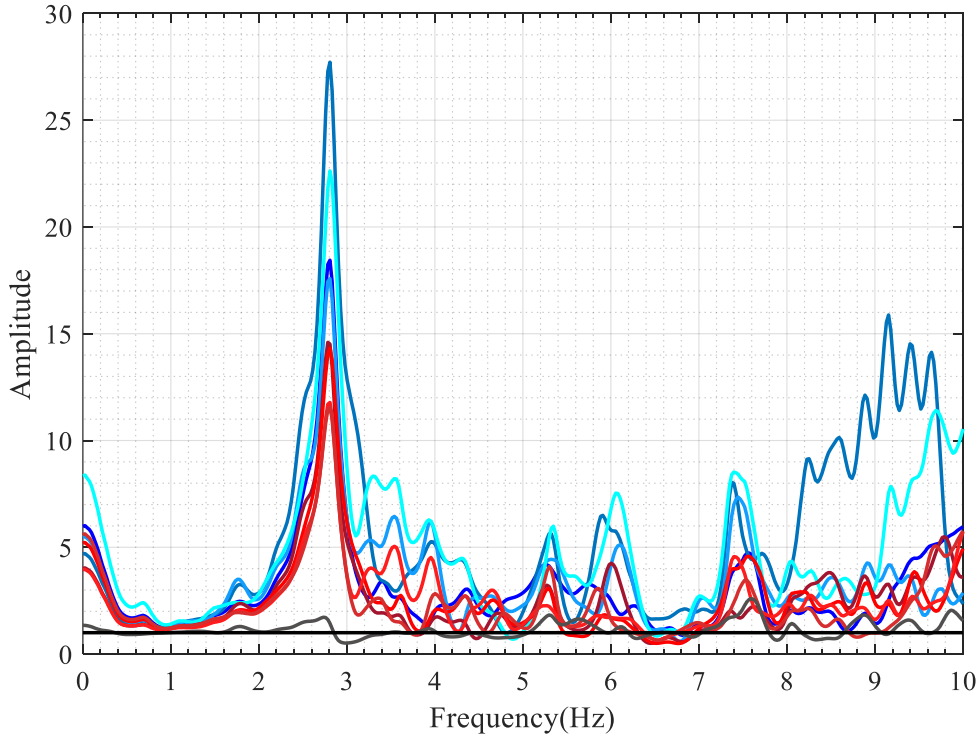

Figure 4.45. Horizontal-Y: TF of the M_W4.4 Yalova earthquake.

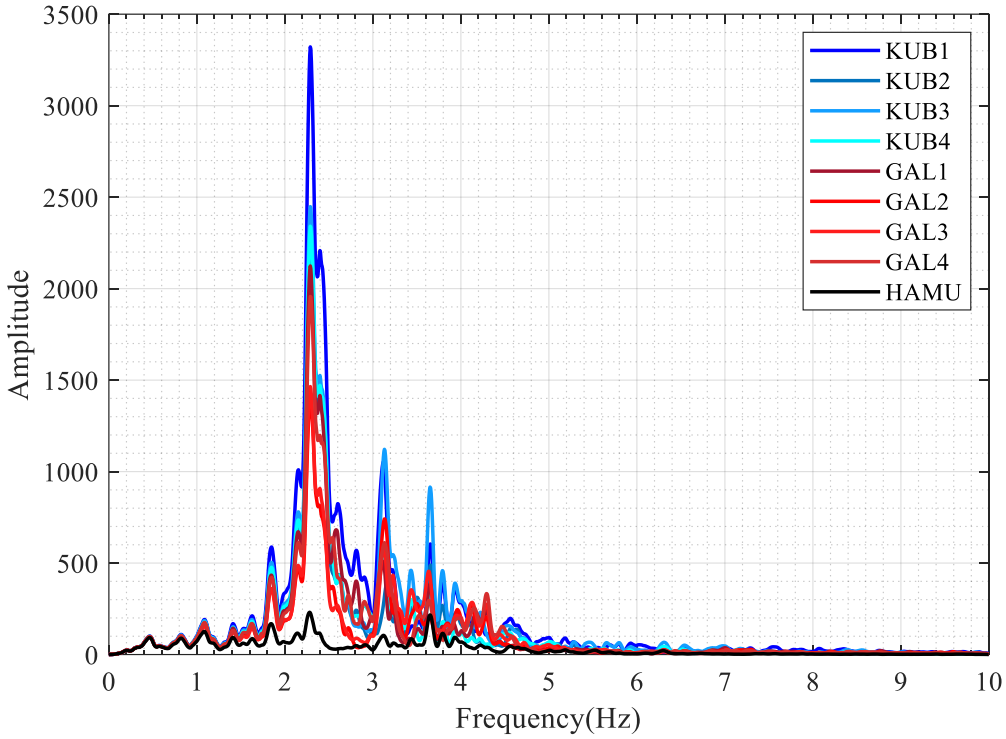

Figure 4.46. Horizontal-X: FAS of the M_W5.7 Silivri offshore earthquake.

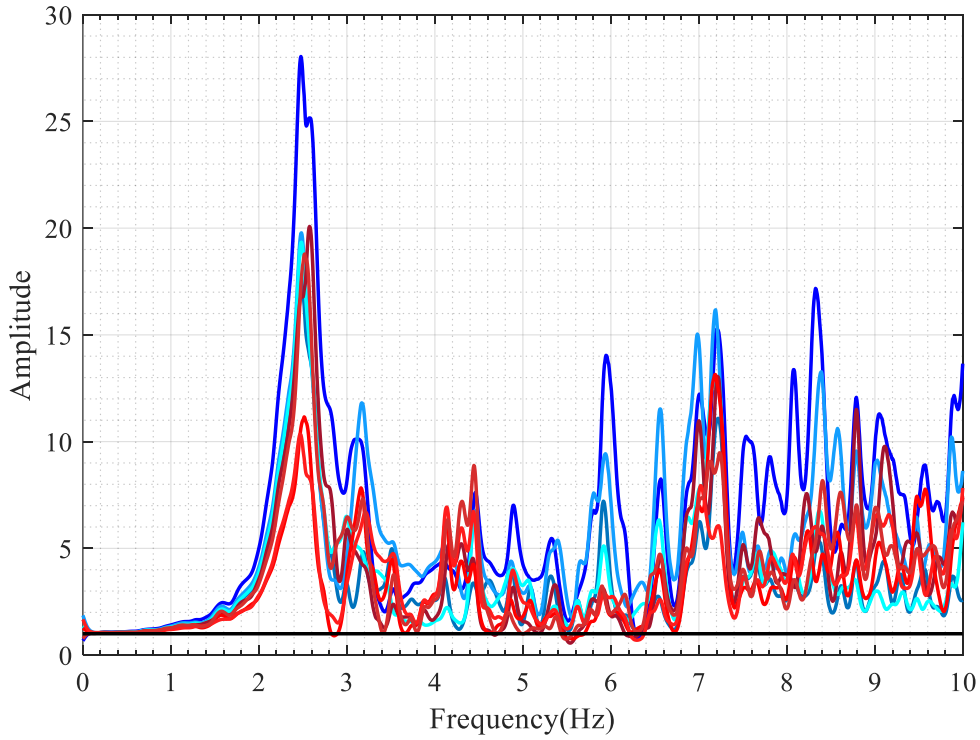

Figure 4.47. Horizontal-X: TF of the M_W5.7 Silivri offshore earthquake.

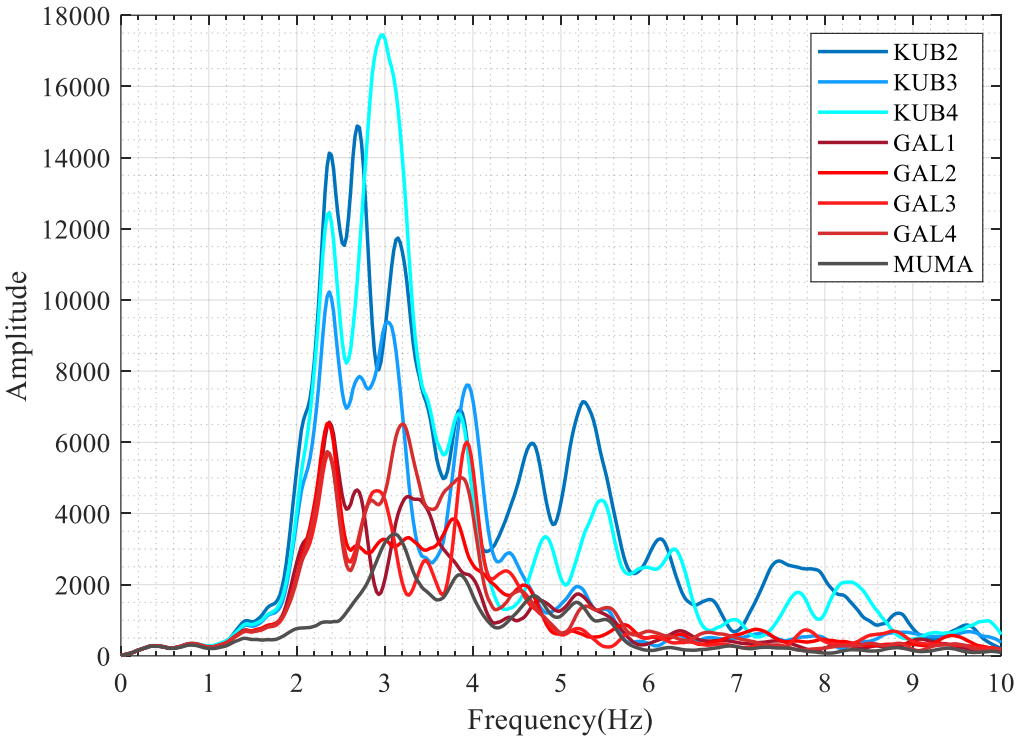

Figure 4.48. Horizontal-Y: FAS of the M_W5.7 Silivri offshore earthquake.

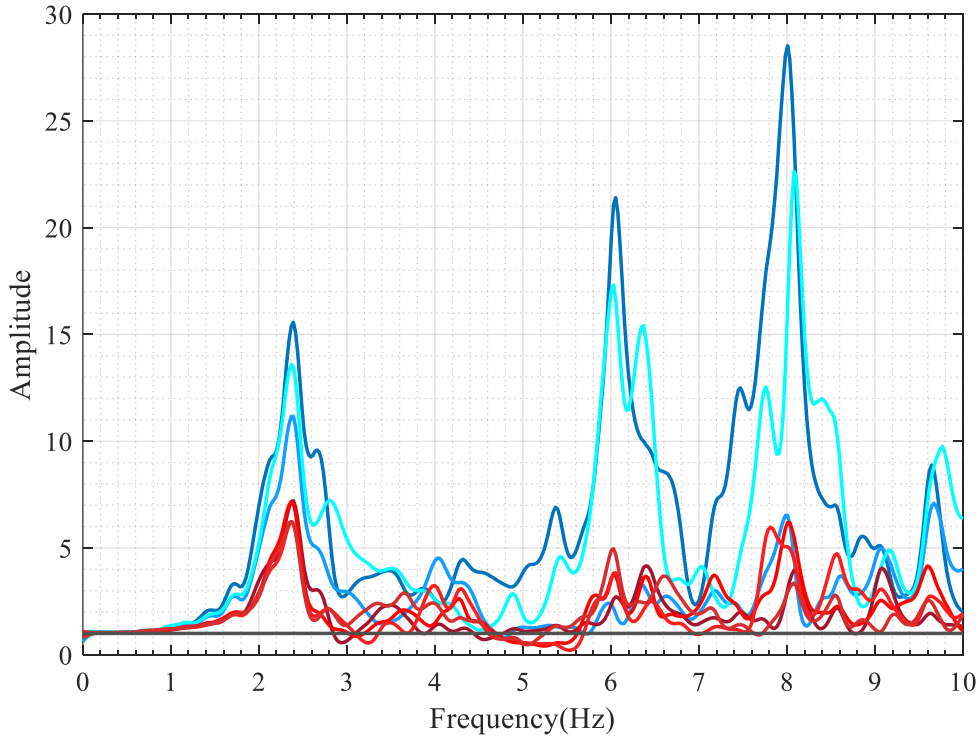

Figure 4.49. Horizontal-Y: TF of the M_W5.7 Silivri offshore earthquake.

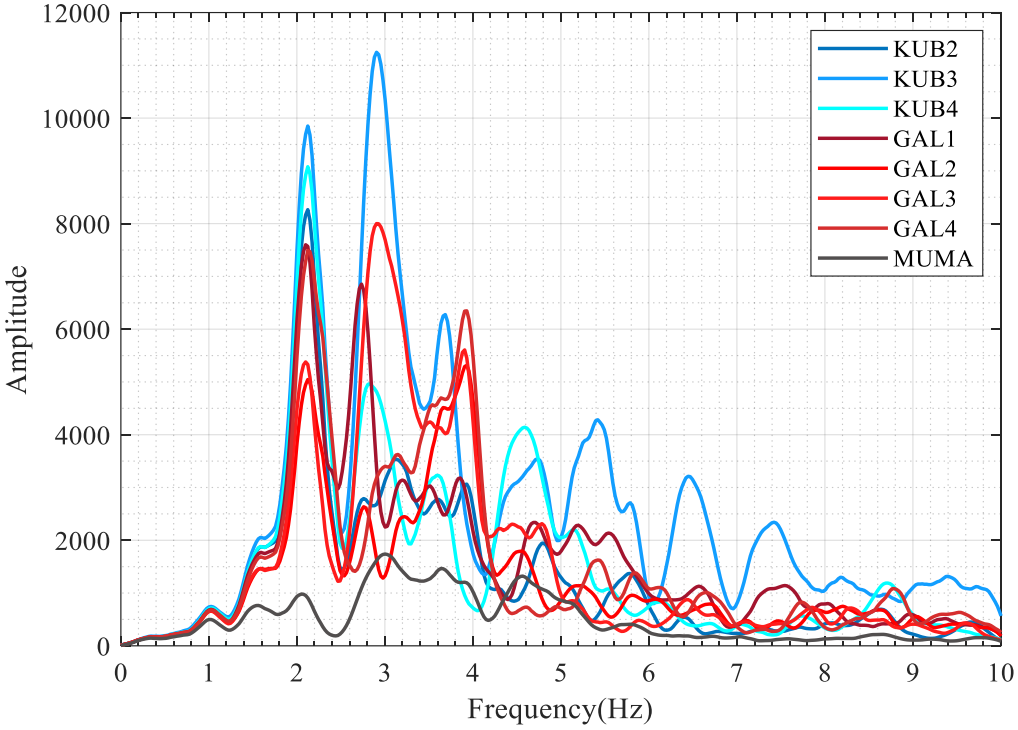

Figure 4.50. Horizontal-X: FAS of the M_W5.7 Aegean Sea earthquake.

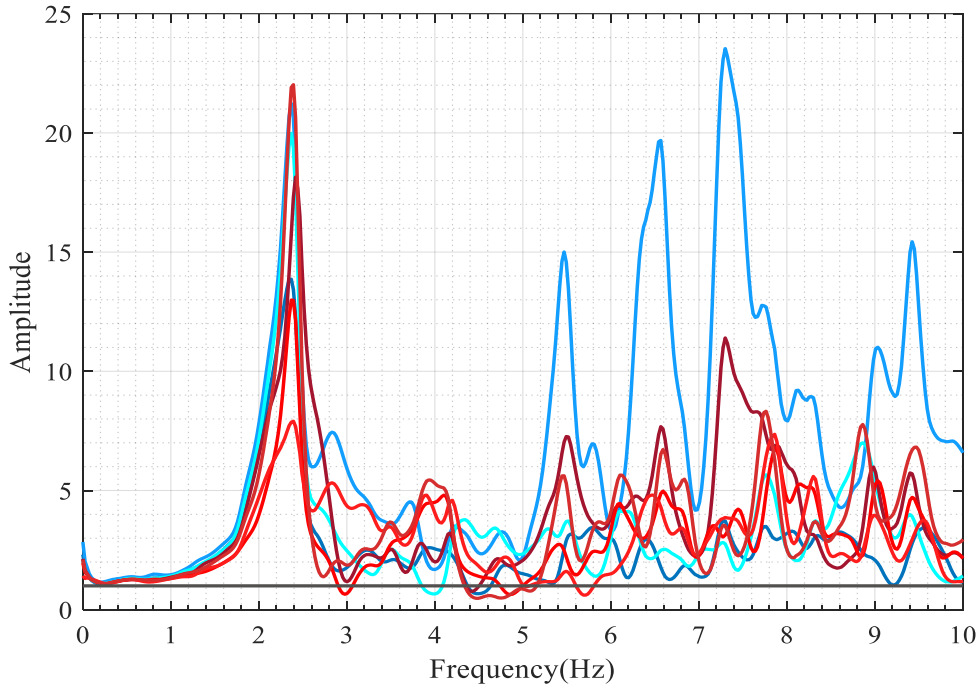

Figure 4.51. Horizontal-X: TF of the M_W5.7 Aegean Sea earthquake.

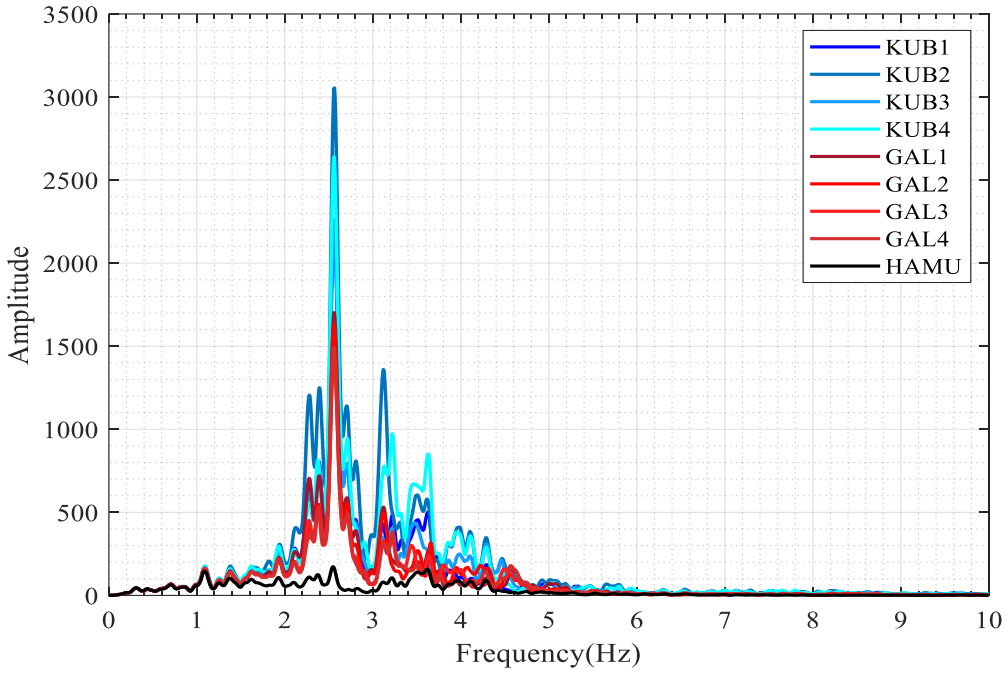

Figure 4.52. Horizontal-Y: FAS of the M_W5.7 Aegean Sea earthquake.

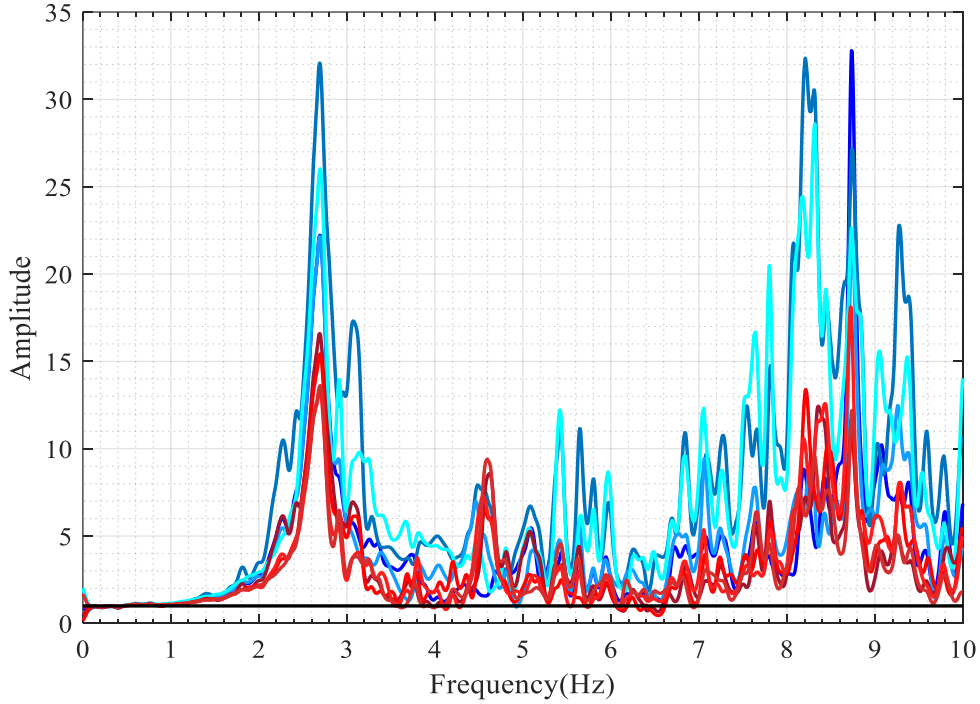

Figure 4.53. Horizontal-Y: TF of the M_W5.7 Aegean Sea earthquake.

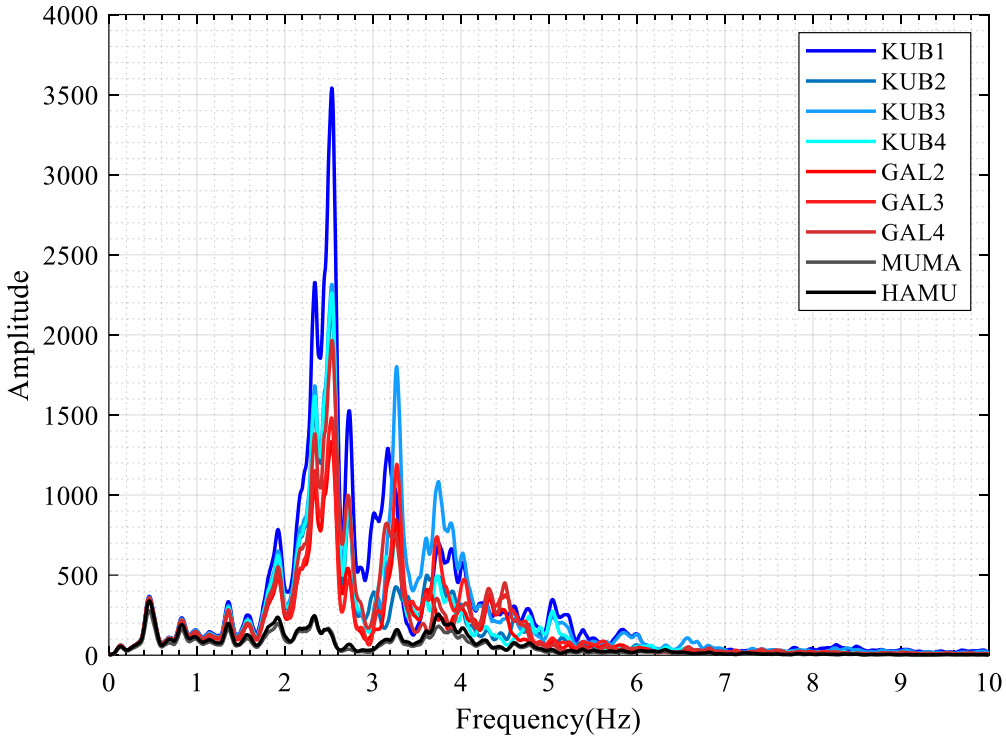

Figure 4.54. Horizontal-X: FAS of the M_W6.1 Aegean Sea earthquake.

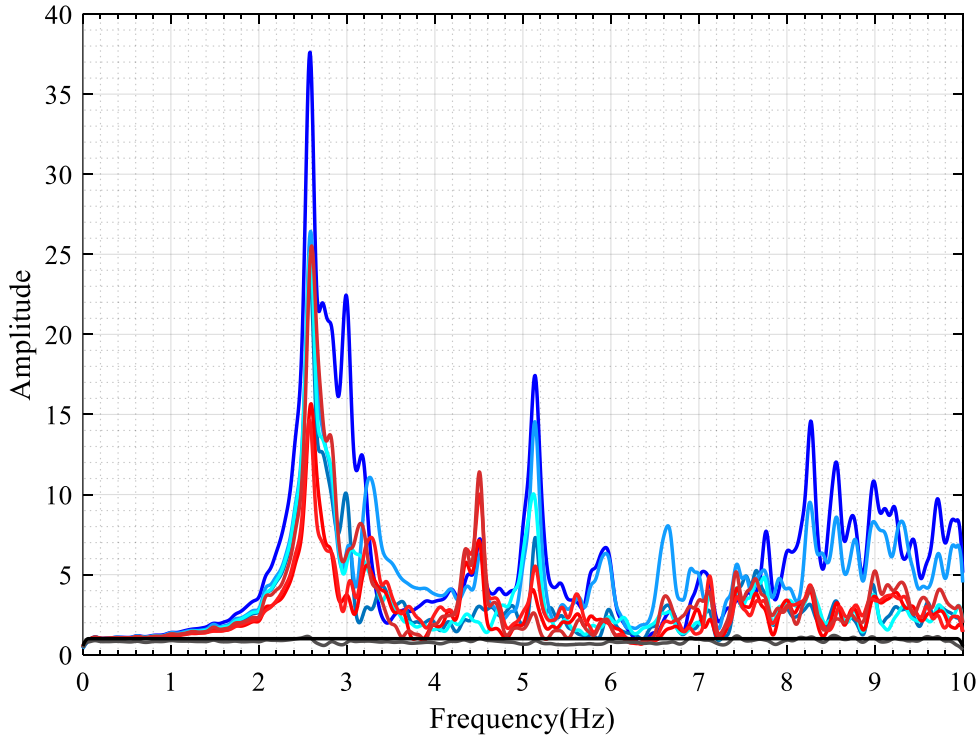

Figure 4.55. Horizontal-X: TF of the M_W6.1 Aegean Sea earthquake.

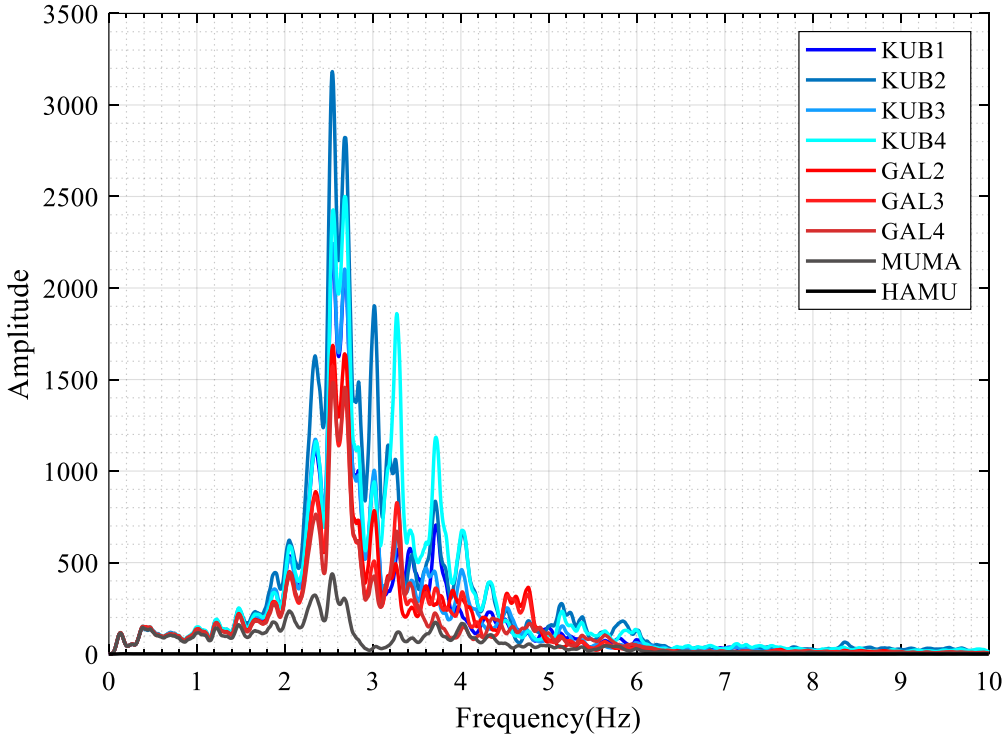

Figure 4.56. Horizontal-Y: FAS of the M_W6.1 Aegean Sea earthquake.

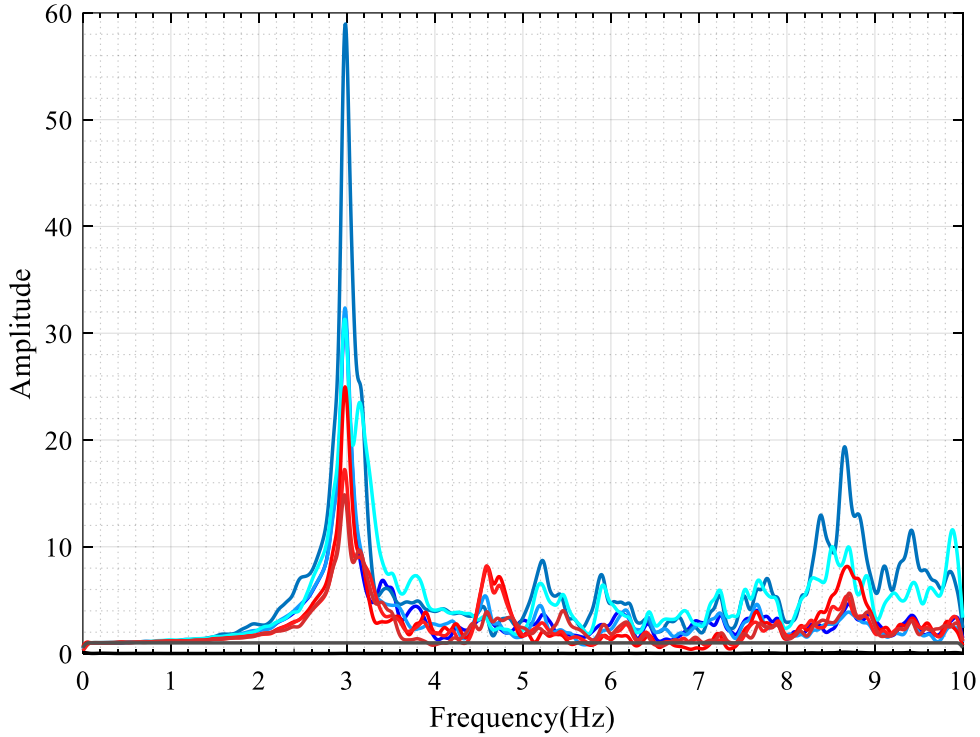

Figure 4.57. Horizontal-Y: FAS of the M_W6.1 Aegean Sea earthquake.

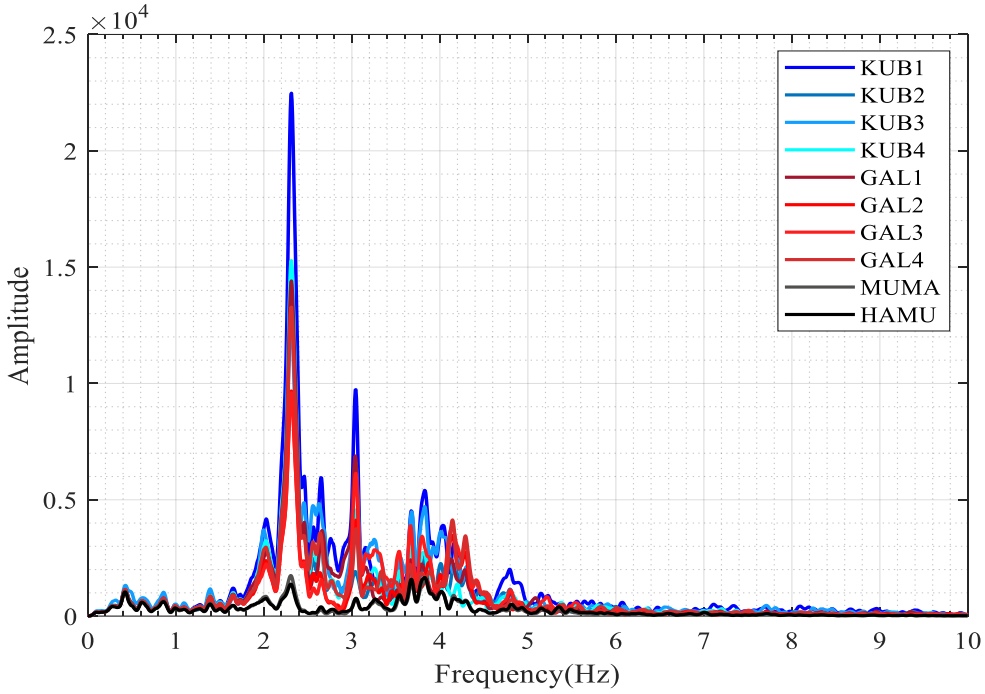

Figure 4.58. Horizontal-X: FAS of the M_W6.8 Aegean Sea earthquake.

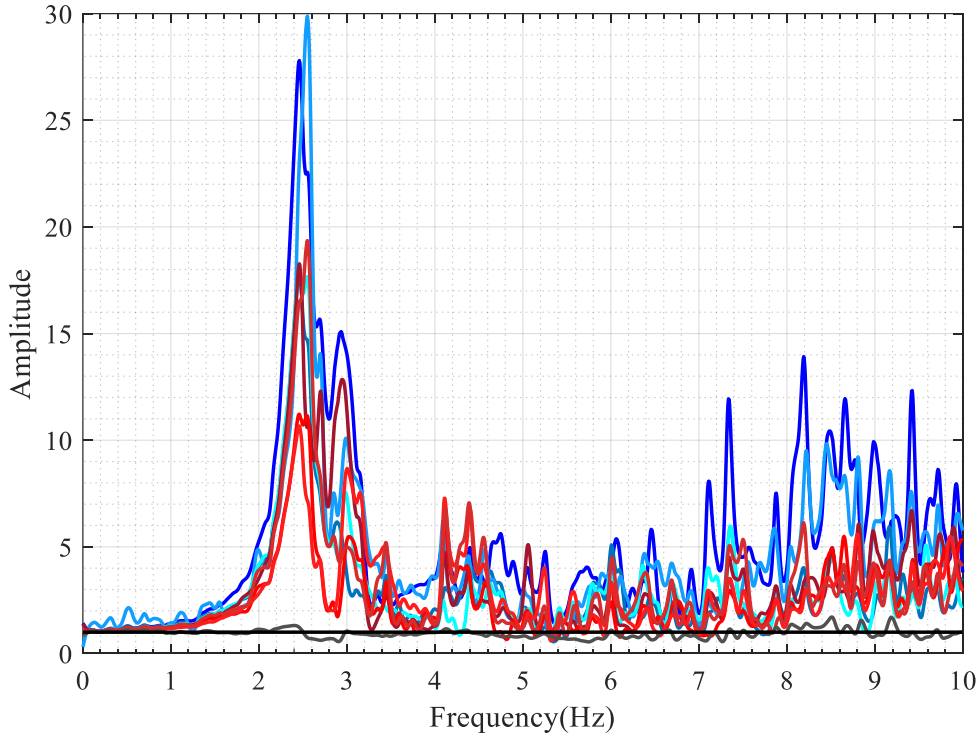

Figure 4.59. Horizontal-X: TF of the M_W6.8 Aegean Sea earthquake.

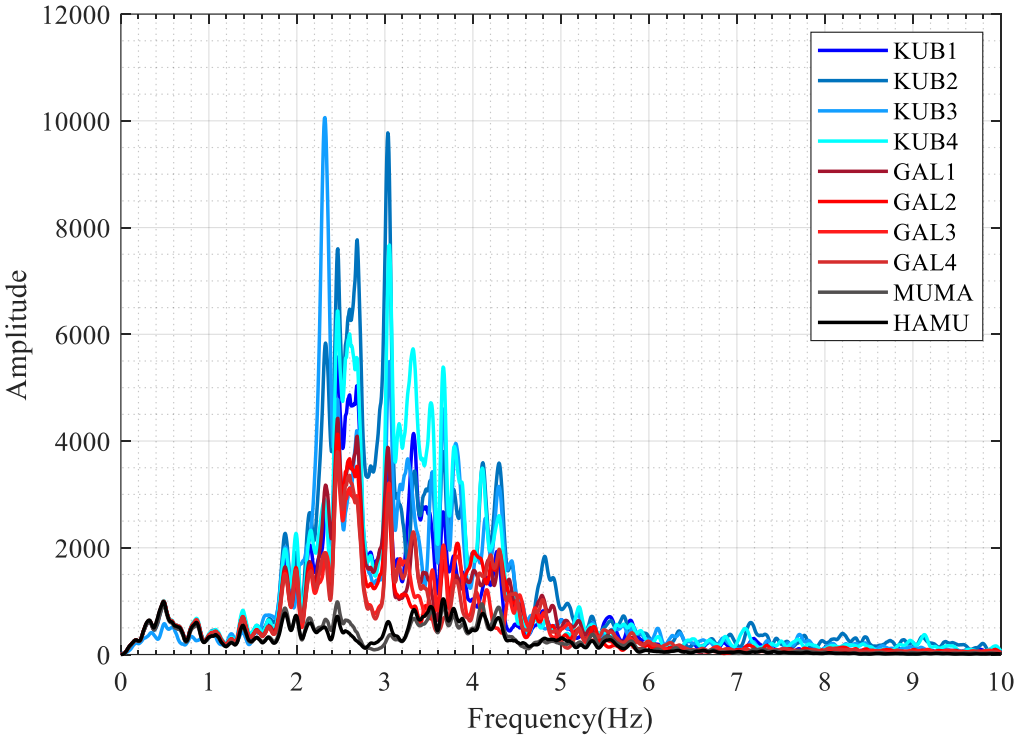

Figure 4.60. Horizontal-Y: FAS of the M_W6.8 Aegean Sea earthquake.

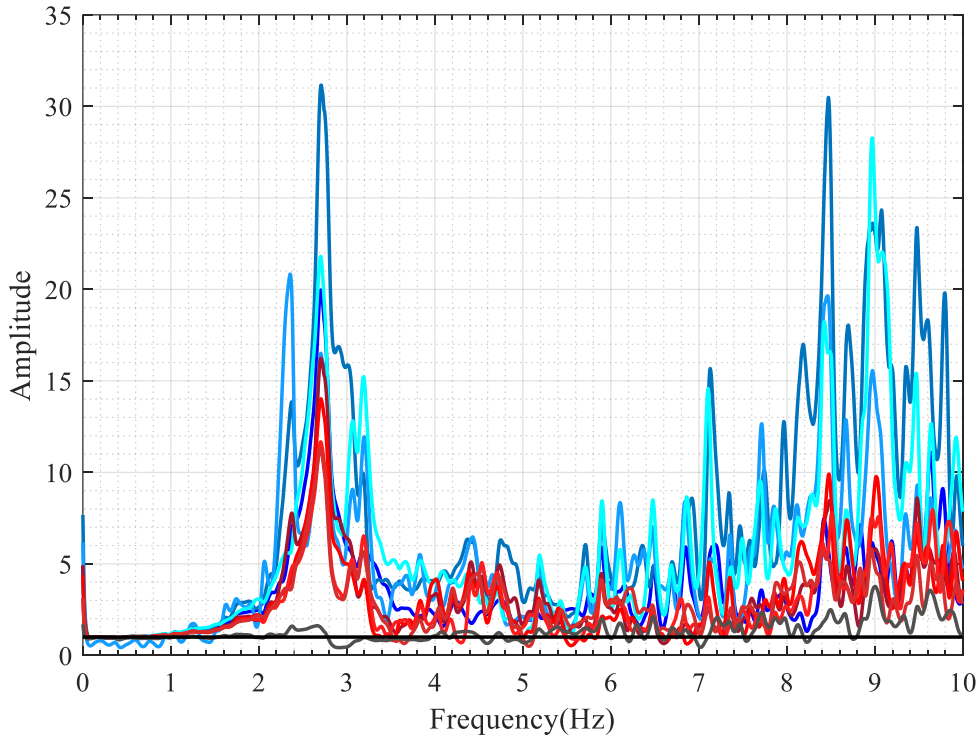

Figure 4.61. Horizontal-Y: TF of the M_W6.8 Aegean Sea earthquake.

4.2.3. Particle Motions and Mode Shapes

How a particular structural reference point, which can be represented at the location of the sensor in our approach, vibrates during an earthquake can be shown by utilising displacement time series. For depicting the movement of a specific point in a structure, the particle motion method gives the shape content and its displacement amplitudes by combining its two horizontal counterparts perpendicular. Furthermore, related modal shapes can be obtained by applying narrow band-pass filters around the modal frequencies to the signal.

A single particle motion allows a sensor-based assessment; meanwhile, it is also favourable that combining several sensors to observe the entire structural response. Particle motions belonging to fundamental events with large acceleration amplitudes are studied to understand the behaviour and response levels of the primary structural system of the mosque during strong excitations. At the first glance, the structural system was found more vibratory in the southern portion since the displacements at three locations where sensors KUB1, KUB2 and GAL1 are placed had been reached more significant levels than others (Figure 3.3). An attempt to comprehend this observation can be made.

Once the particle motions are plotted, the response levels within the structure can be evaluated by visually drawing a comparison among the sensors. Obtained displacement maxima along both X- and Y-axis are used to compute horizontal areas the structure had displaced during the strong excitation (Figure 4.62). Only earthquakes with the largest acceleration amplitudes are considered with the complete sensor-status at the dome and gallery levels (In table 3.1, five earthquakes numbered 22, 57, 74, 68, and 94, whose magnitudes varies from 3.9 to 6.8). In each sensor, geometric means of displacement areas are calculated. The geometric means of estimated areas are also determined for each sensor group. Among four dome-level sensors, those coded by KUB1 and KUB2 are more responsive in the order of 9% and 10.6%, respectively. On the other hand, the response level at sensor GAL1 is significantly higher, 24.9%, than the group average. Overall, it can be

said that the mosque is more responsive on the southern side, i.e., the triangular part framing the south pendentive (please refer to figure 3.3).

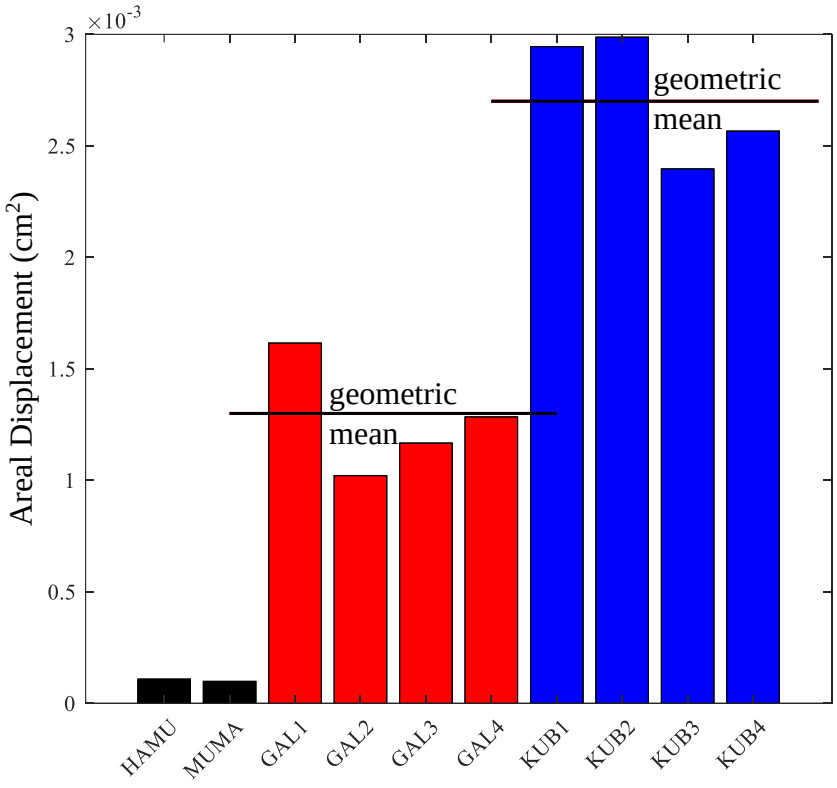

Figure 4.62. The sensor-based comparison of displacements.

The direction that an earthquake originates from may dominate the particle motions. For two earthquakes with moderate and large magnitudes, it is observed that the displacement levels were increased along with the direction of origination. Response levels would have been affected by the azimuthal properties of these selected earthquakes, all of which originated from the southeast and west, i.e., azimuthally 150º - 260º (Figure 4.63). This defined portion of the prayer hall more or less corresponds to the same that monitored with these sensors reaching larger response levels. Figures Figure 4.64 (the M_W6.8 Aegean Sea) and Figure 4.65 (the M_W4.3 Kazikli/Gursu) exhibit particle motions of the mosque, allowing a visual evaluation. An apparent example is evident for how the indicated portion differs in structural response. It should also be taken into consideration that the pillars GAL1 and GAL4 associated with extend to the deeper, and it was shown that this could be a reason for

the larger amplitudes. As well as, this could be another factor governing the response levels of the primary system.

Eight earthquakes with the most significant acceleration levels are considered and analysed for defining mode shapes and determining the narrow band-pass filters around the modes among all the catalogue events. These are provided in Table 4.2. Frequencies are identified using input-to-output transfer functions since the mosque is subjected to the SSI. In our methodology, sensor HAMU at the basement level was the reference station for the input. However, sensor MUMA at the ground level had to be used as input since the HAMU was dysfunctioning during two events, all of which are indicated with an asterisk in the table.

Table 4.2. Narrow band-pass filtering gaps (Hz).

Earthquake	**1st**	**2nd**
	X	**Y**
6.8 Aegean Sea	2.40-2.60	2.64-2.74
*6.1 Aegean Sea	2.48-2.68	2.80-2.85
*5.7 Silivri Offshore	2.25-2.45	2.34-2.44
5.7 Aegean Sea	2.40-2.60	2.64-2.74
4.4 Yalova	2.55-2.70	2.70-2.90
4.3 Kazikli	2.55-2.68	2.75-2.90
4.0 Cinarcik	2.48-2.68	2.70-2.85
3.9 Marmara Sea	2.43-2.63	2.70-2.85

The Sultan Ahmet Mosque is a massive and complex structure, hence resulting in a complex seismic response that other effects should be considered. Beyond material characteristics or non-linearity, it is intended to develop an approach within the scope of approaches that can be associated with structural vibrations. In this context, an animation module to depict particle motions is scripted on MatLab. The use of this module has benefited us in two ways. First, it eased the determination/identification process of mode shapes. The second one is that the whole motion isolated within time windows became possible and associable with earthquake-wave characteristics changing in time. The dominance of vibrations from the body wave portion of an earthquake was found out.

In defining the mode shapes, an animation script simultaneously depicting the movement in each sensor is used. The main events in Table 4.2 are used for analyses, and the first two vibrational modes exhibiting lateral motions are sampled. The 1st mode mainly was found diagonal with a tendency to the y-axis, i.e., it was not highly dominant along a horizontal axis (Figure 4.66). On the other hand, lateral motions dominantly from the origin toward +/– y-axis was revealed for the 2nd mode. The maximum displacement levels were reached during the M_W5.7 Silivri earthquake in 2019. Although there was an inactive sensor at the dome base (KUB1), the 2nd mode shape is given with this event (Figure 4.67).

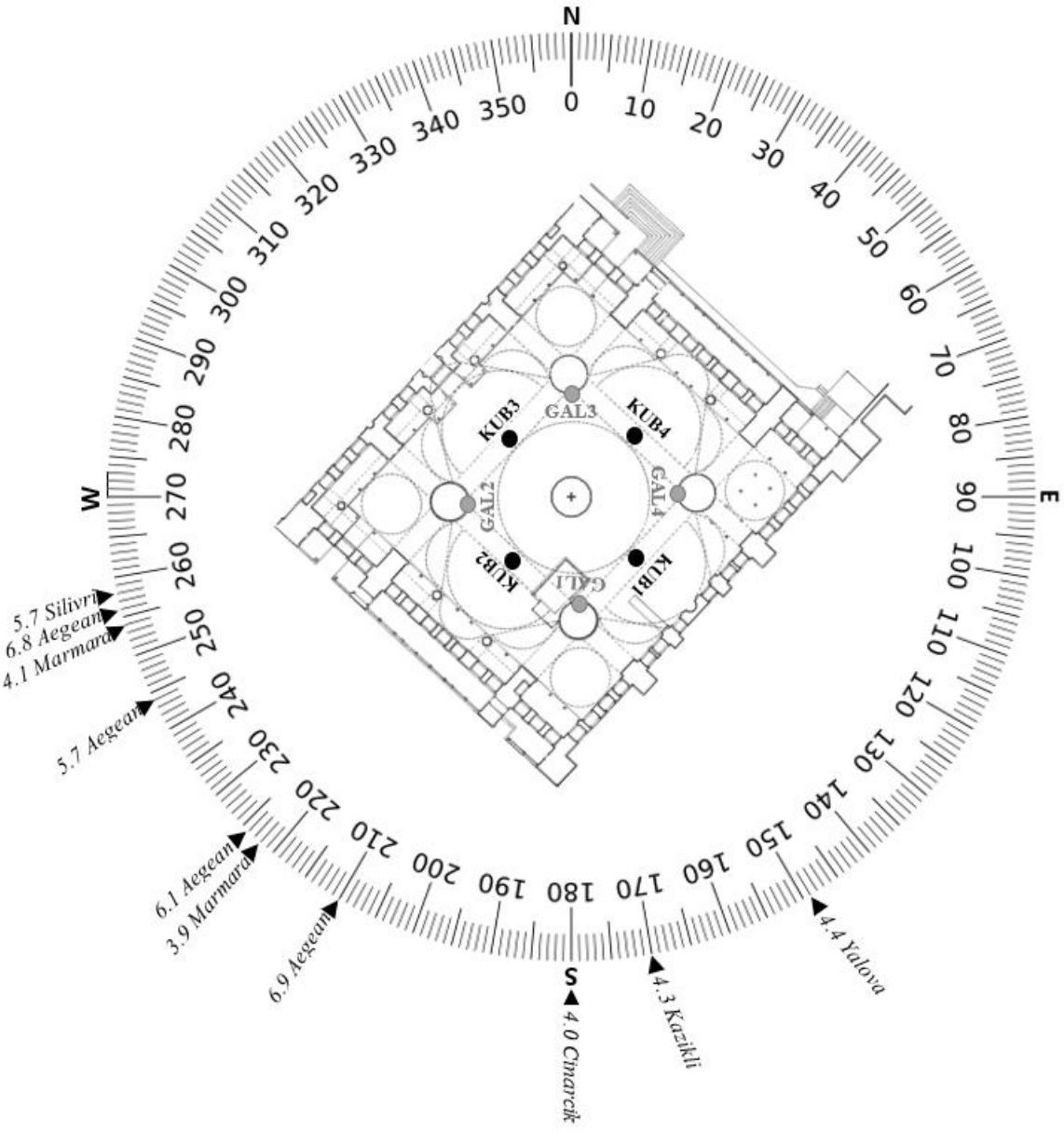

Figure 4.63. Origins of the selected earthquakes with respect to the mosque.

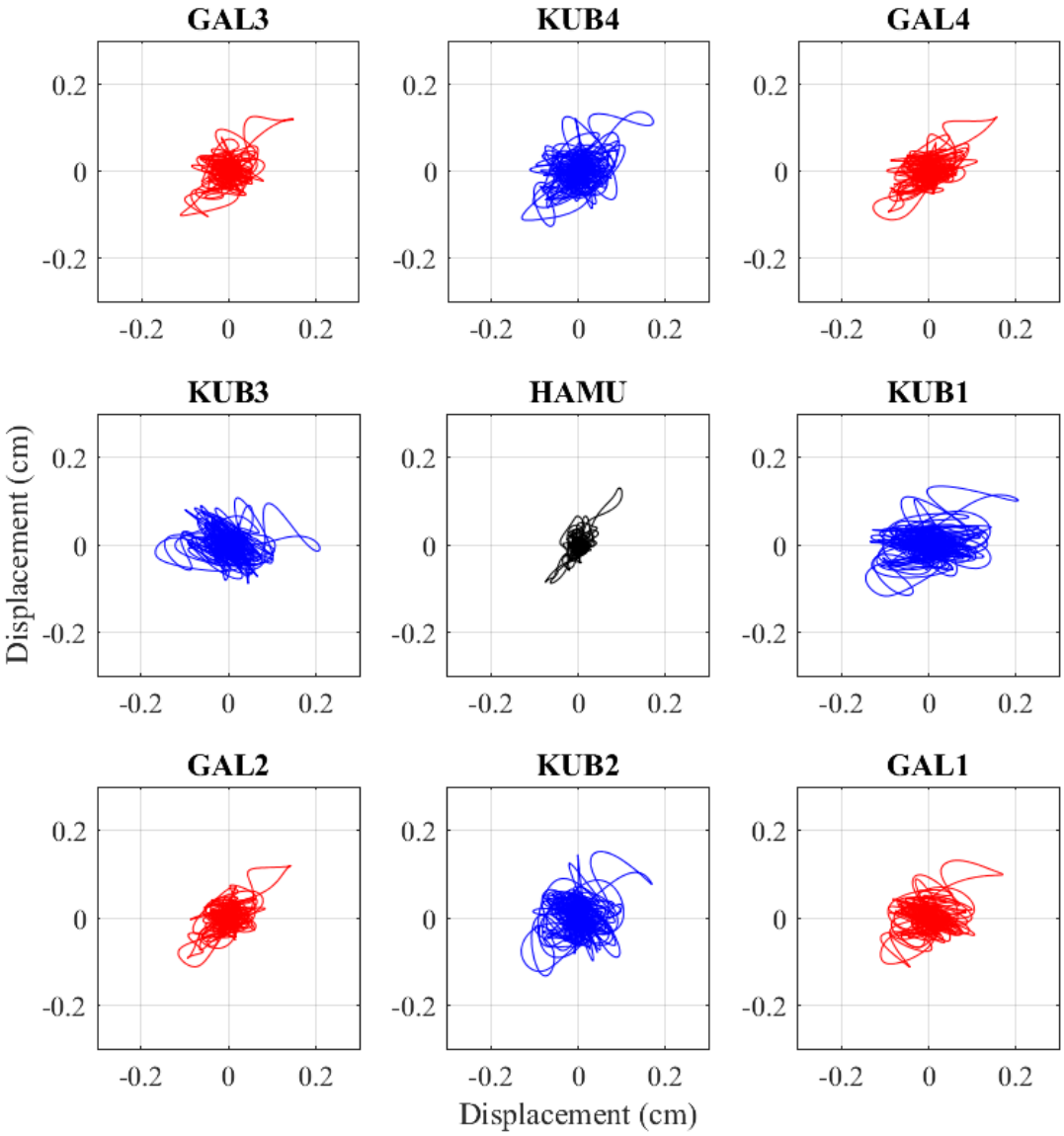

Figure 4.64. The entire particle motion observed during the M_W6.8 Aegean Sea event.

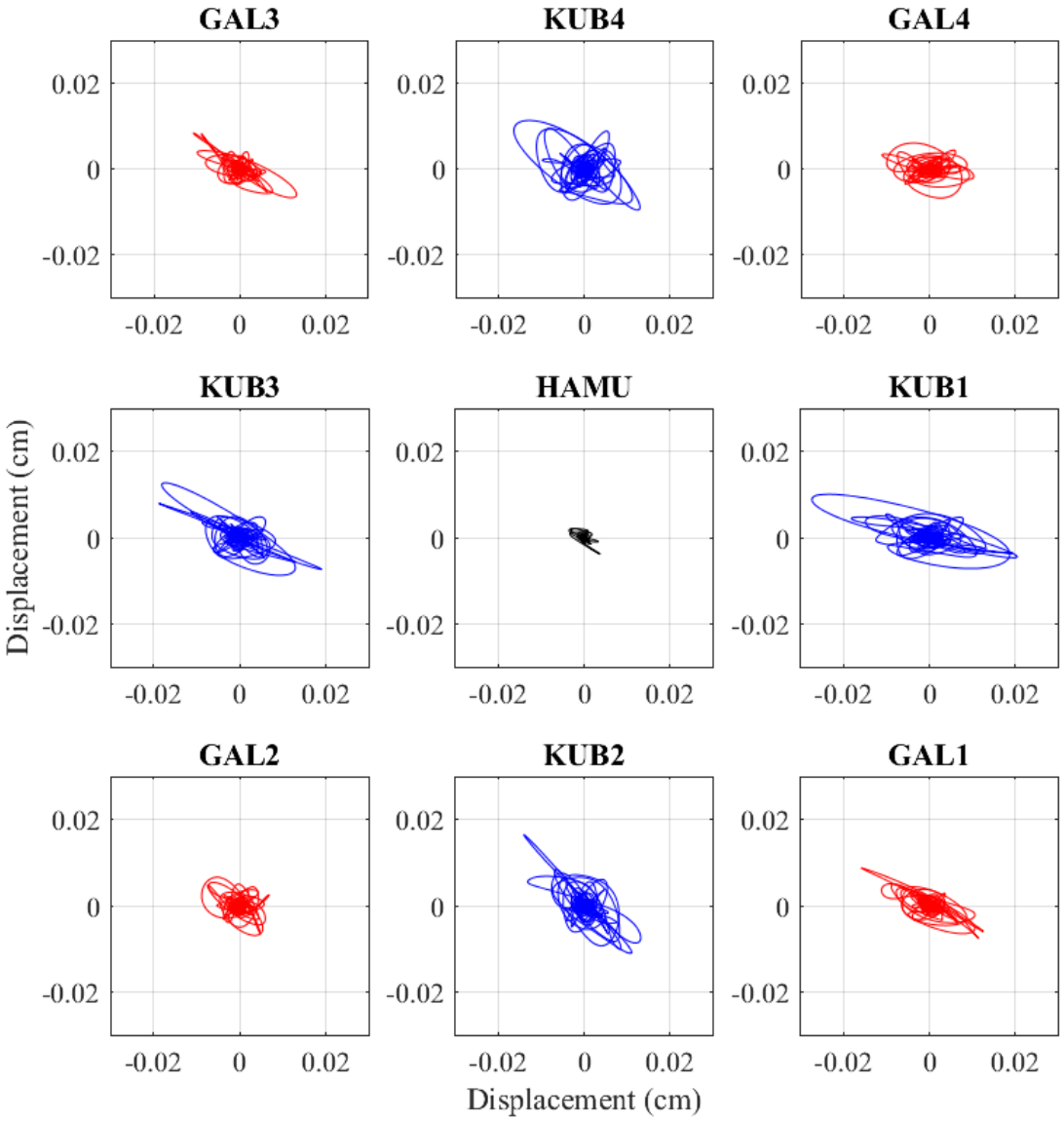

Figure 4.65. The entire particle motion observed during the M_W4.3 Kazikli/Gursu event.

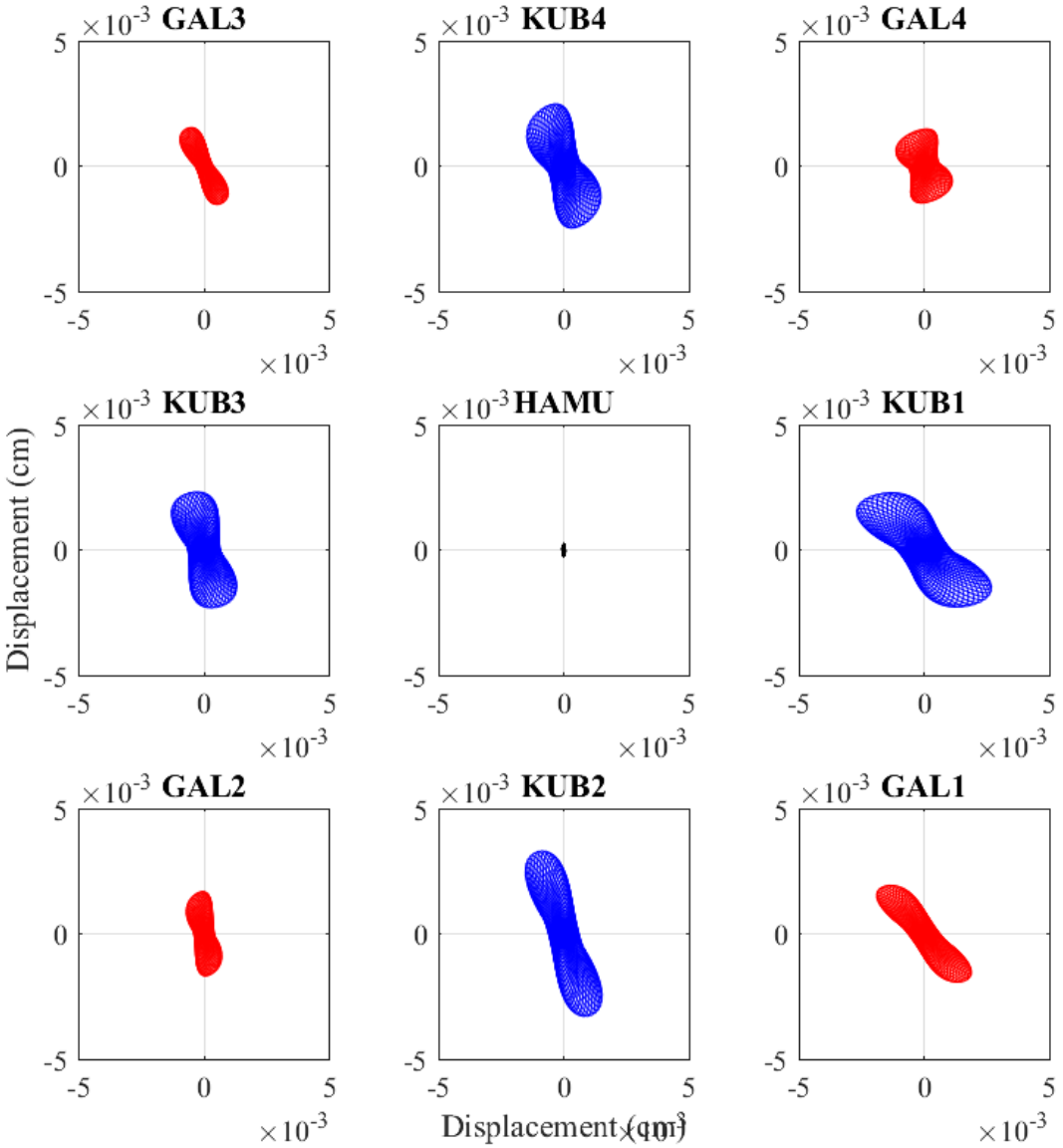

Figure 4.66. The 1st mode shape (lateral) observed during the M_W4.3 Kazikli earthquake.

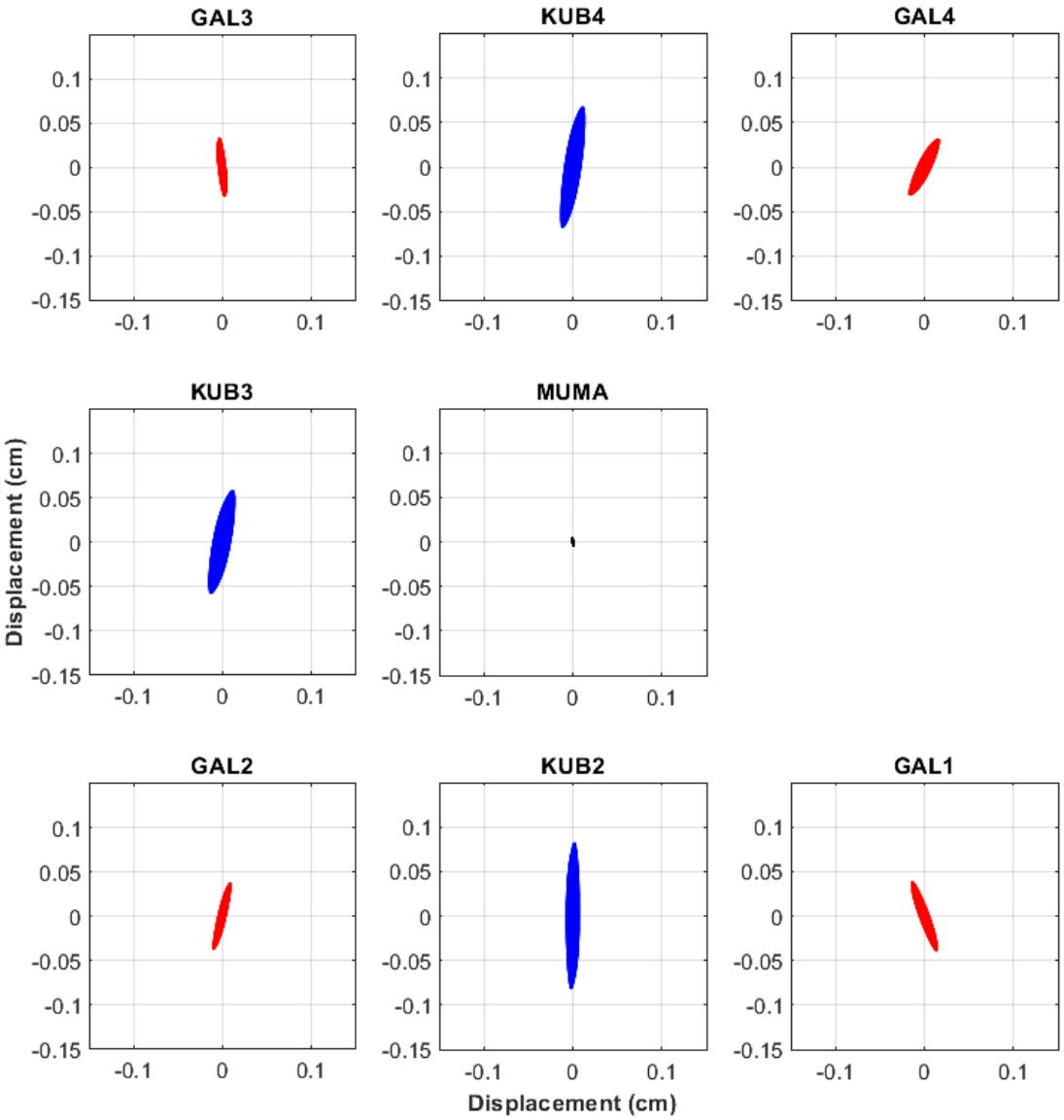

Figure 4.67. The 2nd mode shape (lateral) observed during the M_W5.7 Silivri offshore earthquake.

5. ROCKING

With respect to its foundation, the rigid-body motion of an entire structure is the brief definition of rocking (Safak and Cakti, 2014). This behaviour is mainly observed in the high-rise, especially slender, structural systems. In our case, minarets would be a proper element for this kind of assessment but no minaret vibrations had been monitored.

The fact reported for the May 5, 1766 earthquake can be deemed an indicator or clue of rocking response considering a single-degree-of-freedom system, a minaret, i.e., multi-block rigid body. Although the exact collapse mechanism is unknown, ‘Minaret 3’ was collapsed along X direction from its third balcony, over three small domes of outer portico as provided in section 2.3. A minaret has a considerable vulnerability that can be highly affected by its wall thickness and slenderness, and rocking can be an important effect in its response. In theory, the slenderness ratio of this minaret is calculated as approximately 11.05; 36.427 m, length of the slender body / 3.294 m, exterior diameter (IM Architecture, 2017). Several examples based on the slenderness ratio of minarets can be found in the literature; for instance, calculated values 11.87 for the Edirnekapi Mihrimah Sultan Mosque, 5.85 for the Hagia Sophia, and 12.80 for the Suleymaniye Mosque (Cakti, 2020). All of the examples are from Ottoman architecture. Minaret 3 In conclusion, a minaret has still a considerable vulnerability that can be affected by its wall thickness and slenderness. In contrast, the massive masonry structure - the mosque - survived without vital damage.

Although it is most observable in high-rise structures, whether a 400-year-old mosque has a rocking impact in its nature is another matter needed to be questioned. As expected, the rocking evaluation can be generated within the limitations of the monitoring system in the mosque, i.e., an insufficient number of ground-level sensors. A fit technique for our case is first given in the study of Safak and Celebi (1991) and concluded as a rocking analysis technique in 2014 by Safak and Cakti. The approach requires vertical-motion data collected at three or more corners of the foundation and horizontal-motion data of upper structural levels. The first step is determining a common frequency that is identical for all the

recordings, called rocking frequency. After applying a narrow band-pass filter in a range around the determined rocking frequency, the difference taken between the filtered vertical-motion data will represent the rocking vibrations.

The Sultan Ahmet Mosque SHM System have only two sensors that can produce vertical-motion input on the foundation level. The first one is the sensor MUMA installed at the bottom of the southwest main pillar on the prayer hall ground, and the second is the sensor HAMU installed at the southwest corner of the basement floor. Despite the fact that the minimum number of vertical-motion data does not suffice, these two inputs are worth examining. On the other hand, there are eight sensors, GAL and KUB sensors, usable as horizontal-motion inputs. It should be highlighted that the sensors MUMA and GAL1 are placed at the bottom and top edges of the same main pillar, respectively, and the relevant recordings of these two sensors should be assessed more carefully. Thus, GAL sensors located at four corners of the primary structural system of the mosque are the references for the horizontal motion, i.e., concentrated on a box-like frame.

Since the SSI effects are able to influence the response of the mosque, using horizontal input-to-output transfer functions, which represents the fixed-base case, i.e., no SSI, are more reliable than using Fourier transforms. Identified frequency in FAS needed to be also observed in TF comparison. Therefore, the FAS of the vertical recordings is also combined with the TF of horizontal counterparts.

A common range of frequency is obtained in the FAS of the M_W6.5 Aegean Sea earthquake; 1.80-4.50 Hz, which should be investigated in detail (Figure 5.1). Since vertical motion amplitudes significantly lower than horizontal's, they needed to be amplified. In Figure 5.2, identified frequencies for the x-axis are 2.34 and 3.05 Hz. However, these are not detected in the TF (Figure 5.3). In the y-axis, potential rocking frequencies are 2.32, 2.70, 3.03 and 3.82 Hz (Figure 5.4). Only one of them is apparent in the TF; 2.70 Hz (Figure 5.5). According to theresult of the conducted modal analysis, this frequency is the one identified as the 2nd modal frequency.

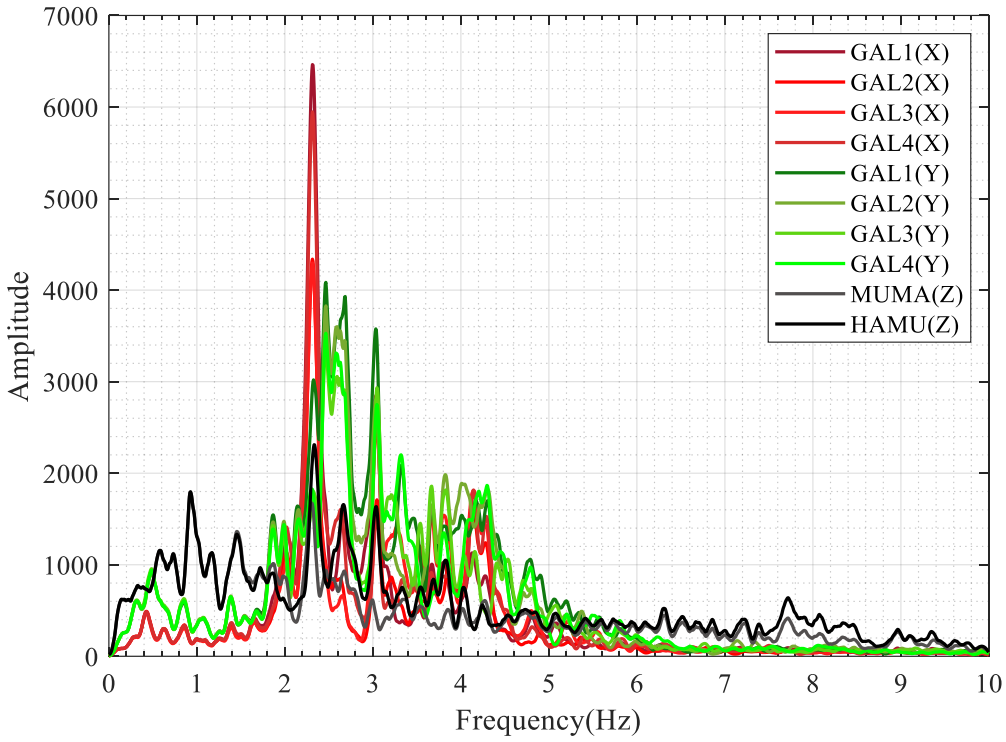

Figure 5.1. The M_W6.8 Aegean Sea Earthquake; FAS of vertical components of ground level sensors, HAMU and MUMA (amplitudes were magnified by 4), and horizontal components of GAL sensors (amplitudes of horizontal X were divided by 2).

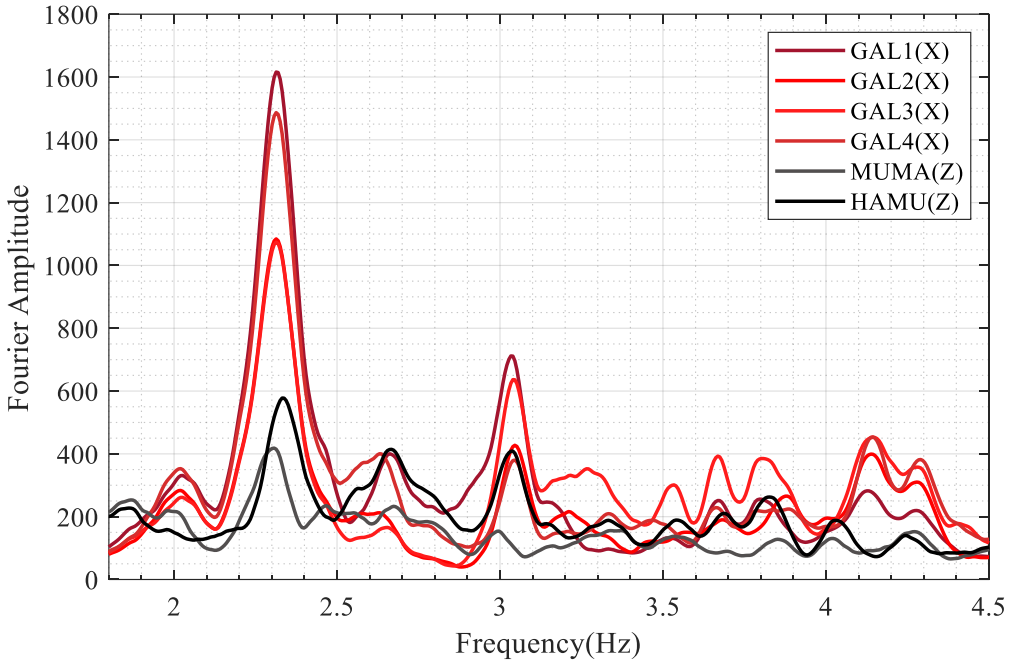

Figure 5.2. The M_W6.8 Aegean Sea Earthquake; FAS of vertical components of ground level sensors and GAL sensors (amplitudes of horizontal X were divided by 8).

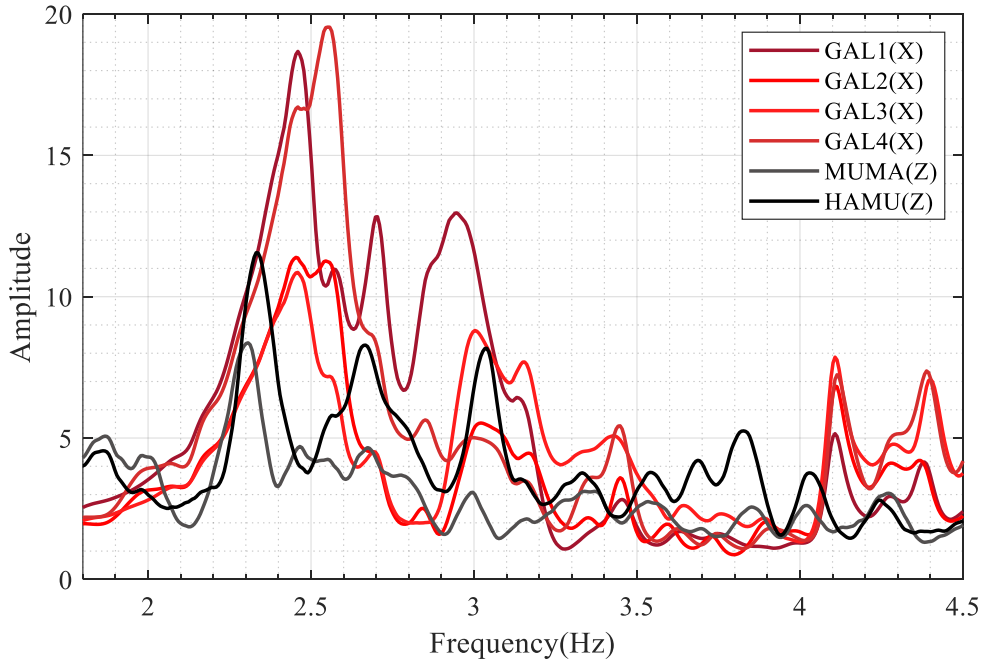

Figure 5.3. The M_W6.8 Aegean Sea Earthquake; FAS of HAMU and MUMA, and TF of GAL sensors (amplitudes of HAMU&MUMA were divided by 50).

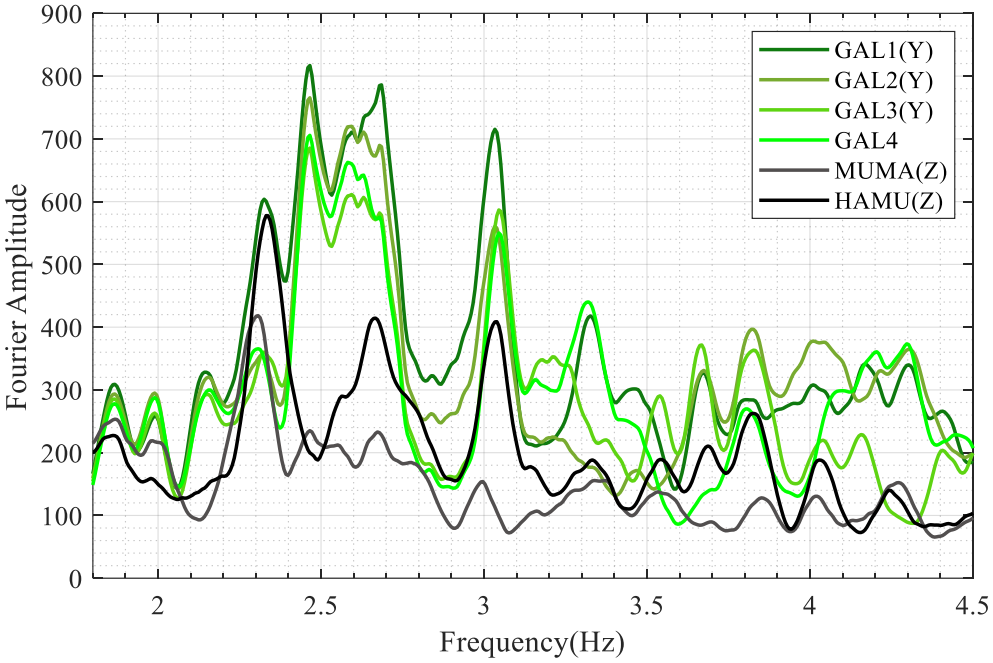

Figure 5.4. The M_W6.8 Aegean Sea Earthquake; FAS of vertical components of ground level sensors and GAL sensors (amplitudes of horizontal Y were divided by 5).

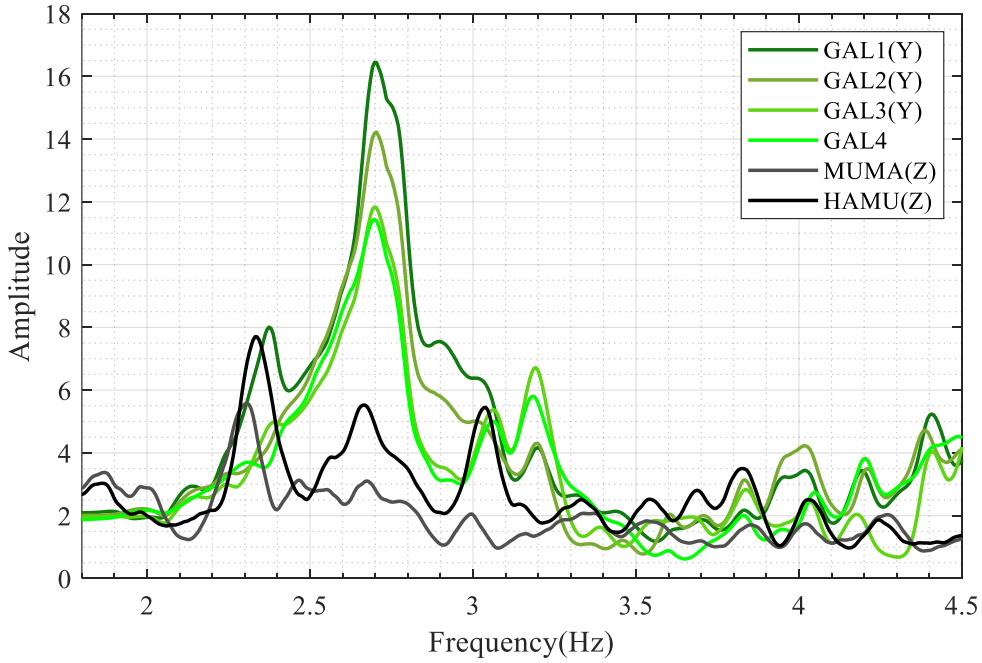

Figure 5.5. The M_W6.8 Aegean Sea Earthquake; FAS of HAMU and MUMA, and TF of GAL sensors (amplitudes of HAMU&MUMA were divided by 75).

The same procedure is also applied for a moderate magnitude earthquake: the M_W4.4 Yalova. The frequency range common for all in the FAS is 2.20-4.80 Hz (Figure 5.6). None of the determined frequencies in the X-axis (2.48 and 4.25 Hz) is also observable in the TF (Figure 5.7 and Figure 5.8). In Y-axis, any overlapped frequency cannot be detected (Figure 5.9 and Figure 5.10).

It is concluded that the mosque has not exhibited rigid body vibrations, i.e., rocking, as part of its seismic response. Although this type of response is not detected in the primary structural system, the minarets would be a suitable case study for this investigation. As initially mentioned, the Sultan Ahmet minarets, especially the taller four at the each corner of the prayer hall, with greater slenderness ratios can be modelled and evaluated by dynamic testing. It is known that they are vulnerable because of their particular geometry and able to collapse during strong seismic excitation, as in the history.

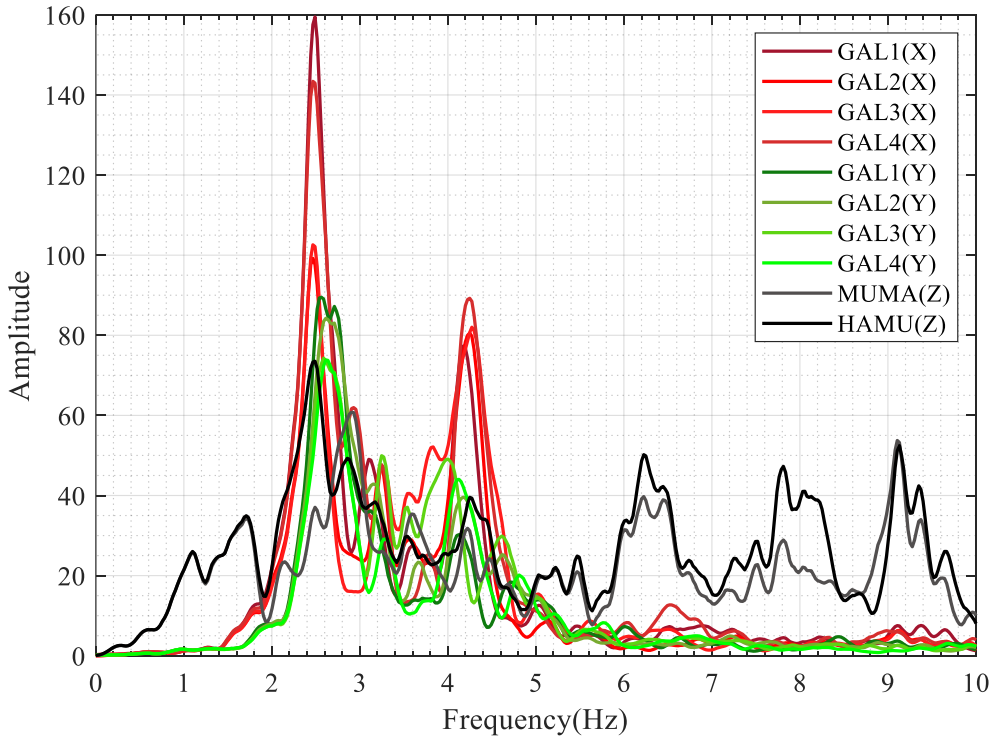

Figure 5.6. The M_W4.4 Yalova Earthquake; FAS of vertical components of ground level sensors, HAMU and MUMA, and horizontal components of GAL sensors (amplitudes of horizontal X and Y were divided by 10).

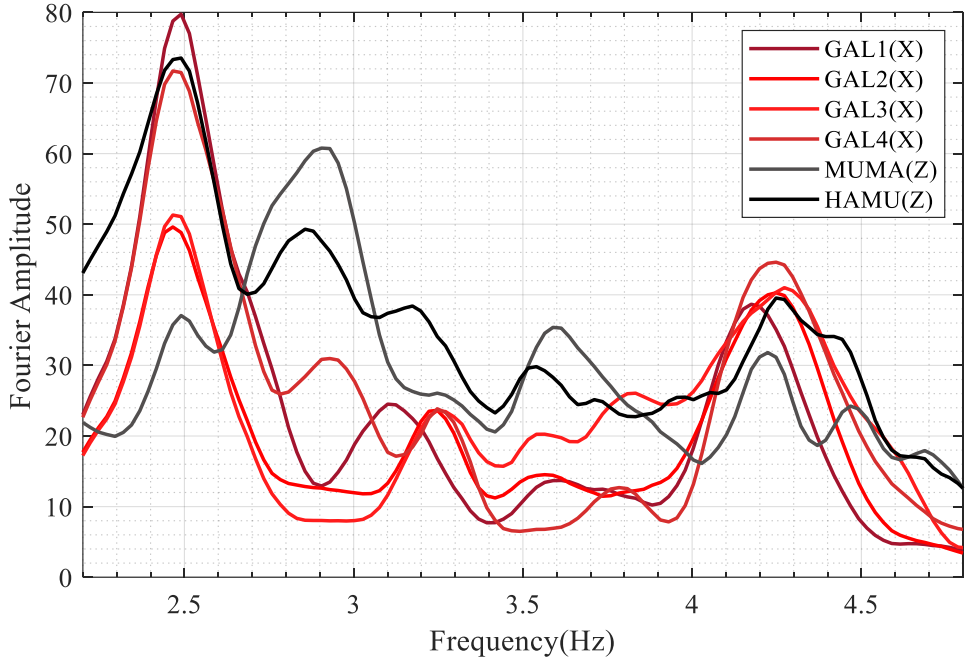

Figure 5.7. The M_W4.4 Yalova Earthquake; FAS of vertical components of ground level sensors and GAL sensors (amplitudes of HAMU&MUMA were divided by 20).

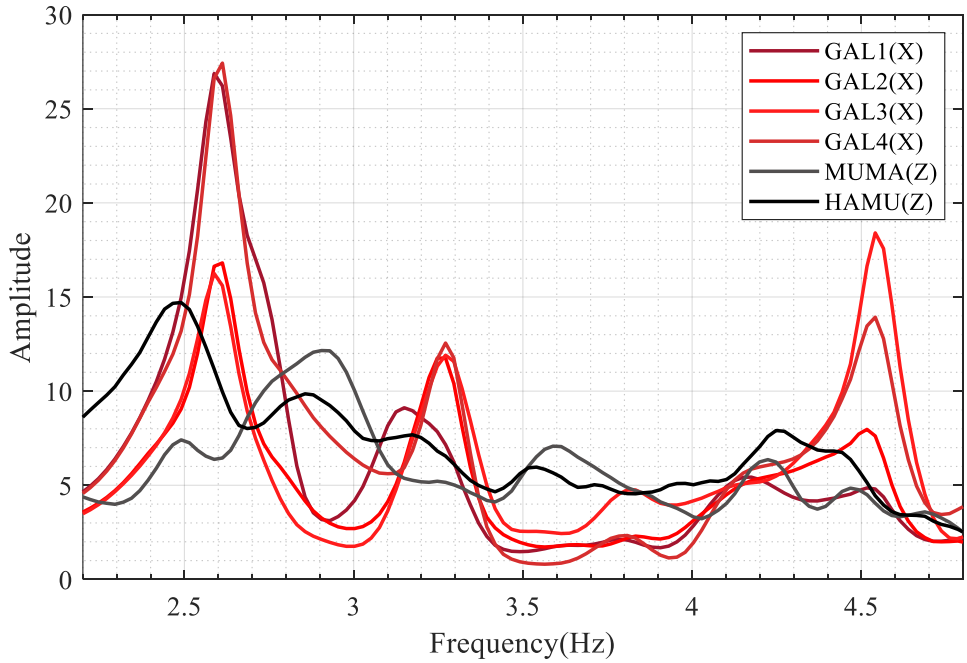

Figure 5.8. The M_W4.4 Yalova Earthquake; FAS of HAMU and MUMA, and TF of GAL sensors (amplitudes of HAMU&MUMA were divided by 5).

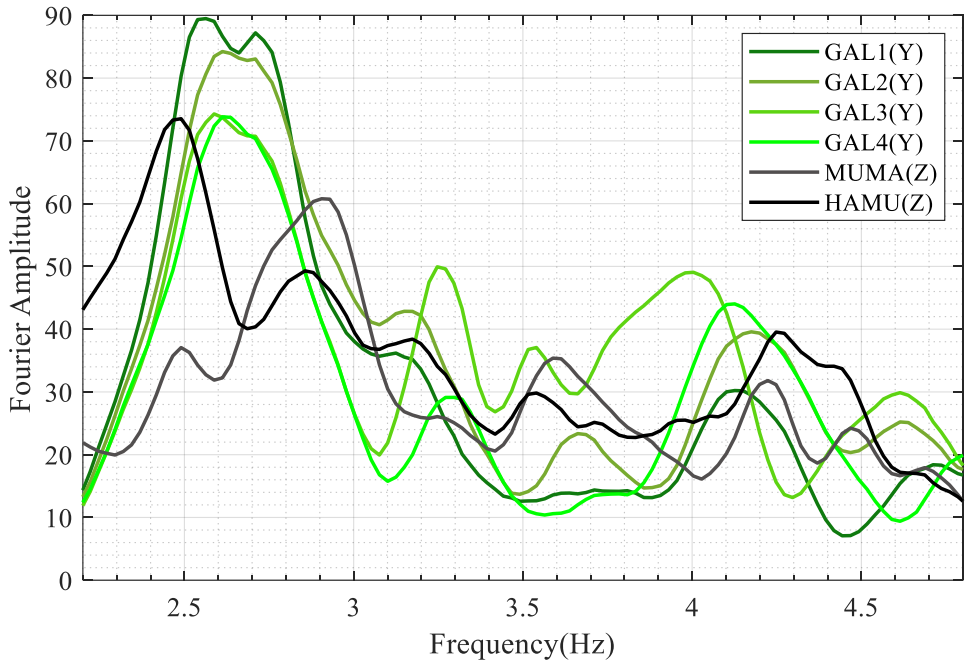

Figure 5.9. The M_W4.4 Yalova Earthquake; FAS of vertical components of ground-level sensors and GAL sensors (amplitudes of horizontal Y were divided by 5).

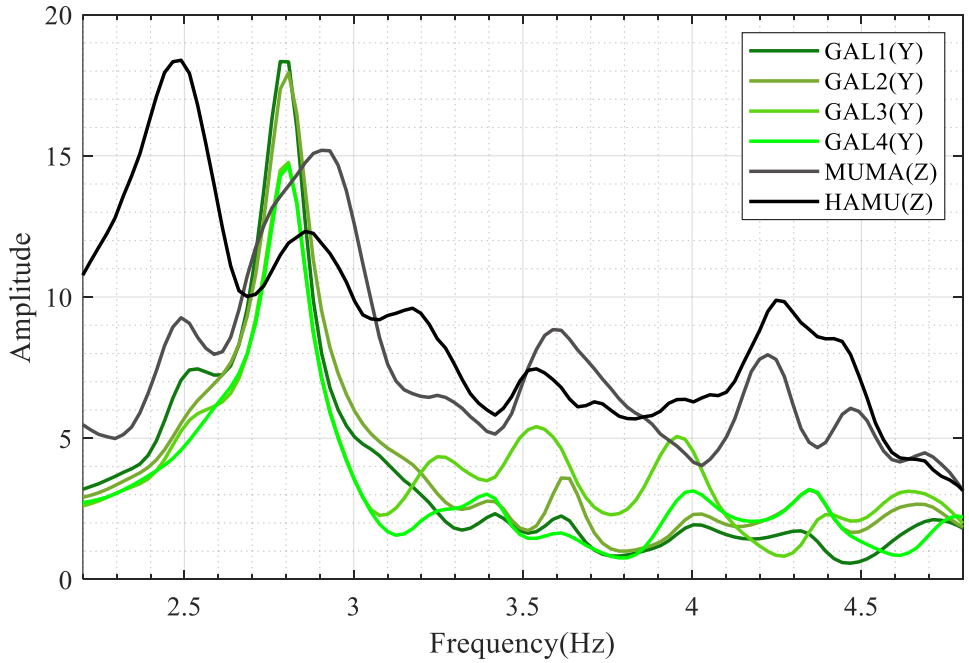

Figure 5.10. The M_W4.4 Yalova Earthquake; FAS of HAMU and MUMA, and TF of GAL sensors (amplitudes of HAMU&MUMA were divided by 4).

6. CONCLUSION

In this thesis, dynamic response of the Sultan Ahmet Mosque to seismicity is characterised. Data set of earthquakes recorded by an SHM system deployed in 2012 are utilised to conduct the time- and frequency-domain analyses.

The final catalogue compiling 103 usable earthquakes is studied. Considering M_W (2.1 - 6.9) and epicentral distance (< 400 km), the system has sensitively functioned. Also, events are depicted with their azimuthal properties, and most of the events originated from the south-east, south and south-west.

In the time domain, acceleration/velocity/displacement peaks are obtained. Each value set in four different structural levels shows the unique feature that can be attributed to its position. From the basement to the dome level, response amplitudes increase. It is observed that four dome-level sensors installed over the keystones of each main arch exhibit in-plane and out-of-plane behaviour as expected. Four others installed where the main arches springing from the pillars resulted in amplitudes in a lower order than the dome. Between the sensors in this sensor group, those at the pillars on the qibla side resulted in relatively higher amplitudes, which could be a consequence of their extra extension in the basement level. The change of amplitudes at the upper structure with earthquake magnitude and input excitation resulted in moderate and positive correlations, respectively. Within the limits of the entire data set, the latter correlation is promising. With further research employing machine learning, a trained model can give predictions as results for large magnitude earthquakes that are expected in the Marmara region.

The first two modal frequencies are identified in the 2.00-3.00 Hz band. These variations of dominant frequencies led us to reveal the affecting factors and the dependence of two frequency bands on time, annual changes and ground excitation individually. The main result found is that the dominant frequency tends to decrease with increasing amplitudes of ground excitation. On the other hand, there is no permanent frequency drop that can be associated

with strong seismic activity, and tension ring installation has no impact on the crowning dome in the frequency domain. Annual change of frequency does not seem affected directly by temperature since the fundamental governing parameter is the ground motion amplitude for the mosque.

In particle motion evaluations, the southern portion of the mosque, i.e., the pendentive formed within KUB1-GAL1-KUB2 sensors, is found more responsive during seismic excitation. The first two mode shapes are lateral through the Y-axis.

By examining the frequency content in Fourier amplitude spectra and transfer functions, it is revealed that the mosque is subjected to soil-structure interaction, which is a must to take into account in further analytical studies.

Examining both a major and moderate earthquake in main horizontal directions, rigid body vibrations, i.e., rocking, are not detected as part of the seismic response of the mosque.

REFERENCES

Acikgoz, S. and M.J. DeJong, 2014, ‘‘The Rocking Response of Large Flexible Structures to Earthquakes’’, *Bulletin of Earthquake Engineering*, Vol. 12, pp. 875-908.

AFAD (Turkish Disaster and Emergency Management Presidency), *Earthquake Hazard Map for Turkey,* 2018, https://tdth.afad.gov.tr/TDTH/main.xhtml, January 2021.

AFAD (Turkish Disaster and Emergency Management Presidency), *Turkish Seismic Building Code*, Ankara, Turkey, 2018.

Aktas, H. (Architect\Project Manager, The Sultan Ahmet Mosque Restoration), personal communication, 24 October 2019.

Ambraseys, N.N., 2001, ‘‘The earthquake of 10 July 1894 in the Gulf of Izmit (Turkey) and its relation to the earthquake of 17 August 1999’’, *Journal of Seismology,* Vol. 5, pp. 117–128.

Ambraseys, N.N., 2009, *Earthquakes in the Mediterranean and Middle East: a multidisciplinary study of seismicity up to 1900,* Cambridge University Press, Cambridge.

Ambraseys, N.N. and C.F. Finkel, 1991, ‘‘Long-term Seismicity of Istanbul and of the Marmara Sea Region’’, *Terra Nova*, Vol. 3, pp. 527-539.

Ambraseys, N.N. and J.A. Jackson, 2000, ‘‘Seismicity of the Sea of Marmara (Turkey) since 1500’’, *Geophysical Journal International*, Vol. 141, Issue 3, F1-6.

Alyanak, Ç., 2019, Anatolian Agency Archive, *Blue Mosque'ta Kapsamlı Restorasyon* (in Turkish), https://www.aa.com.tr/tr/kultur-sanat/blue-mosqueta-kapsamli-restorasyon/1481837, Dec 2019.

Barthès, C.B., 2012, *Design of Earthquake Resistant Bridges Using Rocking Columns*, Ph.D. thesis, University of California, Berkeley.

Boğaziçi University, Kandilli Observatory and Earthquake Research Institute (BOUN-KOERI), 2021, *Regional Tsunami-Earthquake Monitoring Center: Earthquake Catalog*, http://www.koeri.boun.edu.tr/, January 2021.

Bohnhoff, M., F. Bulut, G. Dresen, P.E. Malin, T. Eken and M. Aktar, 2013, ‘‘An Earthquake Gap South of Istanbul’’, *Nature Communications*, 4:1999.

Cakti, E., O. Saygili, J.V. Lemos and C.S. Oliveira, 2016, ‘‘Discrete Element Modeling of a scaled Masonry Structure and Its Validation’’, *Engineering Structures*, 126, pp. 224-236.

Cakti, E. and E. Safak, 2019, ‘‘Structural Health Monitoring: Lessons Learned’’, In: Seismic Isolation, Structural Health Monitoring, and Performance Based Seismic Design in Earthquake Engineering, *International Congress on Advanced Earthquake Resistant Structures*, Samsun, 24-28 October 2016, Springer, Cham, Switzerland, pp. 145-164.

Cakti, E., O. Saygili, J.V. Lemos and C.S. Oliveira, 2020, ‘‘Nonlinear Dynamic Response of Stone Masonry Minarets under Harmonic Excitation’’, *Bulletin of Earthquake Engineering*, 18, pp. 4813-4838.

Cooley, J.W. and J.W. Tukey, 1965, ‘‘An Algorithm for the Machine Calculation of Complex Fourier Series’’, *Mathematics of Computation,* Vol. 19, No. 90, pp. 297-301.

Dar, E. and E. Cakti, 2018, ‘‘Vibration Based Identification of Historical Structures by Machine Learning for Dynamic Events and Atmospheric Conditions’’, *European Geosciences Union General Assembly*, 8-13 April 2018, Vienne, Austria.

Erdik, M., 2013, ‘‘Aya İrini Kilisesi Deprem Performans Değerlendirmesi ve Güçlendirme Projesi Hazırlanması’’ (in Turkish), 4. Tarihi Yapıların Korunması ve Geleceğe Güvenle Devredilmesi Sempozyumu, TMMOB-IMO, November 27-29, 2013, İstanbul, Turkey.

Erdogan, Y.S., T. Kocaturk and C. Demir, 2019, ‘‘Investigation of the Seismic Behavior of a Historical Masonry Minaret Considering the Interaction with Surrounding Structures’’, *Journal of Earthquake Engineering,* Vol. 23, No. 1, pp.112-140.

Evren, E., Z. Cakır, H. Mintas, H.M. Ceylan, M. Sav, M. Tuzer, and D. Meral, 2012, ‘‘Sultan Ahmet Camii’nde Arkeojeofizik Çalışmalar’’ (in Turkish), *Vakıf Restorasyon Yıllığı,* issue 4, pp. 99 – 112.

Eyice, S., 1963, *İstanbul Minareleri* (in Turkish), Güzel Sanatlar Akademisi Türk Sanatı Tarihi Enstitüsü Yayınları, Istanbul.

Finkel, C.F. and N.N. Ambraseys, 1997, ‘‘The Marmara Sea Earthquake of 10 July 1894 and Its Effects on Historic Buildings’’, *Anatolia Moderna-Yeni Anadolu,* Tome 7, pp. 49-58.

Freely, J., 2011, *A History of Ottoman Architecture*, WIT Press, Boston.

Goodwin, G., 2012, *Osmanlı Mimarlığı Tarihi* (in Turkish), Kabalcı Yayınevi, Istanbul.

He, J. and Z.F. Fu, 2001, *Modal Analysis*, Butterworth-Heinemann, Oxford.

İM Architecture (İM Mimarlık Restorasyon Ltd. Şti.), 2017, restoration surveys and technical drawings of the Sultan Ahmet Mosque, Istanbul.

Kafadar, N. (technical staff of the Structural Health Monitoring Laboratory, DEE, KOERI), personal communication, 24 February 2020.

Konstantinidis, D. and N. Makris, 2005, ‘‘Seismic Response Analysis of Multidrum Classical Columns’’, *Earthquake Engineering and Structural Dynamics*, 34, pp. 1243-1270.

Kramer, S.L., 1996, *Geotechnical Earthquake Engineering*, Prentice Hall, New Jersey.

Mayer, L., 1810, *Views in the Ottoman Dominions, in Europe, in Asia, and some of the Mediterranean Islands*, P. Bowyer, London.

Mazlum, D., 2011, *1766 İstanbul Depremi Belgeler Işığında Yapı Onarımları* (in Turkish), İstanbul Araştırmaları Enstitüsü Yayınları, Istanbul.

Munafò I., Malagnini, L., and Chiaraluce, L., 2016, ‘‘On the Relationship between M_W and M_L for Small Earthquakes’’, *Bulletin of the Seismological Society of America*, Vol. 106, No. 5, pp. 2402 – 2408.

Müller-Wiener, W., 2016, *İstanbul'un Tarihsel Topografyası: 17. Yüzyıl Başlarına Kadar Byzantion – Konstantinopolis – İstanbul* (in Turkish), Yapı Kredi Yayınları, Istanbul.

Nayır, Z., 1975, *Osmanlı Mimarlığında Sultan Ahmet Külliyesi ve Sonrası (1609-1690)* (in Turkish), Ph.D. thesis, Istanbul Technical University.

Ordu, M., (Art Historian, The Sultan Ahmet Mosque Restoration), *personal communication*, 24 October 2019.

Özkılıç, S. K., 2015, *1894 Depremi ve İstanbul* (in Turkish), Türkiye İş Bankası Kültür Yayınları.

Priestley, M.J.N., R.J. Evison and A.J. Carr, 1978, ‘‘Seismic Response of Structures to Rock on Their Foundations’’, *Bulletin of the New Zealand National Society for Earthquake Engineering*, Vol. 11, No. 3, pp. 141-150.

Rüstem, Ü., 2016, ‘‘The Dome-Closing Ceremony of the Sultan Ahmed Mosque*’’*, *Muqarnas*, Vol. 33, Brill, pp. 253-299.

Sayin, G.P., 1999, *Structural Identification of the Sultan Ahmet Mosque through Dynamic Response Studies*, M.Sc. thesis, Bogazici University.

Safak, E. and M. Celebi, 1991, ‘‘Seismic Response of Transamerica Building. II: System Identification’’, *Journal of Structural Engineering*, Vol. 117, No. 8, pp. 2405-2425.

Safak, E., 1995, ‘‘Detection and Identification of Soil-Structure Interaction in Buildings from Vibration Recordings’’, *Journal of Structural Engineering*, Vol. 121, pp. 899 – 906.

Safak, E., 1997, ‘‘Models and Methods to Characterize Site Amplification from a Pair of Records’’, *Earthquake Spectra*, Vol. 13, No. 1, pp. 97-129.

Safak, E. and E. Cakti, 2014, ‘‘Simple Techniques to Analyze Vibration Records from Buildings’’, In: EWSHM, *7th European Workshop on Structural Health Monitoring*, 8-11 July 2014, IFFSTTAR, Inria, Université de Nantes, Nantes, France.

Sébah & Joaillier Photograph No:104, with the permission of Fabrizio Casaretto (who archives Sébah & Joaillier collection).

Sengor, A.M.C., O. Tuysuz, C. Imren, M. Sakınc, H. Eyidogan, N. Gorur, X.L. Pichon and C. Rangin, 2005, ‘‘The North Anatolian Fault: A New Look’’, *Annual Review of Earth and Planetary Sciences*, Vol. 33:1, pp. 37-112.

Sesetyan, K., U. Hancılar, E. Safak, E. Caktı, S. Kara, O. Uzunkol, B.E. Konukcu, S. Gunay, H. Mehmetoglu, Y. Mentese, K. Duran, and T. Kahraman, 2020, *İstanbul İli Fatih İlçesi Olası Deprem Kayıp Tahminleri Kitapçığı* (in Turkish), Istanbul Metropolitan Municipality.

Yenihayat, N. and E. Cakti, ‘‘Explosion Records in Historical Structures’’, *4th International Conference on Earthquake Engineering and Seismology*, 11-13 October 2017, Anadolu University, Eskişehir/Turkey.

Yim C.S., A.K. Chopra and J. Penzien, 1980, Rocking Response of Rigid Blocks to Earthquakes, Earthquake Engineering and Structural Dynamics, Vol. 8, pp. 565 – 587.